CONTINGENCY RANKING FOR ON-LINE VOLTAGE STABILITY ASSESSMENT

ZHIHONG JIA

INFORMATION TO USERS

This manuscript has been reproduced from the microfilm master. UMI films the text directly from the original or copy submitted. Thus, some thesis and dissertation copies are in typewriter face, while others may be from any type of computer printer.

The quality of this reproduction is dependent upon the quality of the copy submitted. Broken or indistinct print, colored or poor quality illustrations and photographs, print bleedthrough, substandard margins, and improper alignment can adversely affect reproduction.

In the unlikely event that the author did not send UMI a complete manuscript and there are missing pages, these will be noted. Also, if unauthorized copyright material had to be removed, a note will indicate the deletion.

Oversize materials (e.g., maps, drawings, charts) are reproduced by sectioning the original, beginning at the upper left-hand corner and continuing from left to right in equal sections with small overlaps.

Photographs included in the original manuscript have been reproduced xerographically in this copy. Higher quality 6" x 9" black and white photographic prints are available for any photographs or illustrations appearing in this copy for an additional charge. Contact UMI directly to order.

Bell & Howell Information and Learning
300 North Zeeb Road, Ann Arbor, MI 48106-1346 USA
800-521-0600

UMI®

CONTINGENCY RANKING FOR ON-LINE VOLTAGE STABILITY ASSESSMENT

by

© Zhihong Jia, B.ENG., M.ENG.

A thesis submitted to the School of Graduate

Studies in partial fulfillment

of the requirements for the degree of

Master of Engineering

Faculty of Engineering and Applied Science

Memorial University of Newfoundland

June 1999

St. John's Newfoundland Canada

Abstract

Voltage stability is one of the challenging problems in power system operation. This thesis deals with fast algorithms for Contingency Screening and Ranking (CS&R) for power system voltage stability studies. CS&R is one of the important components of on-line voltage stability assessment. Its purpose is to rapidly and accurately determine which contingencies may cause power system voltage instability according to their severity.

First, two popular voltage stability analysis methods, Continuation Power Flow (CPF) and minimum singular value of Jacobian matrix, are studied in this thesis. Then, several existing CS&R methods are reviewed. Two of them, Reactive Support Index (RSI) and Generalized Curve Fitting (GCF) methods, are investigated in detail.

Finally, based on the GCF method, two novel methods for CS&R are proposed in this thesis. After employing the two improved methods, *reselecting curve fitting points* and *filtering out unreasonable nose points*, the simulation results show that the proposed methods have the ability to provide a fast estimate of voltage stability margins and thus select the most severe contingencies. The proposed methods have been applied for different power systems. These methods have the potential to be implemented in any on-line voltage stability assessment scheme.

Acknowledgements

I would like to thank and express my indebtedness and deepest gratitude to my supervisor Dr. B. Jeyasurya for his constant advice, encouragement and guidance during all stages of this research.

I take this opportunity to express my profound gratitude to my parents and my wife for their constant support and encouragement during my study in Canada.

I also acknowledge the assistance received from Dr. J. J. Sharp, Dr. M. R. Haddara, the staff at CCAE, faculty, and friends.

Finally, I would like to acknowledge financial support from the School of Graduate Studies, and the Faculty of Engineering and Applied Science at Memorial University of Newfoundland.

Contents

Abstract ..... **I**

Acknowledgements ..... **II**

Contents ..... **III**

List of Figures ..... **VI**

List of Tables ..... **IX**

1 Introduction **1**

1.1 Introduction 1

1.2 Aim of the Thesis 5

1.3 Organization of the Thesis 5

2 Power System Voltage Stability **7**

2.1 Introduction 7

2.2 Voltage Stability 7

2.3 Voltage Stability: Static or Dynamic? 14

2.4 Concepts Related to Voltage Stability: PV Curves, QV Curves, and Margins 15

2.5 Voltage Stability Indices 20

2.6 Summary 31

3 Contingency Screening and Ranking Methods 32

3.1 Introduction 32

3.2 Operating States 33

3.3 Voltage Stability Assessment 35

3.4 Methods for Contingency Screening and Ranking 37

3.5 Summary 52

4 Simulation Results for Contingency Screening and Ranking 53

4.1 Introduction 53

4.2 Continuation Power Flow Results for Contingency Screening and Ranking 54

4.3 Simulation Results of Reactive Support Index (RSI) 59

4.4 CS&R Results Obtained by GCF 66

4.5 Summary 81

5 Proposed Methods for Contingency Screening and Ranking 83

5.1 Introduction 83

5.2 Reselecting Curve Fitting Points 84

5.3 Filtering out Unreasonable Nose Points 86

5.4 Simulation Results for Reselecting Curve Fitting Points (R-GCF) 88

5.5 Simulation Results for Reselecting Curve Fitting Points and Filtering out Unreasonable Nose Points 101

5.6 Summary 108

6 Conclusions **110**

6.1 Contributions of this research 110

6.2 Suggestions for future work 114

References **115**

Appendix A Summary of Different Power System Models 119

Appendix B 197-bus BC Hydro Power System Summary 123

Appendix C 1254-bus Ontario Hydro Power System Summary 129

List of Figures

Figure 2.1 A two-machine power system 8

Figure 2.2 A simple radial power system 11

Figure 2.3 A PV curve for an infinite source at a constant power factor 15

Figure 2.4 PQ curves for load buses 17

Figure 2.5 Illustration of stability margin 19

Figure 2.6 Illustration of continuation power flow method 22

Figure 2.7 Voltage profiles at buses 3,4, and 5 for the 5-bus power system 25

Figure 2.8 Voltage profiles at buses 4, 16 and 24 for the New England 39-bus power system 25

Figure 2.9 Minimum singular value index for the 5-bus power system 29

Figure 2.10 Minimum singular value index for the New England 39-bus power system 30

Figure 2.11 Minimum singular value index for a 63-bus power system 30

Figure 3.1 Power system operating states 34

Figure 3.2 Functional representation of VSA environment 36

Figure 3.3 Illustration of multiple load flow method 40

Figure 3.4 Illustration of V-Q curve fitting method 44

Figure 3.5 Illustration of generalized curve fitting method 45

Figure 3.6 Illustration of reactive support index 50

Figure 3.7 Illustration of iterative filtering 51
Figure 4.1 Single line diagram of the 5-bus system 54
Figure 4.2 PV curves for both pre-contingency and line 1,2,and 3 outages at bus 5 for the 5-bus power system 56
Figure 4.3 PV curves for both pre-contingency and line 4, 5, 6, and 7 outages at bus 5 for the 5-bus power system 57
Figure 4.4 Line outage contingencies and their margins 58
Figure 4.5. Normalized RSI index for the 5-bus system 61
Figure 4.6 Normalized RSI index for the 118-bus system 63
Figure 4.7 Normalized RSI index for the 600-bus system 65
Figure 4.8 Ranking results obtained by GCF for the 5-bus system 68
Figure 4.9. Single line diagram of the 39-bus power system 69
Figure 4.10 Normalized GCF index for the 39-bus system 70
Figure 4.11 Normalized GCF index for the 118-bus system 72
Figure 4.12 Normalized GCF index for the 300-bus system 74
Figure 4.13 Normalized GCF index for the 600-bus system 76
Figure 4.14 Normalized GCF index for the 197-bus power system 78
Figure 4.15 Normalized GCF index for the 1254-bus power system 80
Figure 5.1 Illustration of the generalized curved fit method 84
Figure 5.2 The flow chart to obtain the stressed case for each contingency 85
Figure 5.3 Abnormal nose point obtained by GCF (extremely big) 86
Figure 5.4 Abnormal nose point obtained by GCF (Negative margin) 87

Figure 5.5 Illustration of a 'band-pass filter' 88

Figure 5.6 Normalized R-GCF index for the 5-bus system 89

Figure 5.7 Normalized R-GCF index for the 39-bus power system 91

Figure 5.8 Normalized R-GCF index for the 118-bus power system 92

Figure 5.9 Normalized R-GCF index for the 300-bus power system 94

Figure 5.10 Normalized R-GCF index for the 600-bus power system 96

Figure 5.11 Normalized R-GCF index for the 197-bus power system 98

Figure 5.12 Normalized R-GCF index for the 1254-bus power system 100

Figure 5.13 Normalized F-GCF & R-GCF index for the 118-bus power system 102

Figure 5.14 Normalized F-GCF & R-GCF index for the 300-bus power system 103

Figure 5.15 Normalized F-GCF and R-GCF index for the 600-bus power system 104

Figure 5.16 Normalized F-GCF &R-GCF index for the 197-bus power system 105

Figure 5.17 Normalized F-GCF & R-GCF index for the 1254-bus power system 106

Figure B.1 Main structure of BC Hydro power system 127

Figure B.2 Geographic location of BC Hydro transmission network 128

Figure C.1 Main structure of Ontario Hydro power system 131

Figure C.2 Geographic location of Ontario Hydro transmission network 134

List of Tables

Table 2.1 Minimum singular values and loading levels for the 5-bus system 28

Table 2.2 Minimum singular values and loading levels for the New England 39-bus system 28

Table 4.1 Impedances and line charging for the 5-bus system 55

Table 4.2 Scheduled generation, loads, and desired bus voltage for the 5-bus system 55

Table 4.3 Voltage collapse points, margins, and ranking results for each line outage contingency in the 5-bus power system 58

Table 4.4 Scheduled generation of the two generators and their reactive limits for the 5-bus system 60

Table 4.5 Reactive power provided by two generators at stressed case for each line contingency when the generator's reactive power limit is open 60

Table 4.6 Normalized ranking results for the 5-bus system using CPF and RSI 62

Table 4.7 The 10 critical branch outage contingency margins obtained by RSI and CPF for the 118-bus power system 64

Table 4.8 The 10 critical branch outage contingency margins obtained by RSI and CPF for the 600-bus power system 66

Table 4.9 Fitting points selected for line 1 and line 2 outages in the 5-bus system 67

Table 4.10 Margins obtained by GCF and CPF for the 5-bus system 68

Table 4.11 The 10 critical branch outage contingency margins obtained by GCF and CPF for the 39-bus power system 71

Table 4.12 The 10 critical branch outage contingency margins obtained by GCF and CPF for the 118-bus power system 73

Table 4.13 The 10 critical branch outage contingency margins obtained by GCF and CPF for the 300-bus power system 75

Table 4.14 The 10 critical branch outage contingency margins obtained by GCF and CPF for the 600-bus power system 77

Table 4.15 The 10 critical branch outage contingency margins obtained by GCF and CPF for the 197-bus power system 79

Table 4.16 The 10 critical branch outage contingency margins obtained by GCF and CPF for the 1254-bus power system 81

Table 5.1 Line outage contingency margins obtained by R-GCF and CPF for the 5-bus system 90

Table 5.2 The 10 most critical branch outage contingency margins obtained by R-GCF and CPF for the 39-bus system 91

Table 5.3 The 10 most critical branch outage contingency margins obtained by R-GCF and CPF for the 118-bus system 93

Table 5.4 The 10 most critical branch outage contingency margins obtained by R-GCF and CPF for the 300-bus system 95

Table 5.5 The 10 most critical branch outage contingency margins obtained by R-GCF and CPF for the 600-bus system 97

Table 5.6 The 10 most critical branch outage contingency margins obtained by R-GCF and CPF for the 197-bus system 99

Table 5.7 The 10 most critical branch outage contingency margins obtained by R-GCF and CPF for the 1254-bus system 100

Table 5.8 The 10 most critical branch outage contingency margins obtained by F-GCF & R-GCF, and CPF for the 118 bus-system 103

Table 5.9 The 10 most critical branch outage contingency margins obtained by F-GCF & R-GCF, and CPF for the 300-bus system 104

Table 5.10 The 10 most critical branch outage contingency margins obtained by F-GCF & R-GCF, and CPF for the 600-bus system 105

Table 5.11 The 10 most critical branch outage contingency margins obtained by F-GCF & R-GCF, and CPF for the 197-bus system 106

Table 5.12 The 10 most critical branch outage contingency margins obtained by F-GCF & R-GCF, and CPF for the 1254-bus system 107

Table 5.13 The misclassification of the proposed methods 108

Table 5.14 CPU time for the 10 most critical contingencies to different systems 108

Table A.1 5-bus power system component data 119

Table A.2 5-bus power system base-case load flow summary 119

Table A.3 New England 39-bus power system component data 120

Table A.4 New England 39-bus system base case load flow summary 120

Table A.5 IEEE 118-bus power system component data 120

Table A.6 IEEE 118-bus power system base case load flow summary 121

Table A.7 IEEE 300-bus power system component data 121

Table A.8 IEEE 300-bus power system base case load flow summary 121

Table A.9 600-bus power system component data 122

Table A.10 600-bus power system base case load flow summary 122

Table B.1 BC Hydro main power plant summary 125

Table B.2 WSCC 8313- bus power system component data 126

Table B.3 WSCC 8313-bus power system base case load flow summary 126

Table B.4 BC Hydro 197- bus power system component data 126

Table B.5 BC Hydro 197-bus power system base case load flow summary 126

Table C.1 Ontario Hydro main generator summary 132

Table C.2 NEPP 13,715- bus power system component data 132

Table C.3 NEPP 13,715-bus power system base case load flow summary 133

Table C.4 Ontario Hydro 1254- bus power system component data 133

Table C.5 Ontario Hydro 1254-bus power system base case load flow summary 133

Chapter 1

Introduction

1.1 Introduction

Electric energy is one of the most fundamental requirements of modern industrial society. Electric power is produced at generating stations and transmitted to consumers through a complex network of individual components in transmission lines, transformers, and switching devices. The power system is mainly made up of generation, transmission, distribution and its auxiliary system.

Power generation, in the electric industry, means conversion of energy from a primary form to the electrical form. The current sources of all the electricity distributed by utilities come from the conversion of chemical energy of fossil fuels, nuclear fission energy, and the kinetic energy of water which is allowed to fall through a difference of elevation. A transmission system interconnects all major generating stations and main load centers in the system. In addition to its original function of moving energy over long distances, it also ties together the important generation station and primary substations. It forms the backbone of the integrated power system and operates at the highest voltage levels (typically, 230kV and above), while the generator voltages are usually in the range

of 11 to 35 kV, which are stepped up to the transmission voltage level. The distribution system represents the final stage in the transfer of power to the individual customers. The primary distribution voltage is typically between 4.0 kV and 34.5 kV. Small industrial customers are supplied by primary feeders at this voltage level. The secondary distribution feeders supply residential and commercial customers at 120/240 V.

The secure operation of electric power systems is very important. There are many factors affecting the secure operation of power systems, such as overload of power system equipment (transmission lines, transformers etc.) and angular stability of synchronous generators. The maximum temperature of a conductor determines the thermal limit. Conductor temperature affects the conductor sag between towers and the loss of conductor tensile strength due to annealing. If the thermal limit is exceeded for a long time, it may cause the conductor to ground clearance to shorten, and the conductor will not shrink to its original length when cooled. Angular (transient) stability is another factor. Power systems rely on synchronous machines for generation of electrical power. A necessary condition for satisfactory system operation is that all synchronous machines remain in synchronism or 'in step'. This aspect of stability is influenced by the dynamics of generator rotor angles and power-angle relation [1]. If the systems are subjected to some disturbances, such as load increase, switching operations, and faults with subsequent circuit isolation, these disturbances may set up an oscillation that causes the system to swing beyond the critical point [2]. Recovery would be impossible in this situation, and, as a result, generators will lose their angular stability.

Nowadays, line and transformer thermal limits have become less restrictive as the power systems have become more dense. Fast fault clearing, high performance excitation

systems, and other controls have raised the transfer limits in stability limited systems [1]. However, due to the economic and environmental considerations, it has become increasingly difficult for many utilities to add new transmission or generation facilities to their systems. Despite restrictions in system expansions, customer load often continues to grow, and utilities are forced to operate power systems under increasingly stressed conditions. This has led to the emergence of new forms of system instability. One such form of system instability, which has stirred much interest in the research community in recent years, is voltage instability. Voltage instability has become more limiting than angular instability, and in some systems it has been responsible for severe system disturbances including major blackouts [1, 3]. As a result, much attention has been given to the study of voltage stability and the development of analytical tools capable of studying this phenomenon.

One of the most important functions in security assessment of power systems is contingency analysis. The results of this type of analysis allow power systems to be operated defensively. Many of the problems that occur in a power system can cause serious trouble so quickly that the operator cannot take action fast enough to prevent it. This is often the case with cascading failures. Because of this aspect of system operation, computers for power system operation are equipped with contingency analysis programs that model possible system troubles before they arise. These programs are part of the security assessment programs and are useful to the power system operators. These make it possible for the power system to be operated in such a way that most of the contingencies do not cause serious disturbance to the power system operation.

Fast and accurate ranking of contingencies are vital for the secure and economic operation of power systems. Due to an increase in transmission requirements and environmental pressure, utilities are being forced to maximize the transmission capabilities of the existing transmission lines. This effectively means that in order to maintain system security and stability, there is a demand for on-line contingency screening and ranking.

One of the major stumbling blocks to on-line contingency screening and ranking is the heavy computational burden imposed by most of the power system analysis software. Thus, computation speed, which in turn depends on the computer hardware specifications, is the deciding factor which determines the on-line implementation of power system security assessment functions. The initial investments required for sophisticated computing equipment are so high that in most cases utilities are not able to afford them. This prompted researchers to look at alternatives to raw computing power.

Power system engineers are always investigating innovative and challenging ways to enhance the performance of power systems. Recently, there has been considerable interest in the fast algorithms for contingency screening and ranking suitable for on-line voltage stability assessment [4,5,6,7]. However, to the best of the author's knowledge, some of these methods are computationally demanding, while some are sensitive to different power systems [4,5,6,7]. When the latter methods are applied, the ranking results are quite accurate for some test systems, but not for others. In some cases, they cannot even provide any useful information about the severity of each of the contingencies.

1.2 Aim of the Thesis

The focus of the research presented in this thesis is on the Contingency Screening & Ranking (CS&R) methods suitable for on-line voltage stability assessment. Considering the factors described above, this research is to meet the following objectives:

- Simulate two popular voltage stability indices.
- Investigate several existing contingency screening and ranking methods.
- Propose a novel contingency screening and ranking method suitable for on-line analysis.
- Carry out the proposed method on various power systems including several IEEE standard power systems and two North American power systems.

1.3 Organization of the Thesis

Chapter 2 of this thesis discusses the concepts of voltage stability, several indices of voltage stability, and the simulations of these indices on two small power system models.

Chapter 3 focuses on Contingency Screening and Ranking (CS&R) methods. First, operating states of a typical power system are explained. Then, the voltage stability assessment environment is described. Finally, several existing methods for on-line contingency screening and ranking are presented.

Based on the CS&R algorithms presented in Chapter 3, two of them, Reactive Support Index (RSI) and Generalized Curve Fitting (GCF) methods, are investigated using a variety of power systems in Chapter 4. Their simulation results are also compared

with those of the Continuation Power Flow (CPF) method, which has accurate performance.

In view of the poor performance of GCF for several larger power systems, a novel on-line contingency screening and ranking method based on GCF is proposed by the author in Chapter 5. In addition, the simulations of the proposed method are carried out on several power systems including BC Hydro 197-bus system and Ontario Hydro 1254-bus system. The ranking results are compared with those of CPF method.

In Chapter 6, the summary of the thesis highlighting the contribution of the research and recommendations for future work are outlined.

Chapter 2

Power System Voltage Stability

2.1 Introduction

In this chapter, the theory of voltage stability will be presented, followed by a debate, *Voltage stability—Static or Dynamic?* Then, several concepts (PV curves, QV curves, and voltage stability margins) related to voltage stability will be described. Finally, two types of voltage stability indices, direct index and indirect index, will be introduced. The simulation results, based on these indices, will also be presented on a 5-bus and New England 39-bus power system model.

2.2 Voltage Stability

It has been long recognized that there is strong coupling between real power transmission (MW) and rotor angle, and reactive power transmission (MVAR) and the voltage [1,2]. In other words, the availability of MW is dictated by the machine angle, which in turn is decided by the input to the prime movers. On the other hand, voltage is related to the MVAR availability at that point. To understand the above concepts,

consider a simple power system. It is known that real and reactive power transmission depends on the voltage magnitude and angle at both the sending end and the receiving end. Figure 1 shows a two-machine system. The relationship between voltages and angles at both ends can be derived as follows:

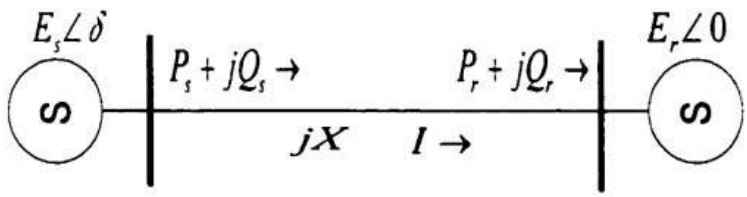

Figure 2.1 A two-machine power system [3]

$$\begin{aligned}\bar{S}_r &= P_r + jQ_r = \bar{E}_r I^* \\ &= E_r\left[\frac{E_s\cos\delta + jE_s\sin\delta - E_r}{jX}\right]^* \\ &= \frac{E_sE_r}{X}\sin\delta + j\left[\frac{E_sE_r\cos\delta - E_r^2}{X}\right]\end{aligned} \tag{2.1}$$

$$P_r = \frac{E_sE_r}{X}\sin\delta = P_{max}\sin\delta \tag{2.2}$$

$$Q_r = \frac{E_sE_r\cos\delta - E_r^2}{X} \tag{2.3}$$

Similarly, for the sending end:

$$P_s = \frac{E_sE_r}{X}\sin\delta = P_{max}\sin\delta \tag{2.4}$$

$$Q_s = \frac{E_s^2 - E_sE_r\cos\delta}{X} \tag{2.5}$$

where:

E_s : the sending end voltage (kV);

E_r : the voltage at the receiving end (kV);

X : the reactance of transmission line (ohm);

δ : the power angle of a synchronous machine (rad);

I : the current through the transmission line (kA);

S_r : the receiving end complex power (MVA);

P_s : the sending end real power (MW);

Q_s : the sending end reactive power (MVar);

P_r : the receiving end real power (MW);

Q_r : the receiving end reactive power (MVar).

Voltage instability can be ascribed to the lack of VAR support needed to maintain the voltage profile at a specified value [3]. For real power at the receiving end of the system, equation (2.2) clearly shows that when P_r increases, the prime mover must provide more energy to increase the power angle δ so as to balance the power. As a consequence, Q_r, reactive power at the receiving end, will decrease or even become negative due to the decrease of $cos\delta$. On the other hand, as shown in equation (2.5), Q_s, the reactive power at the sending end, will increase sharply. Therefore, the difference between the reactive powers at both the sending end and the receiving end (i.e. the reactive power loss across the transmission line) will increase remarkably. Transmission lines become a drain of reactive power. Generally, in case of heavy load, more than one

unit of reactive power will be required for each additional unit of real power transmitted. When the required reactive power exceeds the limit that the generator can provide, the system will collapse.

According to the reference [3], the definitions of voltage stability and voltage collapse are given as follows:

> "A power system at a given operating state and subject to a given disturbance is ***voltage stable*** if voltages near loads approach post-disturbance equilibrium values. The disturbed state is within the region of attraction of the stable post-disturbance equilibrium."
>
> "A power system at a given operating state and subject to a given disturbance undergoes ***voltage collapse*** if post-disturbance equilibrium voltages are below acceptable limits."
>
> "Normally, voltage collapse may be total or partial (blackout). To some extent, ***Voltage instability*** and ***voltage collapse*** are used somewhat interchangeable."

Thus, voltage collapse is an extreme form of voltage instability. As opposed to angle instability, the main dynamics involved in voltage collapse is the load dynamics. Hence voltage stability has also been called load stability [2]. During the period of voltage decay, other dynamics no less important come into play. These are generator excitation control, on-load tap changers (OLTCs), static *Var* compensator (SVC) controls, thermostat controlled loads etc. Since all of the above controls have a longer response time (in seconds), the dynamics are termed as slow dynamics. Typically, the response time may range from 10-20 seconds up to several minutes. Next, we will

examine how voltage stability can develop in a simple radial system and show how the various controls listed above contribute to voltage instability.

Consider the radial power system shown in Figure 2.2, which consists of generators feeding three different types of distribution systems through a heavily loaded transmission line [8].

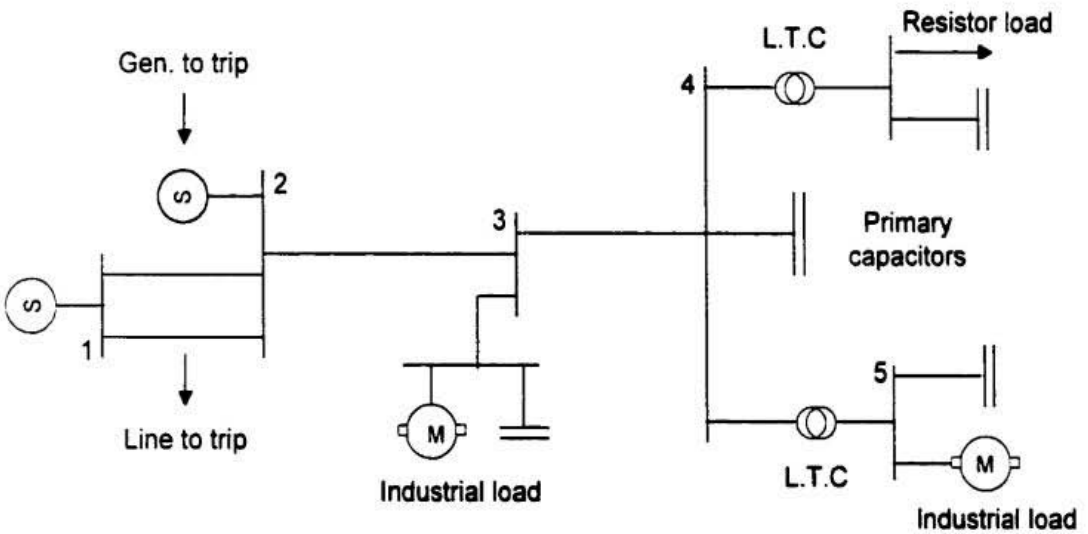

Figure 2.2 A simple radial power system

The three different types of loads are

1) Type 1 is a domestic load which is mostly a heating and lighting load and is relatively a high power factor load. This type of load tends to drop with drop in voltage.

2) Type 2 is an industrial load on a load tap changer (LTC). Most of the industrial load comprises of induction motors and does not vary with voltage.

3) Type 3 is an industrial load not on LTC.

In this heavily loaded system operating near its voltage stability limit, a small increase in load (active or reactive), a loss of generation or shunt compensation, or a drop in sending end voltage, for example, can bring in voltage instability. Assuming that one of the above mentioned changes happen, and the receiving end voltage falls, several mechanisms come into play. Since residential loads are voltage dependent, the active and reactive loads drop with drop in voltage. The industrial active and reactive loads dominated by induction motors change only by a small amount. Thus, the overall effect may be the stabilization of voltage at a value slightly less than the rated value. The next action is the operation of distribution transformer tap changers to restore distribution voltages. The residential active load will increase while the industrial reactive load will decrease. The increasing residential load will outweigh the decrease in reactive load, causing the transformer primary voltage to fall further. The increased primary reactive losses will further drop the transformer primary voltage. In this scenario, the OLTCs (on load tap changer) may be close to their limits, primary voltage at around 90% and distribution voltage below normal. As voltage sensitive controlled loads (residential) creep back toward full power, primary and secondary voltages will drop further. The Type 3 industrial loads, in other words, those without OLTCs will be exposed to reduced voltage levels. This greatly increases the stalling of induction motors (stalling occurs when load torque is greater than developed torque). When a motor stalls, it will draw increasing reactive current, bringing down the voltage on the bus. This results in a "cascade" stalling of other induction motors, resulting in a localized voltage collapse. Since most large induction motors are controlled by magnetically held contactors, the

voltage collapse would cause most motors to drop off from the system. This loss of load will cause the voltage to recover. However, the recovered voltage will again result in the contactor closing, and the motor stalling and collapse. Thus, this loss and recovery of load can cause alternate collapse and recovery of voltage. The effect of automatic voltage regulation (AVR) may be explained as follows: As the voltage drops the AVR steps in and increases the reactive generation. This increases the field current and when the current limit is reached, the excitation limiters come into play and voltages are allowed to drop. Nearby generators may pick up the reactive load, but this may last only for a few minutes if they too reach their excitation limits.

Thus, from the above discussion, it is clear that voltage stability is essentially "slow" dynamics and is affected by the nature and type of load, transformer tap changer action, or generator AVR control.

To sum up, the various important factors contributing to voltage instability are:

1) Stressed power, in other words, high active and reactive loading due to excessive load or line or transformer outages.
2) Inadequate fast reactive power resources available locally, aggravated by action of field current limiters of generators.
3) Load response at low voltages.
4) Tap changer response to distribution voltage magnitude and prop up loads as primary voltages continue to fall.

2.3 Voltage Stability: Static or Dynamic?

The above scenario, which describes how a voltage collapse can evolve in a system, shows that the time frame for a collapse to occur can be within minutes depending on the response of the various controls involved. Traditionally, dynamic analysis, as applied to angle stability, has limited itself to the generator dynamics during the transient phase in milliseconds. However, the time frame for voltage stability is much larger and the computation requirements, if the generator dynamics are to be taken into account for such a long period of time, would be prohibitive. In view of the longer time frame involved, voltage stability has often been viewed as a steady state problem suitable for static analysis [1]. Also, since a major factor in voltage instability is the availability of reactive power, the problem is ideal for power flow analysis. The static approach can offer an insight into the phenomena and can indeed give an approximate, yet acceptable solution which is computationally much simpler compared to the dynamic approach. However, since the effect of load dependency on voltage is of importance in voltage stability, it is desirable that the static load flow approach can be modified suitably to incorporate the voltage dependency on load. This "quasi static" model can give a reasonable accuracy without a corresponding increase in computation requirement. Thus, it may be seen that there is a trade off involved in both approaches, and since engineering solutions should be practical and economical and not necessarily ideal, the static approach is widely used by most utilities. Recently, many static approaches for voltage stability have been proposed [9-14].

2.4 Concepts Related to Voltage Stability: PV Curves, QV Curves, and Margins

PV curves and QV curves are two widely used curves in power system stability analysis. These two methods determine steady-state loadability limits which are related to voltage stability.

2.4.1 PV Curves

PV curves are a widely used traditional voltage stability analysis method in power systems. In a power system, PV curves can be obtained if the receiving end voltage V is plotted against the real power P when the load at the receiving end is increased.

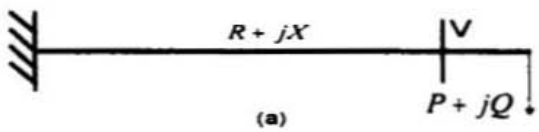

a) An infinite source power system

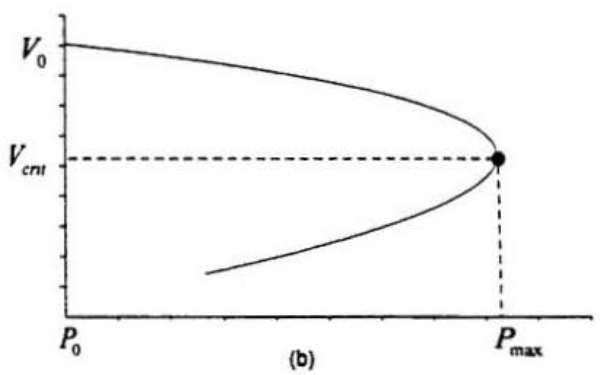

Figure 2.3 A PV curve for an infinite source at a constant power factor

Consider the very simple system of Figure 2.3(a). If the load is increased at constant power factor from the initial value of $P_0 + jQ_0$, the PV curve shown in Figure 2.3(b) can be obtained, which shows the change in load bus voltage as a function of active power at the load bus. When the load is increased, a maximum power transfer limit is reached at the 'nose', P_{max}, determined by the network impedance, sending end voltage, and load power factor. Beyond P_{max}, no additional active power can be transferred. The voltage at P_{max}, referred to as the critical voltage V_{crit}, is the bus voltage at which instability will occur. The top half of the PV curve can be referred to as stable region and the bottom part as the unstable region.

PV curves are useful for conceptual analysis of voltage stability and for the study of radial system. Recently, this method has also been used for large meshed network where P is the total load in an area and V is the voltage at a critical or representative bus[6].

2.4.2 QV Curves

The procedure for obtaining the QV curves is similar to that for PV curves outlined above. QV curves can be obtained by plotting voltage at a bus against the reactive power at the same bus. In the QV curve, voltage V is on the X-axis and the reactive power Q on the Y-axis. For the different values of P shown in Figure 2.3(a), when increasing the reactive power Q, we can plot the QV curves shown in Figure 2.4. For large systems, the curves are obtained by a series of power flow simulations.

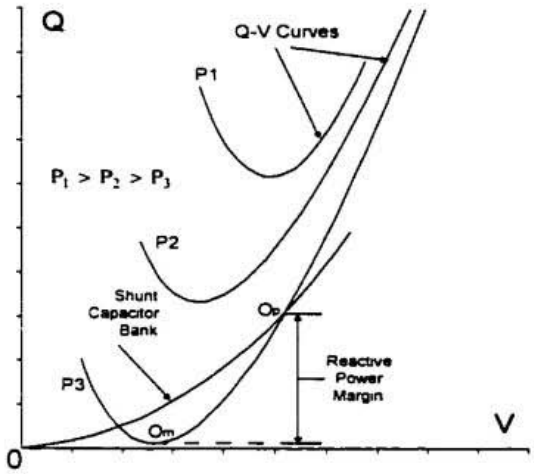

Figure 2.4 PQ curves for load buses

Q-V curves have several advantages:

- The characteristics of test bus shunt reactive compensation (capacitor, SVC, synchronous condenser, STATCOM [15], UPFC [16]) can be plotted directly on the QV curve. The operating point (O_p) is the intersection of QV curve and the reactive compensation characteristic. This is useful since reactive compensation is often a solution to voltage stability problems.
- Voltage security is closely related to reactive power, and a QV curve gives the reactive power margin at the test bus. The reactive power margin is the MVar distance from the operating point (O_p) to the bottom of the curve (O_m).

QV curves are used in many utilities. Since the method only artificially stresses a single bus without considering its influence to the whole systems, the conclusions should be confirmed by more realistic methods. Nowadays, this method has been expended to include the MVar at the whole system instead of only on particular bus.

2.4.3 Stability Margin

Stability margin (or loading margin) is an important concept in power systems. It is a measure of proximity to either: (i) a post-contingency loadability limit, or (ii) a secure operation limit.

> ***A margin*** to voltage collapse is defined as the largest load change that the power system may sustain at a bus or collective of buses from a well-defined operating point. It may be measured in MVA, MW, or MVar. Also, many effects influence the stability margin, such as reactive power limitation of generators, load changes, or equipment outage [1,3].

In a system shown in Figure 2.5(a), for example, a load is supplied through a small impedance transmission line, by a generator G_1 which is in turn connected through relatively large impedance transmission line to an infinite bus. Here, the generator and load are analogous to some local area of load and generation in an actual power system, while the infinite bus represents the remote generation or a neighboring utility.

Consider the first situation in which generator G_1 has unlimited reactive capability. If the load is increased, with active power increased on G_1 accordingly, PV curve 1 shown in Figure 2.5(b) is obtained and its stability margin is P_{max1}-P_0.

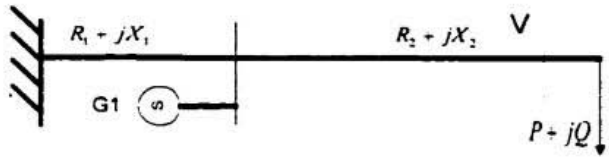

(a) A radial power system

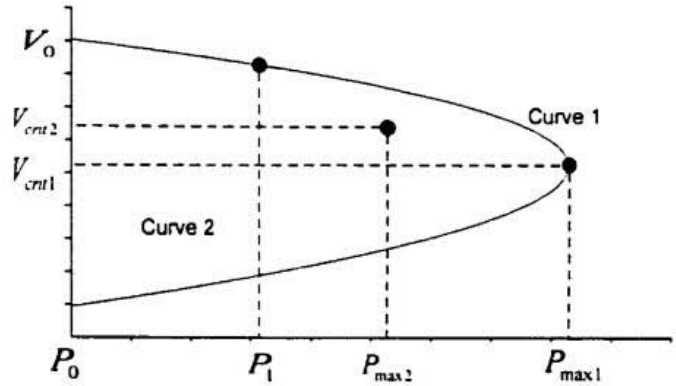

(b) PV curves for a radial system at different conditions

Figure 2.5 Illustration of stability margin [17]

In real life, however, generators do not have infinite reactive capability. Consider the second situation in which the reactive limit of G_1 is assumed to be Q_{Gmax}. If the load is once again increased from its initial value and the active power of G_1 is increased accordingly, the PV curve 2 in Figure 2.5(b) is obtained. It is seen that PV curve 2 follows the same trajectory as curve 1 until a certain active load P_1 at which G_1 hits its reactive power limit Q_{Gmax}.

From the above example, the stability margin of curve 1 is greater than that of curve 2 (i.e. $P_{max1}-P_0 > P_{max2} - P_0$). However, the critical voltage of curve 1 is smaller than that of curve 2 (i.e. $V_{crit1} < V_{crit2}$). Therefore, the margin is a good indicator of the proximity to voltage instability rather than voltage level.

Voltage Stability margin is the basic and widely accepted index to voltage collapse because it has following advantages:

(1) The margin is straightforward, well accepted and easily understood.

(2) The margin is an accurate index that takes full account of the power system non-linearity and limits such as reactive power limitation of generators.

However, it also has several disadvantages. One of them is that the calculation of margin is time consuming.

2.5 Voltage Stability Indices

Performance indices to predict proximity to voltage collapse problems have been of considerable interest to researchers and technical staff in power system operation, as these indices could be used on-line or off-line to help operators determine how 'close' the system is to collapse. The objective of these indices is to define a scalar magnitude that can be monitored as system parameters change. If this index exceeds a predefined threshold, the preventive or corrective control actions will be triggered. Therefore, these voltage stability indices should have a 'predictable' shape and be 'smooth', so that acceptable predictions may be made; furthermore, they should be computationally inexpensive, particularly for on-line system monitoring. Generally, these indices can be classified into two types: direct indices and indirect indices. The first are originally developed to compute the collapse point by solving the nonlinear power system equations to obtain the stability margin, while the second only use information at the operating

point. In this section, two widely used methods, continuation power flow and minimum singular value methods, will be introduced.

2.5.1 Continuation Power Flow (CPF) Method

There are many iterative methods available to solve load flow equations, such as Gauss-Seidel and Newton-Raphson methods [18]. Under a certain load increasing pattern, these methods can only calculate the upper portion of a PV curve until the power flow equations become singular and fail to be solved. In recent years, the continuation method has been used to obtain the power flow solution at any load level [19,20]. This enables the user to obtain the nose of the PV curve as well as the operating points (unstable) on the lower portion of the PV curve. This method has the following advantages:

(1) There is clear demarcation of limit.

(2) There is information regarding the "unstable" region of operation.

(3) It is possible to obtain the unstable equilibrium points (i.e. low voltage as well as normal operating voltage solution for a given load). These points form the basis for direct security assessment based on energy function methods, as well as other methods, for contingency screening and ranking.

In general, the continuation power flow analysis uses an iterative process involving predictor and corrector steps, as depicted in Figure 2.6. From a known initial solution (A), a tangent predictor is used to estimate the solution (B) for a specified pattern of load increase. The corrector step then determines the exact solution (C) using a

conventional power flow analysis with the system load assumed to be fixed. The voltages for a further increase in load are then predicted based on a new tangent predictor. If the new estimated load (D) is now beyond the maximum load on the exact solution, a corrector step with loads fixed would not converge; therefore, a correct step with a fixed voltage at the monitored bus is applied to find the exact solution (E). As the voltage stability limit is approached, the size of load increase has to be reduced gradually during the successive predictor steps to determine the exact maximum load.

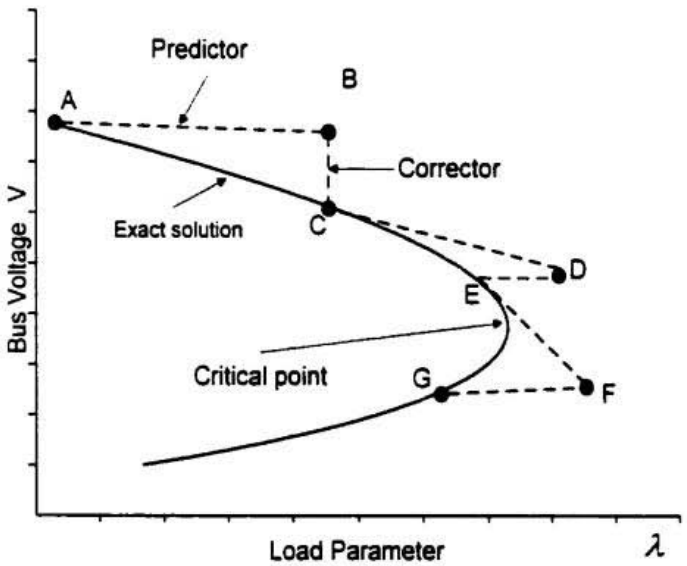

Figure 2.6 Illustration of continuation power flow method [1]

The behavior of a power system can be described by a set of differential equations of the form

$$\dot{x} = f(x, \lambda) \tag{2.6}$$

where

x : the n-vector of state variables (voltage magnitudes and angles at all the buses)

λ : a parameter used to represent the change in demand at all the buses.

For slow variation of the parameter, the power system can be modeled by a series of steady-state solutions to equation (2.6) obtained for different values of λ. These solutions are obtained by computing the equilibrium points given by the solution to the non-linear equation

$$f(x,\lambda) = 0 \tag{2.7}$$

In terms of the familiar power flow equations, the above set may be written as

$$\begin{aligned} P_{Gi}(\lambda) - P_{Li}(\lambda) &= \sum_{j\in} V_i V_j (G_{ij}\cos\theta_{ij} + B_{ij}\sin\theta_{ij}) \\ Q_{Gi}(\lambda) - Q_{Li}(\lambda) &= \sum_{j\in} V_i V_j (G_{ij}\sin\theta_{ij} - B_{ij}\cos\theta_{ij}) \end{aligned} \tag{2.8}$$

where

$$\begin{aligned} P_{Gi}(\lambda) &= P_{Gio}(1+\lambda K_{Gi}) \\ P_{Li}(\lambda) &= P_{Lio}(1+\lambda K_{Li}) \\ Q_{Li}(\lambda) &= Q_{Lio}(1+\lambda K_{Li}) \end{aligned} \tag{2.9}$$

P_{Lio}, Q_{Lio} are the active and reactive load at bus i, and P_{Gio} is the active generation at bus i in the base case.

Comparing the equations (2.7) and (2.8), it can be found that variables λ and x can be de-coupled or separated. Therefore, equation (2.7) can be rewritten more compactly as:

$$f(x,\lambda) = F(x) + \lambda b = 0 \tag{2.10}$$

The direction vector $\boldsymbol{b}$ represents the changes in real and reactive power demand and the changes in real power generation.

The continuation power flow is an iterative process, which is divided into two steps: predictor and corrector. In the predictor step, linear approximation is used to predict the next solution for a change in one of the state variables. This solution will be used as initial condition to the second step, the corrector step. Detailed description can be found in [1].

In order to obtain the voltage profiles at each bus and to assess the voltage collapse distance (stability margin), the real and reactive loads are increased in the load buses in proportion to the bus MVA, assuming constant power factor. The increased real power generations are picked up by all generators in the power systems also in proportion to the generator capability. The continuation power flow method is applied to a 5-bus and New England 39-bus power systems by using the commercial software *VSTAB* [17]. The voltage profiles of several load buses are shown in Figure 2.7 and Figure 2.8 respectively. From these figures, it is visible that both the stable branches and unstable branches of PV curves are obtained. When the loads increase at the extreme condition, all PV curves reach their collapse points at the same time. Details of the 5-bus and New England 39-bus power systems are given in Appendix A.

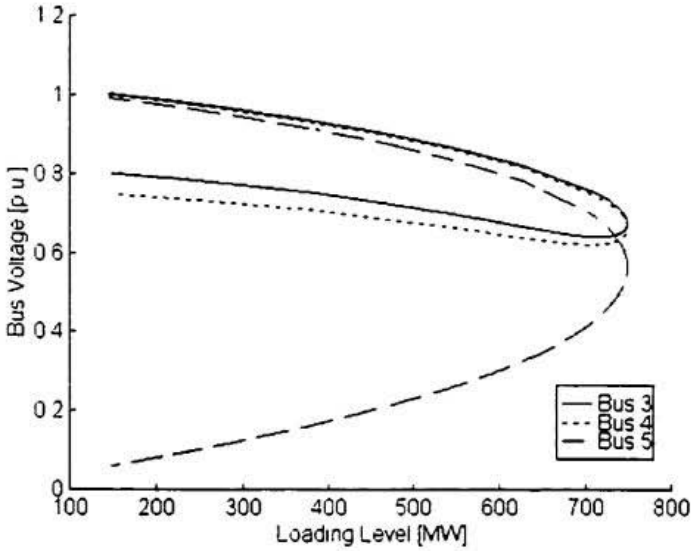

Figure 2.7 Voltage profiles at buses 3,4, and 5 for the 5-bus power system

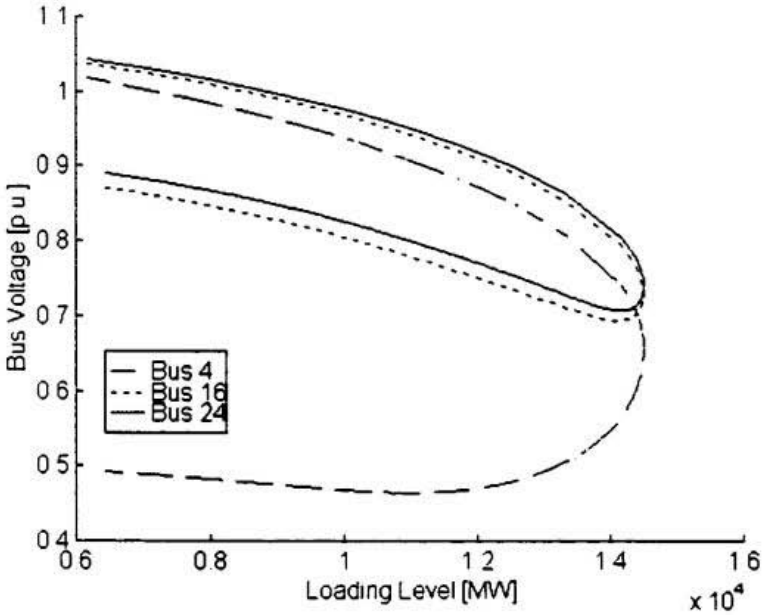

Figure 2.8 Voltage profiles at buses 4, 16 and 24 for the New England 39-bus power system

Even though CPF method can give accurate voltage profiles at each bus and the stability margin for a power system, it needs a lot of computing time. Thus, it is very difficult to use this method for on-line analysis. However, this method is widely used as a standard benchmark to check the accuracy of other methods.

2.5.2 Minimum Singular Value Method

The minimum singular value of power flow Jacobian matrix is an indirect index for voltage stability. When a power system operates close to collapse point, it is found that the Jacobian matrix of the power flow equation will become singular and the inverse of the Jacobian matrix will not exist. Based on the above phenomena, the minimum singular value method was proposed as an index for voltage stability [21].

For the power flow equation (2.7), the power flow Jacobian matrix can be written as:

$$J = \begin{bmatrix} \frac{\partial P}{\partial \delta} & \frac{\partial P}{\partial V} \\ \frac{\partial Q}{\partial \delta} & \frac{\partial Q}{\partial V} \end{bmatrix} \tag{2.11}$$

For this real n×n square Jacobian matrix at the equilibrium point (Z_0, λ_0) of equation (2.7), it can be written as:

$$J = R\Sigma S^T = \sum_{i=1}^{n} r_i \sigma_i s_i^T \tag{2.12}$$

Where the singular vectors r_i and s_i are the i^{th} columns of the orthonormal matrices R and S, and Σ is a diagonal matrix of positive real singular values σ_i, such that $\sigma_1 \geq \sigma_2 \geq \ldots \geq \sigma_n = \sigma_{min}$.

For instance, a given Jacobian matrix

$$J = \begin{bmatrix} 1 & 3 \\ 2 & 4 \end{bmatrix}$$

can be decomposed as:

$$J = \underbrace{\begin{bmatrix} 0.5760 & 0.8174 \\ 0.8174 & -0.5760 \end{bmatrix}}_{R} \times \underbrace{\begin{bmatrix} 5.4650 & 0 \\ 0 & 0.3660 \end{bmatrix}}_{\Sigma} \times \underbrace{\begin{bmatrix} 0.4046 & -0.9145 \\ 0.9145 & 0.4046 \end{bmatrix}^{T}}_{S^{T}}$$

where R is the left singular matrix, and S is the right singular matrix. The minimum singular value of this Jacobian matrix is equal to 0.3660.

When the Jacobian matrix becomes singular,

$$J = \begin{bmatrix} 1 & 3 \\ 2 & 6 \end{bmatrix}$$

it can be decomposed as:

$$J = \underbrace{\begin{bmatrix} 0.4472 & 0.8944 \\ 0.8944 & -0.4472 \end{bmatrix}}_{R} \times \underbrace{\begin{bmatrix} 7.0711 & 0 \\ 0 & 0.0000 \end{bmatrix}}_{\Sigma} \times \underbrace{\begin{bmatrix} 0.3162 & -0.9487 \\ 0.9487 & 0.3162 \end{bmatrix}^{T}}_{S^{T}}$$

The minimum singular value of Jacobian matrix becomes zero. Hence, the application of minimum singular value to voltage collapse analysis can be focused on monitoring the singular value up to the point when it become zero at collapse point.

In this chapter, the minimum singular value method is implemented by using MATLAB [22] program. After specifying the load and generation increasing patterns which are the same as those of section 2.5.1, simulation results for the power systems are

as shown in Table 2.1 and Table 2.2. From these tables, it is clear that when the loading levels increase, their minimum singular values of Jacobian matrixes will decrease.

Table 2.1 Minimum singular values and loading levels for the 5-bus system

Loading Levels (MW)	145	207	269	332	394
Minimum singular values	3.6856	3.5656	3.4271	3.2664	3.0787
Loading Levels (MW)	456	519	581	643	768
Minimum singular values	2.8571	2.5905	2.2601	1.8256	0.2500

Table 2.2 Minimum singular values and loading levels for the New England 39-bus system

Loading Levels (MW)	6150	6735	7319	7903	8488
Minimum singular values	0.6661	0.6569	0.6468	0.6355	0.6231
Loading Levels (MW)	9072	9656	10241	10825	11409
Minimum singular values	0.6092	0.5936	0.5758	0.5552	0.5308

Figure 2.9, and Figure 2.10 graphically show the relationship between the minimum singular values and loading levels. It can be seen that the minimum singular is a non-linear index. Further studies show that the magnitude of the minimum singular value is strongly affected by the dimension of the Jacobian matrix, the network structure, and the number of PV buses. Figure 2.11 shows the simulation results for a 63-bus power system as given in [23]. At heavy load condition, several generators reached their reactive power limits. When the reactive margin of generators vanishes, the buses connecting to these generators will change from PV buses (voltage controlled buses) to

PQ buses (load buses), while the dimension of the Jacobian matrix will increase. As a consequence, the magnitude of the minimum singular value decreases dramatically and has a high non-linear behavior. Therefore, the minimum singular value index is not a good indicator of an approaching voltage collapse.

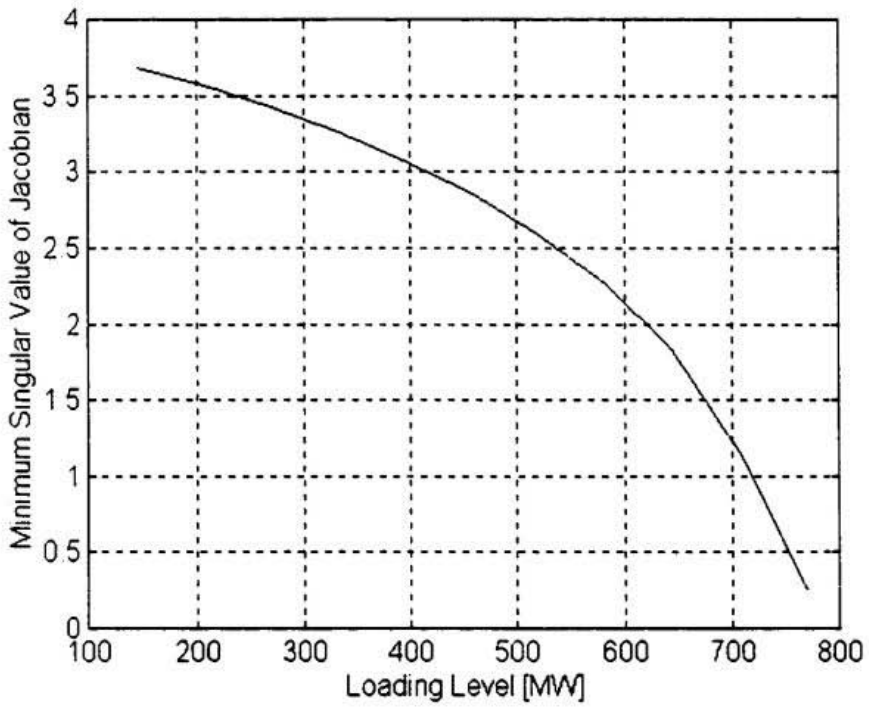

Figure 2.9 Minimum singular value index for the 5-bus power system

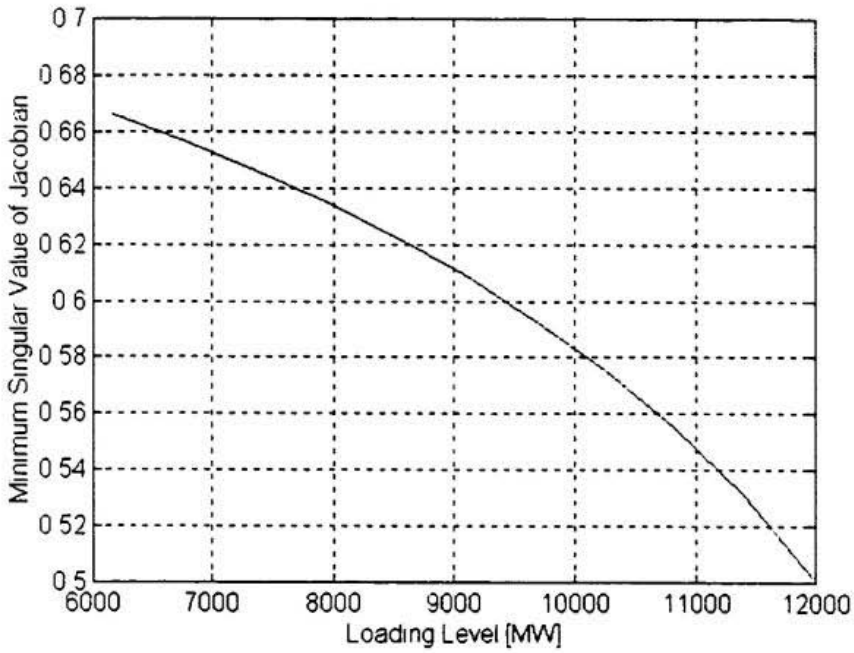

Figure 2.10 Minimum singular value index for the New England 39-bus power system

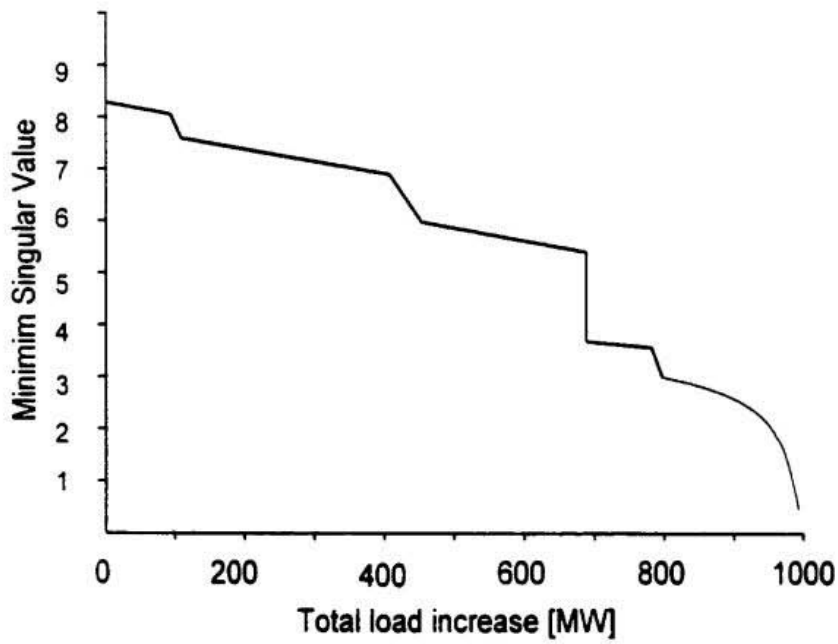

Figure 2.11 Minimum singular value index for a 63-bus power system [23]

2.6 Summary

This chapter has explained the general theory of voltage stability, followed by several concepts related to voltage stability, namely PV curves, QV curves, and stability margin. Two types of voltage stability analysis methods, Continuation Power Flow and Minimum Singular Value, are introduced. The simulation results for the two indices are also presented. The results show that the continuation power flow method can not only provide stability margin, but also give the voltage profiles of all buses in the system. The drawback of this method is that it is time consuming. Normally, this method is widely used as a benchmark to check the accuracy of other methods. Minimum Singular Value is another performance index to indicate how "close" the system is to its voltage collapse point. However, its magnitude is strongly affected by the dimension of Jacobian matrix, the network structure, and the number of PV buses. Thus, its performance is highly non-linear. This drawback affects its applications.

Chapter 3

Contingency Screening and Ranking Methods

3.1 Introduction

Currently, many utilities perform off-line studies to determine voltage stability margin and control actions necessary to ensure stability for a restricted set of system conditions. These results are then complied into a look-up table for use by the system operators. This approach has many drawbacks such as significant amount of off-line analysis, limited number of considered operating conditions, and limited number of considered contingencies. In light of the importance of voltage stability to system performance and the shortcomings of the off-line methods, there exists a strong need for on-line voltage stability assessment method. Translating the available off-line voltage stability assessment tools for on-line use provides many challenges.

An important function in voltage stability assessment tools is contingency screening and ranking. Its objective is to quickly and accurately select a short list of critical contingencies from a large list of potential contingencies and rank them according to their severity. Suitable preventive control actions can be implemented considering contingencies that are likely to affect the power system performance [24,25]. Recently,

many fast algorithms suitable for on-line contingency screening and ranking have been proposed [4,5,26].

In this chapter, power system operating states and voltage stability assessment environment will be introduced. Then many existing contingency screening and ranking methods will be presented. The advantages and limitations of these methods will be described as well.

3.2 Operating States

Power system operation is subjected to two sets of constraints: i) the load constraints, which express that the load demand is met by the system; and ii) the operating constraints, which impose minimum or maximum limits on variables associated with the system components [1].

If both the load and the operating constraints are satisfied, the system is said to be in a normal operating state. On the occurrence of disturbance, the system may either settle down to a new normal state or it may enter other states. The system operating conditions can be classified into five states: *normal, alert, emergency, in extremis*, and *restorative*. Figure 3.1 depicts these operating states and the ways in which transition can take place from one state to another.

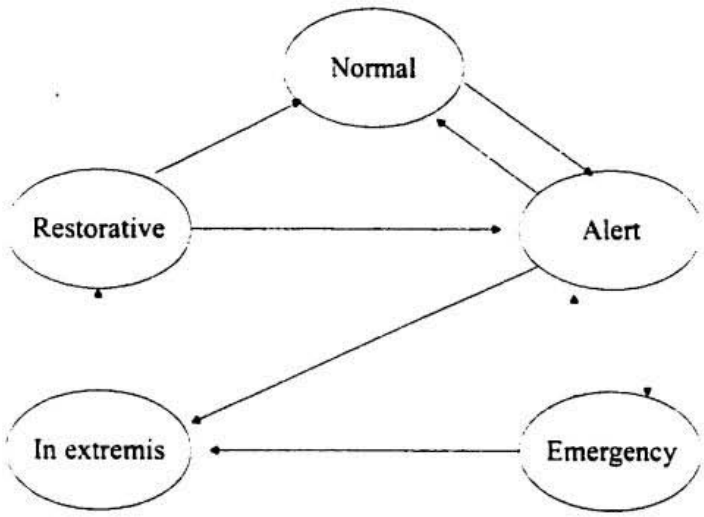

Figure 3.1 Power system operating states [1]

In the *normal state*, all system variables are within the normal range and no equipment is being overloaded. The system operates in a secure manner and is able to withstand a contingency without violating any of the constraints.

The system enters the *alert state* if the security level falls below a certain limit of adequacy, or if the possibility of disturbance increases. In this state, all system variables are within the acceptable range and all constraints are satisfied. However, the system has been weakened to a level where a contingency may cause an overloading of equipment that places the system in an emergency state. If the disturbance is very severe, the *in extremis* (or extreme emergency) state may result directly from the alert state.

The system enters the *emergency state* if a sufficiently severe disturbance occurs when the system is in the alert state. In this state, voltages at many buses are low and/or equipment loading exceeds short-term emergency ratings. The system is still intact and may be restored to the alert state by the initiating of emergency control actions.

If the protective actions are ineffective, the system is *in extremis*. The result is cascading outages and possibly a shut-down of a major portion of the system. Control actions, such as load shedding [24], are aimed at saving as much of the system as possible from a widespread blackout.

The *restorative state* represents a condition in which control action is being taken to reconnect all the facilities and to restore system load. The system transits from this state to either the alert state or normal state, depending on system conditions.

Characterization of the system conditions into five states, as described above, provides a framework in which control strategies can be developed and operator actions identified to deal effectively with each state.

Voltage instability may develop from a few seconds (short-term) to several minutes or longer (long-term). Both are usually considered too fast to be corrected by system operators, and hence corrective actions are implemented through automatic controls. However, the time taken by the long-term instability to develop, while short for a human operator, would be ample for a computer executing efficient software to identify the problem, warn the operator and suggest or trigger corrective actions. Voltage Stability Assessment, based on on-line system analysis and adapting its decision to disturbance of concern, has been investigated with great interest.

3.3 Voltage Stability Assessment

Voltage stability has become one of the most important and urgent problems in modern bulk power supply systems due to the significant number of serious failures believed to have been caused by this phenomenon [1,3]. For many utilities, planning and

operating studies indicate that voltage stability is a limiting operating criterion. It is therefore necessary to develop Voltage Stability Assessment (VSA) tools in today's Energy Management Systems (EMS) for on-line power system voltage stability analysis.

Recently, some possible schemes for on-line voltage stability assessment (VSA) have been proposed [4]. Figure 3.2 shows an overview of the voltage stability assessment environment as discussed in [4]. The VSA environment receives its input from a real time database. This input consists of the current state of power system as determined by a state estimator. In addition, other inputs to VSA include pertinent data required for voltage stability analysis, including all the models of devices and controls.

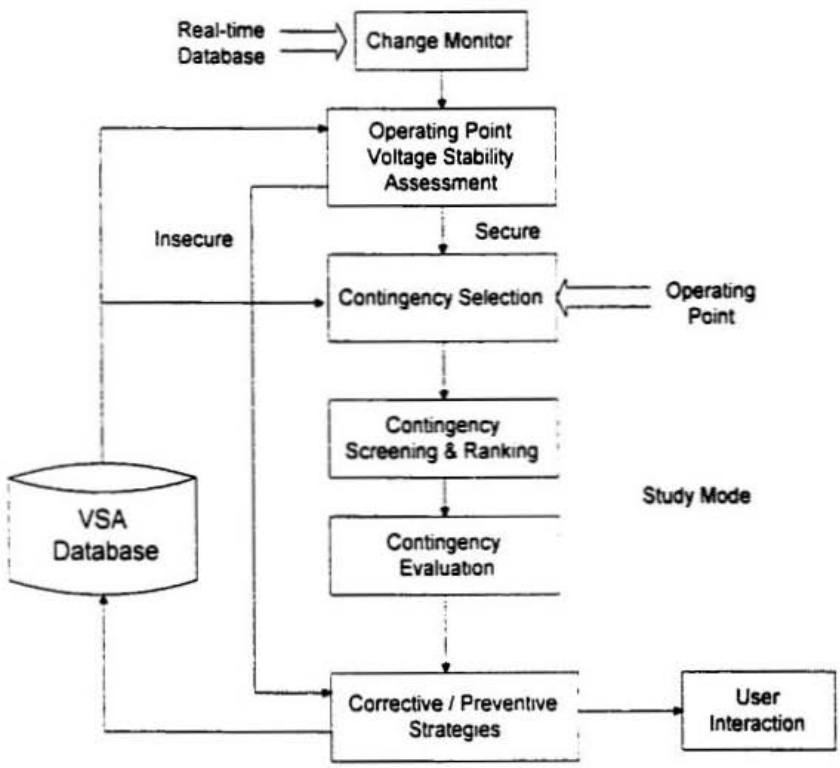

Figure 3.2 Functional representation of VSA environment [4]

The first task within the VSA environment is the assessment of security of current operating point from the voltage stability point of view. This assessment identifies whether the operating point is secure or not. If a credible contingency would cause violation of voltage stability criteria, the system will be deemed voltage insecure. Depending on this outcome, analysis should proceed with the determination of an appropriate corrective strategy, in the insecure case, or to the study mode, in the secure case. The objective of the study mode is to determine from a large set of potential contingencies those that may lead to voltage stability problems. Contingency screening and ranking is an important part of the study mode. The large list of selected contingencies is screened and ranked using fast ranking algorithms. For those contingencies which are likely to be harmful, preventive and corrective strategies (reactive power control, or load shedding) may be developed in terms of control actions to be executed in either a pre-contingency, or post contingency mode [1,20,21]. Preventive control actions move the system state to a voltage secure operating point. Corrective control actions would maintain voltage stability of the system in case severe or unforeseen contingencies happen. Thus, it can be seen that the overall aim of the voltage stability assessment environment is to increase the security of the power system at any given condition.

3.4 Methods for Contingency Screening and Ranking

Obviously, if one were to consider all possible disturbances, it would be impossible to find a secure power system. In practice, system security is checked with reference to a set of credible disturbances, i.e. disturbances with a reasonable probability

of occurrence, referred to as contingencies. A contingency can consist of one or more events occurring simultaneously or at different instants of time, with each event resulting in a change in the state of one or more power system elements. It may be initiated by a small disturbance, a fault, or a switching action. Normally, the following types of switching action should be supported in the definition of a contingency:

1) Breaker opening/closing

2) Shunt capacitor/reactive insertion and/or removal

3) Generator tripping

4) Load shedding

5) Transformer tap changing

6) FACTS device connectivity and operation

7) Automatic transfer tripping (armed remedial action)

However, it is impractical and unnecessary to analyze in detail the impact of every conceivable system contingency. Because of interconnections of power systems, systems are becoming larger and larger. If all contingencies are studied in detail, it will take a long time for calculation. This is intolerant for on-line voltage stability assessment. Further, most contingencies are not severe. Only a limited number of contingencies may impact the security of power system immediately [5]. Hence, only these contingencies will be of immediate concern and must be assessed. Therefore, it is desirable to be able to screen the contingencies such that a list of those most likely to cause problems can be assessed in detail. These contingencies should be ranked according to their expected impact.

As stated in chapter 2, by directly solving non-linear power flow equations for different contingency cases, one can obtain their collapse points and rank them according to their stability margins. This method is accurate, but only suitable for off-line studies rather than for on-line. In order to develop on-line voltage stability tools, many on-line contingency screening and ranking methods are proposed [4,5,6]. Several of them are discussed below.

3.4.1 Multiple Load Flow Method (MLF) [27]

In order to rank contingencies, a method called Multiple Load Flow Method (MLF) was proposed [27]. MLF can compute an approximate margin by using voltage gradients determined at a Stable Equilibrium Point (SEP) of the voltage V versus load λ curve, and at the corresponding Unstable Equilibrium Point (UEP), as shown in Figure 3.3. The margin obtained by MLF is a first order approximation of voltage stability margin; however, since only the relative order of contingencies is of interest for contingency screening and ranking, it is not necessary to predict the actual voltage collapse point. Point C in Figure 3.3 is sufficient to permit the ranking of contingencies for comparison with the ranking produced by the reference method, the continuation-based power flow.

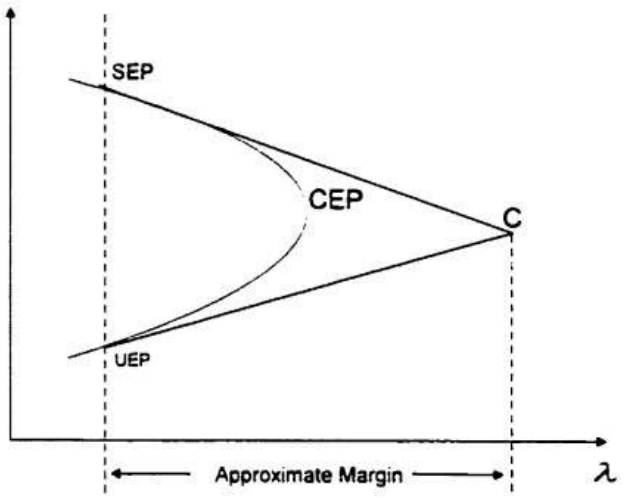

Figure 3.3 Illustration of multiple load flow method

The sensitivity of the bus voltage magnitude at bus ***i*** with respect to system load change is given by

$$\frac{\partial V_i}{\partial \lambda} = \sum_{j \in N} \left(\frac{\partial V_i}{\partial P_j} \frac{\partial P_j}{\partial \lambda} + \frac{\partial V_i}{\partial Q_j} \frac{\partial Q_j}{\partial \lambda} \right) \tag{3.1}$$

where

V_i is the voltage at bus ***i***

P_i is the MW injection at bus ***i***

Q_i is the Mvar injection at bus ***i***

λ is the load change parameter

N is the number of buses

Let ***b*** be the vector defining the direction of change of the system load, such that

$$\frac{\partial P_i}{\partial \lambda} = b_{2*i-1} \quad \text{and} \quad \frac{\partial Q_i}{\partial \lambda} = b_{2*i}$$

and $\partial V_i/\partial P_j$ and $\partial V_i/\partial Q_j$ elements of the inverse Jacobian matrix. Let $m_i^{sep} = \partial V_i^{sep}/\partial \lambda$ be the voltage sensitivity at bus i computed at the SEP, and $m_i^{uep} = \partial V_i^{uep}/\partial \lambda$ be the voltage sensitivity at bus i computed at the UEP, then the equations of the tangents to the curve V versus λ can be computed. From these the Δλ change between the current operating point and the point of intersection of the tangents is given by

$$\Delta\lambda = \frac{V_i^{sep} - V_i^{uep}}{m_i^{uep} - m_i^{sep}} \tag{3.2}$$

The basis of the above method is that there exist two close load flow solutions in heavily loaded power systems. One is the higher voltage (SEP) solution; the other is the lower voltage (UEP) solution.

Multiple Load Flow Method has been reliable in finding the low voltage solutions and more robust than merely starting the power flow with the load bus of interest at some extremely depressed voltage magnitude. However, because MLF method uses first order approximation, its results are not accurate according to reference [4].

3.4.2 Test function method

The test function method is used for the estimation of the critical value of the load parameter λ*. The basic idea of the method is to use a test function t(x, λ) to determine the existence of collapse points bounded by two solutions (x1, λ1) and (x2, λ2) [4]. The test function is defined as

$$t(x,\lambda) = e_i^t J(x,\lambda) v \tag{3.3}$$

where

e_l is the l-unit vector of order n

J is the Jacobian matrix of the system equation (2.8)

v is obtained from the solution to

$$J_{lk} v = e_l \tag{3.4}$$

with J_{lk} defined by

$$J_{lk} = (I - e_l e_l^T) J + e_l e_k^T \tag{3.4}$$

It can be shown that the proposed test function has a value of zero at the collapse point λ^*. This is equivalent to singularity of the Jacobian matrix at the same point.

Using the proposed test function, the authors of [26] computed approximations to the critical values of the load parameter λ^*, as follows

$$\lambda^* = \lambda_1 - \frac{1}{2} \frac{t(x_1, \lambda_1)}{t'(x_1, \lambda_1)} \tag{3.5}$$

for a quadratic (second order) approximation, and,

$$\lambda^* = \lambda_1 - \frac{1}{4} \frac{t(x_1, \lambda_1)}{t'(x_1, \lambda_1)} \tag{3.6}$$

for a quartic (fourth order) approximation.

In the above formulae the derivative t' is computed by using a small perturbation to the parameter λ.

However, test results obtained in reference [4] have shown that the accuracy of this method is not very satisfactory.

3.4.3 V-Q Curve Fitting Method (VQF) [4]

The method in reference [4] is another fast but approximate method for the computation of limit to collapse based on power flow and curve fitting. This method, however, is only applicable to the computation of a reactive power limit to voltage collapse. It determines the limit from the V-Q curve obtained for a particular bus in power system with respect to reactive power changes at that bus.

The basic idea of the method is to use three known points in the V-Q curve and to fit an appropriate curve by the three points. In the experiments reported in [4], a cubic spline was used. The three points used are shown in Figure 3.4. Point P_1 corresponds to the base case condition obtained from the state estimator. Point P_2 is the origin of the coordinate system (0,0), while point P_3 is obtained from a power flow solution with the bus of interest treated as a PV bus with a selected voltage magnitude (say 0.9 per unit). The value of reactive power Q (MVar) obtained at the bus, together with the chosen voltage magnitude, comprise the third point. Given these points the spline can be easily computed. The value of voltage magnitude for which the reactive power is a maximum is then determined, and thus the estimated margin can be computed.

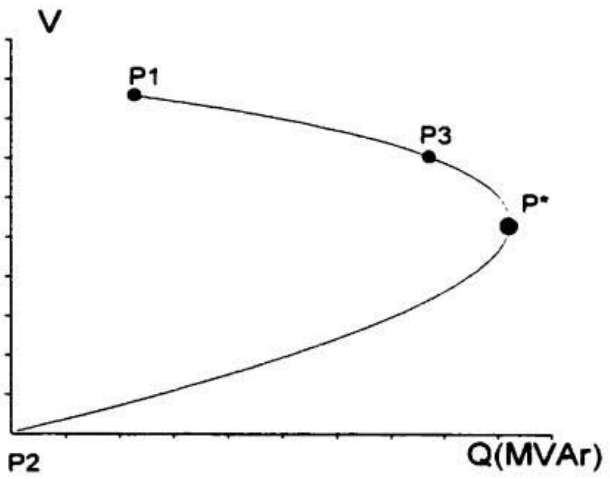

Figure 3.4 Illustration of V-Q curve fitting method

However, the main disadvantage of this method is that the reactive load change is applied only at a single bus, which is not realistic.

3.4.4. Generalized Curve Fit (GCF) [4]

To overcome the disadvantage of the VQF method, reference [4] introduced another approximation method, Generalized Curve Fit (GCF) method, to calculate the nose of PV curve.

The method to compute the stable branch and to get an approximation to the collapse point is obtained by using the curve fitting technique. In general, the stable branch may be approximated by a polynomial of degree *n* of the form

$$\lambda = a_n x^n + \cdots + a_1 x + a_0 \tag{3.7}$$

where the pairs (x,λ) are solutions of equation (2.7) on stable branch. From Figure 3.5, it is clear that the stable branch of the Voltage versus Power curve can be approximated by

a second order polynomial. To fit the desired polynomial, it is sufficient to determine three stable equilibrium points on the curve. One of these points is a given stable equilibrium point obtained from a state estimation solution and denoted by $(x^{(1)}, \lambda^{(1)})$. Two other points can then be computed by increasing the demand λ such that $\lambda^{(3)} > \lambda^{(2)} > \lambda^{(1)}$. The points corresponding to $(x^{(2)}, \lambda^{(2)})$ and $(x^{(3)}, \lambda^{(3)})$ can be obtained using two steps of the continuation power flow.

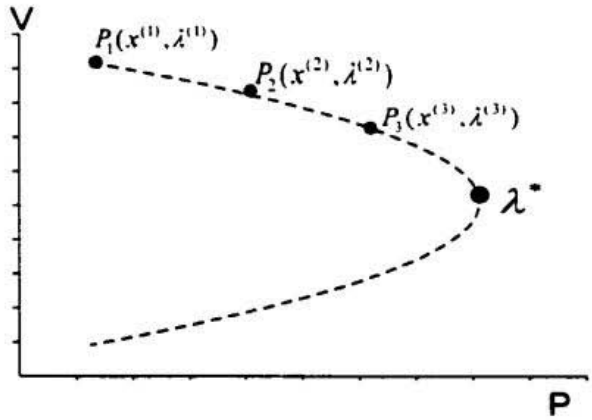

Figure 3.5 Illustration of generalized curve fitting method [4]

The three points $(x^{(1)}, \lambda^{(1)})$, $(x^{(2)}, \lambda^{(2)})$, and $(x^{(3)}, \lambda^{(3)})$ are then used to fit the approximate stable branch

$$\lambda_i = a_{1i} x_i^2 + a_{2i} x_i + a_{3i} \tag{3.8}$$

After the constants a_1, a_2, and a_3 are computed, the voltage collapse index (the load demand limit) λ^* is given by

$$\lambda^* = \left(\sum_{i=1}^{n_c} \lambda_i^* \right) \Big/ n_c \tag{3.9}$$

where

$$\lambda_i^* = -\frac{a_{2i}^2}{4a_{1i}} + a_{3i} \tag{3.10}$$

and n_c is the number of buses where load is changed.

Although the method in this paper gives very accurate ranking for contingencies, the actual margins calculated have relatively noticeable errors. The inaccuracy of this method is that it uses only three points to calculate the collapse point, λ^*, which is out of the range between λ_1 and λ_2. The farther the distance beween the collapse point and λ_3, the bigger the error will be. Therefore, the method is also highly dependent on the location of the three selected points.

3.4.5. Look-ahead Voltage Method [6]

In reference [6], the authors proved that the power flow equations could be expressed as a quadratic function only at the collapse point of a power system. Then, based on this theory, this paper introduced a new curve fitting method by using only two points on the stable branch of the power system solution and the derivative of the second point.

Starting from a power flow solution, say x_1 with the corresponding load level λ_1, the authors calculated another operating point x_2 corresponding to a higher load level λ_2 ($\lambda_2 > \lambda_1$) and its derivative $\dot{x}_2$ with respect to the parameter λ_2. Then, the authors selected the load bus whose drop in voltage magnitude is the largest to be the curve fitting bus. That is, they defined

$$\Delta V_i = \frac{(V_i|_{\lambda=\lambda_1} - V_i|_{\lambda=\lambda_2})}{V_i|_{\lambda=\lambda_1}} \tag{3.11}$$

and chose the maximum value ΔV_i among $\{\Delta V_1, \Delta V_2, \cdots, \Delta V_n\}$. Then the $\lambda - V$ curve of i-th load bus was chosen to derive the load margin. The equation $\lambda = \alpha + \beta V_{i,1} + \gamma V_{i,1}^2$ was used to approximate the $\lambda - V$ curve. After substituting the two points $(V_{i,1}, \lambda_1)$ and $(V_{i,2}, \lambda_2)$, and the derivative $\dot{V}_{i,2}$ at the second point, the authors obtained the values for parameter α, β, and γ from the following equations:

$$\begin{aligned} \lambda_1 &= \alpha + \beta V_{i,1} + \gamma V_{i,1}^2 \\ \lambda_2 &= \alpha + \beta V_{i,2} + \gamma V_{i,2}^2 \\ 1 &= \beta \dot{V}_{i,2} + 2\gamma \dot{V}_{i,2} V_{i,2} \end{aligned} \tag{3.12}$$

Therefore, the difference between the operation point and the collapse point is given by:

$$\overline{\lambda}_{V_{max}} = \alpha - \frac{\beta^2}{4\gamma} \tag{3.13}$$

Moreover, to get a more accurate performance index, this paper also gives a correction. That is, if the selected load bus, whose drop in voltage magnitude is the largest, also has a significant change in angle magnitude, then the performance index can be expressed as

$$\overline{\lambda}_{max} = 0.5(\overline{\lambda}_{V_{max}} + \overline{\lambda}_{\theta_{max}}) \tag{3.14}$$

In the paper, according to the testing results on 39-bus and 1169-bus systems, the errors are very small (<5%). This performance index does work very well.

Unfortunately, there is no method provided to calculate the derivative of the second point. Also, the authors choose the second point, which is placed as far from the

first point as possible. When the second point is located near the collapse point, the result is much more accurate. Otherwise, this performance index will give a larger mismatch. However, in practice, when the second point is being selected, it is very difficult to tell whether this point is near the collapse point or not. If the second point, which is very close to the collapse point, can be obtained beforehand, the stability margin of the power system can be determined immediately without calculating that performance index. This is the main disadvantage of this method.

3.4.6. Reactive Support Index (RSI) and Iterative Filtering [5]

In order to obtain a full-function on-line voltage stability method, BC Hydro proposed two new methods, Reactive Support Index (RSI) and Iterative Filtering, for contingency screening and ranking according to their severity.

Reactive support index

Reactive Support Index (RSI) evolved from the severity indices based on Generalized Curve Fit (GCF) [4] as well as an earlier method developed at B.C Hydro called Reactive Compensation Index (RCI). The RCI method is based on the premise that the distance between the normal case (pre-contingency) nose and the contingency case nose can be approximated by the total reactive injection required at the load buses to establish similar voltage levels for both cases. This method has the following five steps: (1) Obtain a pre-contingency power flow nose (normal case nose) or a very stressed case close to it. (2) Add artificial synchronous condensers at the load buses with settings equal to the load bus voltage value, while the bus voltage angles will be determined. (3) Apply

a certain contingency (say contingency i). (4) Solve the load flow and establish the reactive output of the artificial condensers. (5) Using the artificial condensers' output, calculate the RCI defined as:

$$RCI_i = \sum_{j=1}^{l} m_j \cdot Q_{ji}^n \tag{3.15}$$

where RCI_i is the relative RCI index for contingency i, Q_{ij}^n is the reactive power generation at the artificial dynamic Var resource added at the load bus j, l is the total number of the load buses and m_j is the weighting factor for the Var resource at load bus j.

RCI was later extended by another similar method called Reactive Support Index (RSI), which proved to have a better performance (accuracy, speed, and implementation ease) than RCI.

Unlike the RCI index, which needed artificial reactive sources at load buses, the Reactive Support Index is defined as the extra amount of reactive generation from all the existing dynamic Var devices (generation, SVC, etc.). To establish the extra reactive generation, the reactive limits at the dynamic Var devices are ignored. The RSI has four steps: (1) Obtain a base-case reflecting the nose of the normal case or a very stressed case to the nose. (2) Implement a certain contingency (Steps 1 and 2 are the same as that of RCI). (3) Solve the power flow equation with the dynamic reactive devices limits open. (4) Using the solved power flow solution, calculate the RSI defined as:

$$RSI_i = \sum_{j=1}^{\kappa} [m_j (Q_j^{no} - Q_{ji}^{no})^n] \tag{3.16}$$

where RSI_i is the relative RSI index for contingency i, Q_j^{no} and Q_{ji}^{no} are the reactive generation of *j-th* dynamic Var device in the pre-contingency case and after contingency i

with open reactive limits respectively, g is the total number of the dynamic Var resource, m_j is the weighting factor for the j-th dynamic Var resource and p is a factor reflecting the order of the index for removing the masking effect. According to the experience of BC Hydro, the best result can be obtained when p is set to be 1.

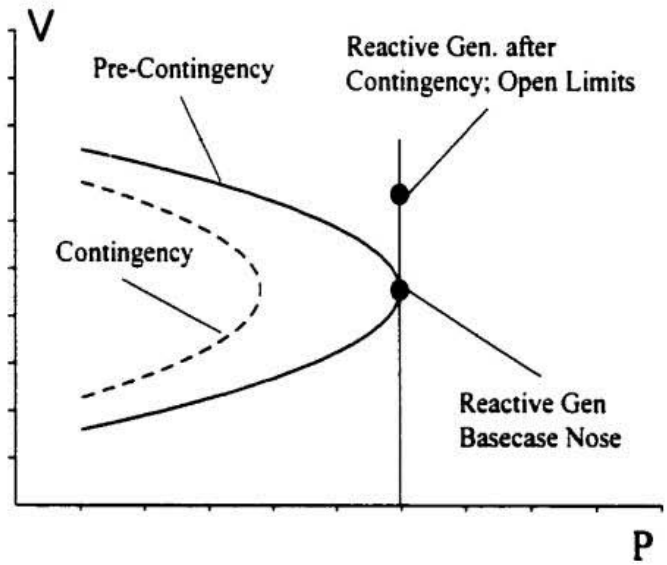

Figure 3.6 Illustration of reactive support index

The RSI method was used to screen and rank the contingencies for the BC Hydro system, which has 1398 buses and 2295 branches, as well as another major utility, which has 1643 buses and 2299 branches. The result shows that RSI method can closely follow the pattern of exact margin which is calculated by a repetitive load flow method. However, this method also misclassifies some contingencies: out of the most critical contingencies, RSI misclassifies 6 for the 1643-bus system. The misclassification is unacceptable if those severe contingencies are removed from the contingency short list.

Iterative Filtering

Figure 3.7 shows a series of Q-V curves for post-contingency system relative to the Q-V curve representing the base-case with no outage. The closer the nose of post-contingency Q-V curve to that of pre-contingency curve, the less severe the contingency, and vice versa. Based on this fact, the Q-V curve can be arbitrarily divided into several segments of Very Mild, Mild, High, and Very High indicating the degree of severity.

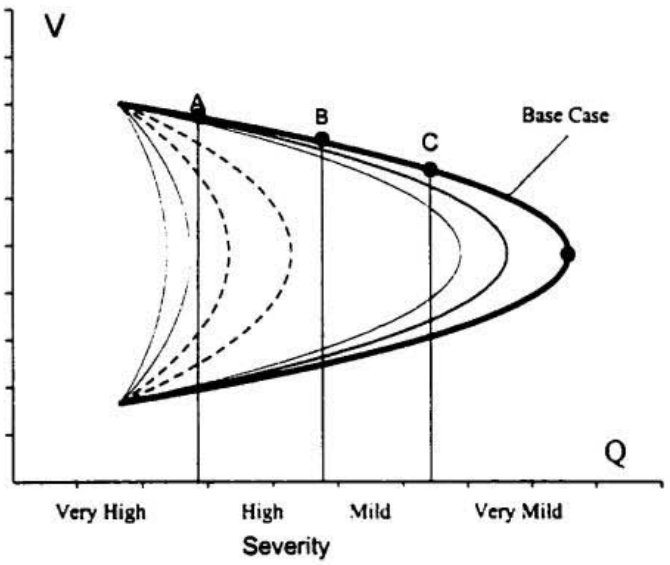

Figure 3.7 Illustration of iterative filtering

At a particular stressed load (say point C), only the load flows with Very Mild contingencies will be solved; others cannot be solved. If the load is decreased to point B, among the unsolved cases, only the Mild contingencies can be solved and so on. Therefore, for a given stressed base case, it is possible for the method to filter out a specified number N which is the most critical of all the contingencies. Theoretically, if

the QV curve is divided into very small segments, this method can precisely rank the contingencies without any error.

According to reference [5], when the iterative filtering and RSI methods are combined together, it gives very accurate ranking results for all selected contingencies.

3.5 Summary

In this chapter, power system operating states and on-line voltage stability assessment (VSA) environment are introduced. Contingency Screening and Ranking (CS&R) plays an important part in VSA. To meet the need for on-line voltage stability assessment tools, many fast algorithms for CS&R have been proposed. Several of them have been discussed in this chapter.

Simulation results for few of the selected methods on different power systems will be presented in the next chapter.

Chapter 4

Simulation Results for Contingency Screening and Ranking

4.1 Introduction

In this chapter, three methods, Continuation Power Flow (CPF), Reactive Support Index (RSI), and Generalized Curve Fit (GCF), are applied to sample power systems. CPF is an accurate method of solving load flow equations and thus obtaining the voltage collapse point, while RSI and GCF methods are two fast ranking algorithms suitable for on-line Contingency Screening and Ranking (CS&R).

The simulation results presented in this chapter are based on a 5-bus, New England 39-bus, IEEE 118-bus, IEEE 300-bus, as well as a 600-bus, BC Hydro 197-bus, and Ontario Hydro 1254-bus power systems. The study can be divided into three parts. The first part will present the ranking results obtained by the CPF method. The second part of the work will calculate the RSI results for 5-bus, 118-bus and 600-bus power systems. The RSI ranking results will also be compared with the accurate ones which are

obtained by CPF. The third part will deal with GCF ranking results. The accuracy of GCF will be compared with CPF as well.

Among these methods, CPF was implemented by *VSTAB* software [17] developed by Powertech Labs Inc. All other programs were written in *MATLAB* [22] by the author.

4.2 Continuation Power Flow Results for Contingency Screening and Ranking

Figure 4.1 shows the single line diagram of a 5-bus power system. The test system has two generators and 7 transmission lines. Bus 1 is the swing bus; bus 2 is a PV bus; and buses 3, 4, and 5 are all PQ buses. The transmission line impedances and line charging admittances in per unit on 100MVA base are given in Table 4.1. The scheduled generation, load, and desired bus voltages are given in Table 4.2.

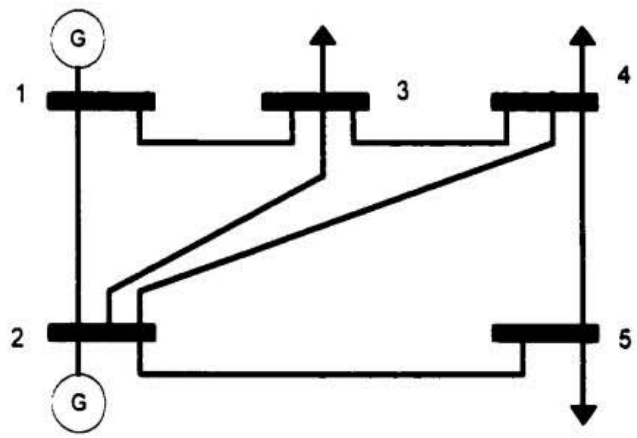

Figure 4.1 Single line diagram of the 5-bus system

Table 4.1 Impedances and line charging for the 5-bus system

Line Number	Bus From To	Line impedance (p.u)	Line charging (p.u)
1	1 - 2	0.02 + j 0.06	0.0 + j 0.030
2	1 - 3	0.08 + j 0.24	0.0 + j 0.025
3	2 - 3	0.06 + j 0.18	0.0 + j 0.020
4	2 - 4	0.06 + j 0.18	0.0 + j 0.020
5	2 - 5	0.04 + j 0.12	0.0 + j 0.015
6	3 - 4	0.01 + j 0.03	0.0 + j 0.010
7	4 - 5	0.08 + j 0.24	0.0 + j 0.025

Table 4.2 Scheduled generation, loads, and desired bus voltage for the 5-bus system

Bus number	Desired bus voltage (p.u)	Generation		Load	
		Megawatts	Megavars	Megawatts	Megavars
1	1.06∠0	109	55.27	0	0
2	1.0	40	-41.24	0	0
3	--	0	0	45	15
4	--	0	0	40	5
5	--	0	0	60	10

To obtain PV curves, the load at each bus is increased proportionally to its MVA, and the generation is also picked up by all generators proportionally to their capabilities. After applying the CPF method to the 5-bus system by using *VSTAB*, the PV curve of the pre-contingency case at a certain bus can be obtained. For this system, the total system load at the base case operating condition is 145.00 MW at which the line outages are assumed to occur. The maximum load can reach 748.34 MW, beyond which no power

flow solution exists. Hence, the margin for the pre-contingency case is 748.34 – 145.00 = 643.34 MW.

Keeping the load increase pattern and generation dispatch scheme as before, if one transmission line among these seven is out of service independently, the PV curves at a certain bus can be obtained by using the CPF method.

Figure 4.2 and Figure 4.3 show PV curves at bus 5 for both pre-contingency and different line outage contingencies by using the CPF method. It is visible that when line 1 or line 6 is out of service, their margins only decrease a little bit; however, if line 5 is disconnected, the margin decreases dramatically.

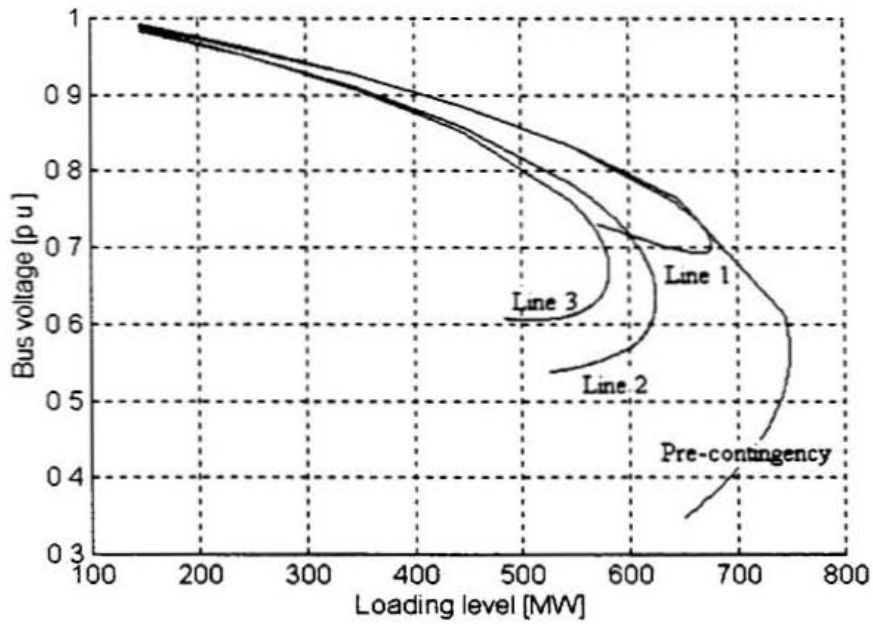

Figure 4.2 PV curves for both pre-contingency and line 1,2,and 3 outages at bus 5 for the 5-bus power system

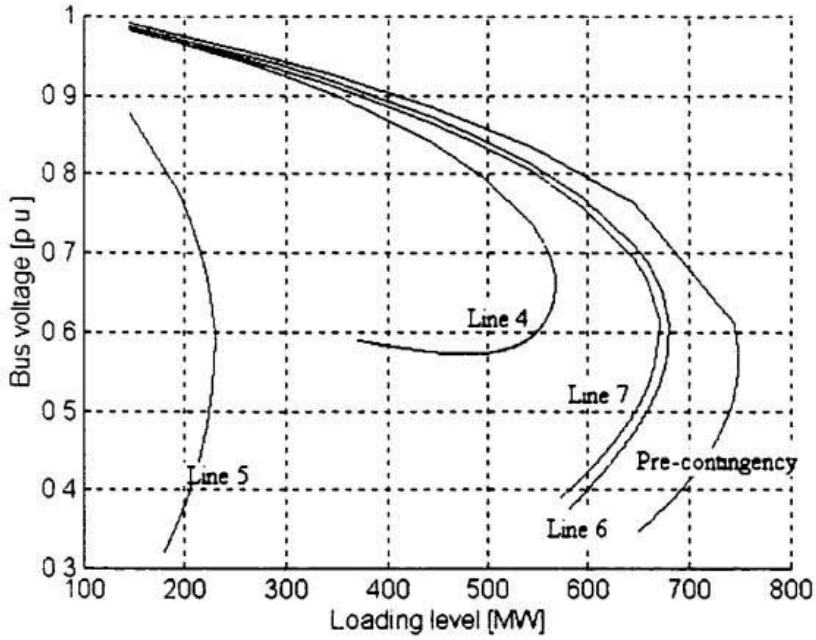

Figure 4.3 PV curves for both pre-contingency and line 4, 5, 6, and 7 outages at bus 5 for the 5-bus power system

Table 4.3 gives the simulation results, which shows the voltage collapse points, margins, and ranks based on their margins for each branch outage contingency for the 5-bus system. Figure 4.4 is a bar chart showing the margins of each line outage contingency. It is evident that when line 5 is disconnected, the loading margin decreases from 643.34 MW to 85.64 MW; while with line 6 out of service, the loading margin only decreases from 643.34MW to 535.64MW. Thus, the outage of line 5 is the most severe contingency for which the post-contingency voltage stability margin is the lowest. Similarly, the loading margins of each branch outage contingency for other systems can be obtained by using the CPF method.

Table 4.3 Voltage collapse points, margins, and ranking results for each line outage contingency in the 5-bus power system

Line Number	Bus From To	Collapse points [MW]	Margins [MW]	Rank
1	1 – 2	676.19	531.19	6
2	1 – 3	624.36	479.36	4
3	2 – 3	580.89	435.98	3
4	2 – 4	567.80	422.80	2
5	2 – 5	230.64	85.64	1
6	3 – 4	680.64	535.64	7
7	4 – 5	671.03	526.03	5

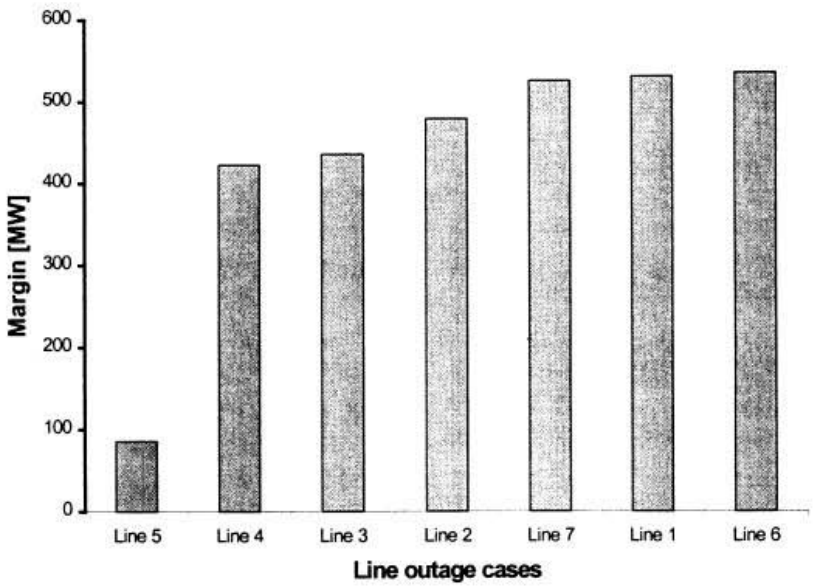

Figure 4.4 Line outage contingencies and their margins

The CPF method is a very accurate method to calculate the collapse points. The results obtained by the CPF method can generally be used to check the accuracy of other methods for continency screening and ranking.

4.3 Simulation Results of Reactive Support Index (RSI)

As discussed in section 3.4.6, Reactive Support Index is a fast ranking algorithm, which has been proposed recently for contingency screening and ranking. It is defined as the extra amount of reactive generation from all the existing dynamic *Var* devices (generation, SVC, etc.). In the following sections, the RSI method will be investigated on several power systems.

4.3.1 RSI simulation for 5-bus system

The generators in the 5-bus power system do not have data on reactive power limitations. In practice, all generators have reactive limitations due to their armature current limit, field current limit, and end region heating limit [1]. In order to simulate the RSI index for the 5-bus system, the reactive power limitations of the generators are assigned by the author based on their real power capability. Table 4.4 shows the parameters assigned to the two generators during the simulation.

Table 4.4 Scheduled generation of the two generators and their reactive limits for the 5-bus system

Bus number	Desired bus voltage (p.u)	Generation		Reactive power limits	
		MW	Mvar	Mvar (Min)	Mvar
1	1.06∠0	110	55.27	-80	80
2	1.0	41	-41.24	-80	80

To obtain the RSI, the load is increased from the operating point 145MW to a stressed point 220MW. At the stressed case, generators 1 and 2 provide reactive power 63.4 *Mvar* and -21.0 *Mvar*, respectively. When the generator reactive power limits are open, the reactive power supplied by each generator can be calculated for each line outage contingency at the stressed case. Table 4.5 shows the results. It is evident that for the most severe contingency, that is, when line 5 is out of service, the reactive power provided by generators 1 and 2 increases dramatically.

Table 4.5 Reactive power provided by two generators at stressed case for each line contingency when the generator's reactive power limit is open

Line Number	Bus		Generator 1	Generator 2
	From	To	[MVar]	[Mvar]
1	1	2	10.3	54.2
2	1	3	31.5	25.7
3	2	3	74.4	-21.5
4	2	4	73.1	-19.3
5	2	5	89.2	30.6
6	3	4	58.7	-13.0
7	4	5	62.4	-14.3

After the above data are substituted into equation (3.16), the RSI results can be calculated. In order to compare the results with those of CPF, the RSI values are normalized using the following equation.

$$RSI_{i(norm)} = \frac{RSI_i - \min(RSI_i)}{\max(RSI_i) - \min(RSI_i)} \tag{4.1}$$

where,

RSI_i : RSI value for the *i-th* branch contingency (Mvar)

$RSI_{i(norm)}$: normalized RSI value for the *i-th* branch contingency

$\min(RSI_i)$: minimum value among all RSI_i (Mvar)

$\max(RSI_i)$: maximum value among all RSI_i (Mvar)

Figure 4.5 shows normalized RSI and CPF ranking results for the 5-bus system. In this figure, the X-axis represents line number, which is sorted according to their margins, while the Y-axis corresponds to the normalized value of voltage stability margin. The scaling of the Y-axis is such that "0" corresponds to the most critical contingency, whereas "1" corresponds to the least severe contingency case. As seen from Figure 4.5, the RSI method closely follows the pattern of the exact margin calculation.

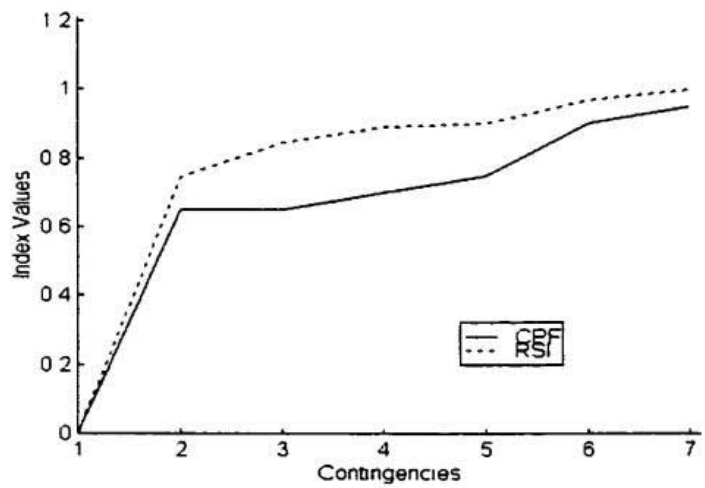

Figure 4.5. Normalized RSI index for the 5-bus system

CPF – Continuation power flow RSI – Reactive support index

The process of calculating RSI values for line 2, line 5, and line 6 is shown below. Substituting the values in Table 4.5 into equation (3.16), the RSI values can be obtained.

$$RSI_2 = (63.4 - 31.5) + (-21.0 - 25.7) = -14.8 \ (MVar)$$

$$RSI_5 = (63.4 - 89.2) + (-21.0 - 30.6) = -77.4 \ (MVar)$$

$$RSI_6 = (63.4 - 58.7) + (-21.0 + 13.0) = -3.3 \ (MVar)$$

By applying equation (4.1), the normalized RSI index values can be obtained. For instance, $RSI_{2(norm)} = \frac{(-14.8) - (-77.4)}{(-3.3) - (-77.4)} = 0.845$, $RSI_{5(norm)} = \frac{(-77.4) - (-77.4)}{(-3.3) - (-77.4)} = 0$, and $RSI_{2(norm)} = \frac{(-3.3) - (-77.4)}{(-3.3) - (-77.4)} = 1$. It is seen that the normalized index value "0" stands for the most critical contingency, whereas "1" corresponds to the least severe contingency. Table 4.6 shows the normalized RSI and CPF index values, as well as their ranking results. It indicates that the RSI method can classify the contingencies of the 5-bus system without any mis-ranking, When comparing the results of CPF and RSI, there are some minor differences, but they do not affect the ranking results.

Table 4.6 Normalized ranking results for the 5-bus system using CPF and RSI

Line Number	Bus From To	CPF		RSI	
		Normalized index	Rank	Normalized index	Rank
5	2 – 5	0	(1)*	0	(1)
1	1 – 2	0.65	(2)	0.746	(2)
2	1 – 3	0.66	(3)	0.845	(3)
4	2 – 4	0.70	(4)	0.891	(4)
3	2 – 3	0.75	(5)	0.903	(5)
7	4 - 5	0.90	(6)	0.967	(6)
6	3 – 4	0.95	(7)*	1.000	(7)

(1)* corresponds to the branch for which the post-contingency margin is the lowest.

(7)* corresponds to the branch for which the post-contingency margin is the largest.

4.3.2 RSI simulation for the 118-bus system

The RSI method is applied to the IEEE 118-bus power system, which contains 179 transmission lines and 54 generators. At the operating point, the system total load is 3668MW. Details of this power system are given in Appendix A. For the pre-contingency case, the maximum power that this system can provide is 7808MW. Therefore, the pre-contingency margin is 4140MW. Once the CPF and RSI methods are applied to this system, the ranking results can be recorded. These results are shown in Figure 4.6. The figure shows that the RSI method can basically follow, with some noise, the pattern of the accurate ranking obtained by the CPF method. Figure 4.6 also indicates that this method still has mis-rankings for several severe contingencies for this power system.

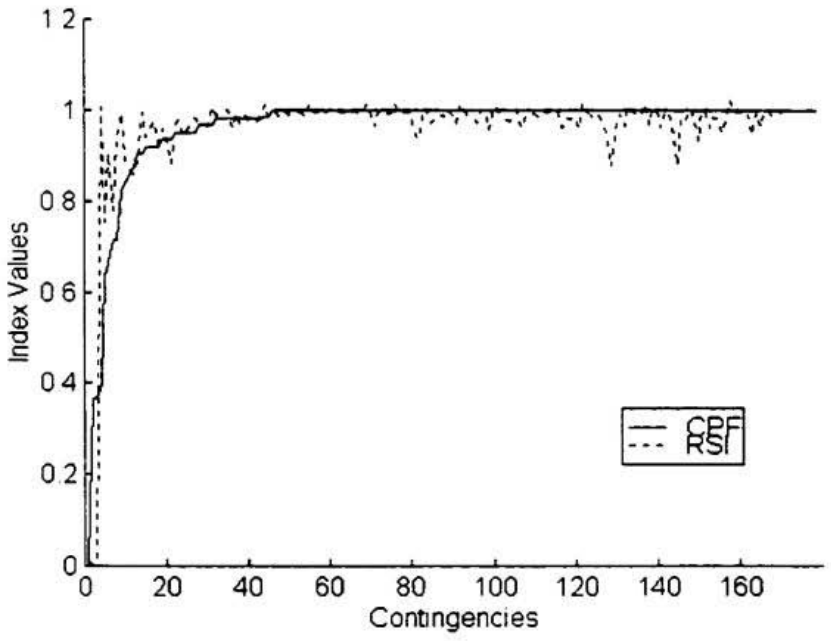

Figure 4.6 Normalized RSI index for the 118-bus system
CPF – Continuation power flow
RSI – Reactive support index

Table 4.7 shows the loading margins and ranks for the 10 worst branch outages of the 118-bus power system. Close examination of Table 4.7 indicates that out of the 10 most critical contingencies, the RSI method misclassifies 5 of them for the 118-bus system.

Table 4.7 The 10 critical branch outage contingency margins obtained by RSI and CPF for the 118-bus power system

Branch Outages		CPF margins Exact		RSI Estimate
From	To	[MW] (rank)	[p.u] (rank)	[p.u] (rank)
8	5	980 (1)	0.230 (1)	0.0112 (3)
8	9	2100 (2)	0.507 (2)	0 (1)
9	10	2120 (3)	0.513 (3)	0.0066 (2)
75	118	2200 (4)	0.531 (4)	1.0076 (167)
38	37	2980 (5)	0.720 (5)	0.7544 (4)
76	77	3060 (6)	0.739 (6)	0.9069 (13)
38	65	3220 (7)	0.777 (7)	0.7778 (5)
100	103	3220 (8)	0.777 (8)	0.9413 (19)
4	5	3580 (9)	0.865 (9)	0.9918 (99)
69	75	3600 (10)	0.870 (10)	0.8928 (12)

4.3.3 RSI simulation for a 600-bus power system

The RSI method was applied to a 600-bus power system, which contains 900 transmission lines and 60 generators. Details of this power system are given in Appendix A. At the operating point, the total load is 24594.6 MW. For the pre-contingency case, the maximum power that this system can provide is 25734.6 MW. The pre-contingency margin is 1140MW. After the CPF and RSI methods are applied to the 150 most critical branch outage contingencies, the detailed ranking results are obtained and shown in Figure 4.7. This figure reveals that the RSI method can detect most severe branch outage contingencies for the 600-bus system, except for several mis-rankings.

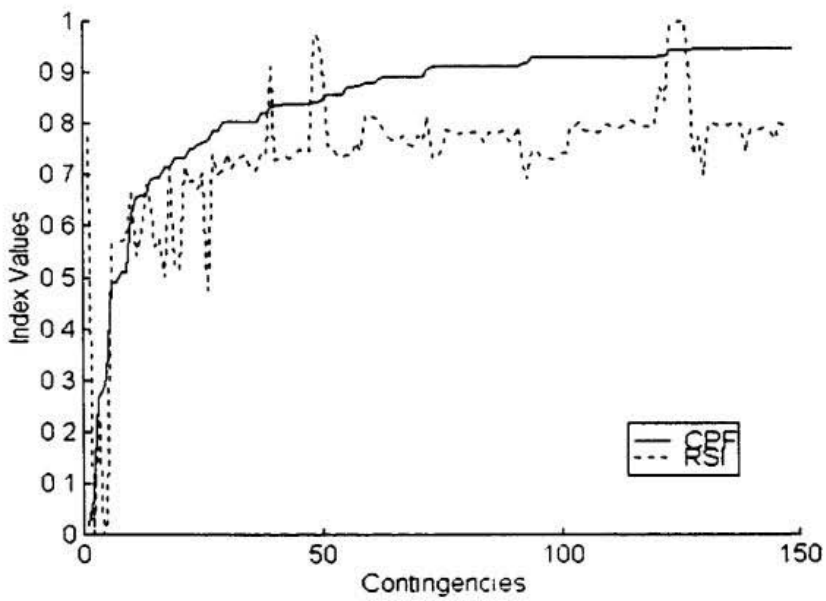

Figure 4.7 Normalized RSI index for the 600-bus system
CPF – Continuation power flow
RSI – Reactive support index

Table 4.7 shows the loading margins and ranks for the 10 worst branch outages of the 600-bus power system. Out of the 10 most critical line outage contingencies, the RSI method misclassifies 6 of them.

Table 4.8 The 10 critical branch outage contingency margins obtained by RSI and CPF for the 600-bus power system

Line Voltage Rating(kV)	Line Outages Bus No.		CPF margins Exact		RSI Estimate
			[MW] (rank)	[p.u] (rank)	[p.u] (rank)
118.1	226	227	20 (1)	0.017 (1)	0.77409 (81)
220	8	299	80.01 (2)	0.070 (2)	0 (1)
500	16	350	300.01 (3)	0.263 (3)	0.26128 (4)
500	9	15	319.99 (4)	0.281 (4)	0.00151 (2)
500	15	19	340.01 (5)	0.298 (5)	0.02769 (3)
220	92	108	549.29 (6)	0.482 (6)	0.56487 (11)
220	92	110	549.29 (7)	0.482 (7)	0.56487 (12)
220	93	112	572.76 (8)	0.502 (8)	0.57198 (13)
220	93	113	572.76 (9)	0.502 (9)	0.57382 (14)
118.05	459	464	700 (10)	0.614 (10)	0.67114 (18)

4.4 CS&R Results Obtained by GCF

GCF is another fast ranking algorithm suitable for online contingency screening and ranking (CS&R). This method has been discussed earlier in section 3.4.4. To assess

the performance of GCF for CS&R, this method is applied to the same power systems as in the RSI algorithm.

4.4.1 GCF simulation for the 5-bus system

To obtain the loading margin for each line outage contingency by GCF, at every load bus in the 5-bus test system shown in Figure 4.1, three points are selected to fit a PV curve. Those three points are located at the stable branch of each PV curve, but are far away from the nose point. Table 4.9 shows the three selected fitting points for line 1 and line 2 outages.

Table 4.9 Fitting points selected for line 1 and line 2 outages in the 5-bus system

Line number	Bus From To	Total load [MW]	Voltage (p.u)		
			Bus 3	Bus 4	Bus 5
1	1 – 2	145.00	0.9940	0.9937	0.9890
		275.00	0.9600	0.9591	0.9503
		355.00	0.9350	0.9338	0.9220
2	1 – 3	145.00	0.9802	0.9823	0.9845
		275.00	0.9284	0.9324	0.9388
		355.00	0.8900	0.8954	0.9049

After the collapse points of all load buses are obtained by the GCF method, the final collapse point of each contingency can be approximated by using their mean value. The load margins obtained by the CPF and GCF methods are shown in Figure 4.8 and Table 4.10.

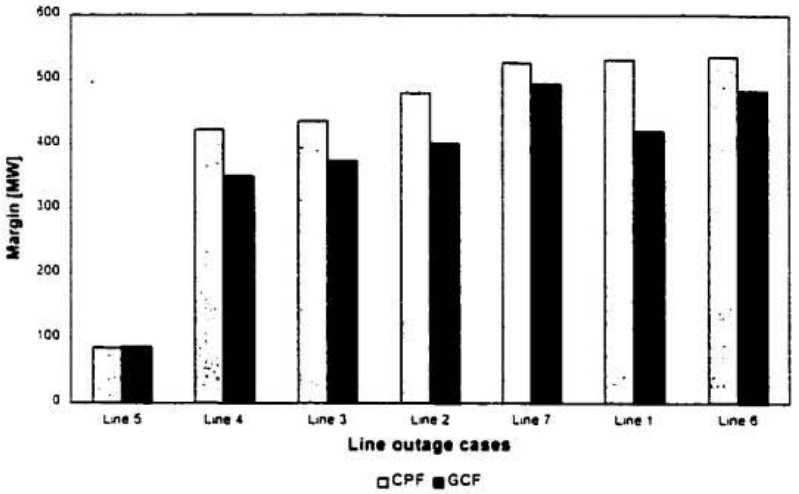

Figure 4.8 Ranking results obtained by GCF for the 5-bus system

Table 4.10 Margins obtained by GCF and CPF for the 5-bus system

Line Number	Bus From To	CPF Margins Exact (rank)	GCF Margins Estimate (rank)
5	2 - 5	85.64 (1)	87.08 (1)
4	2 – 4	422.8 (2)	350.13(2)
3	2 – 3	435.89(3)	374.01(3)
2	1 - 3	479.36(4)	400.89(4)
7	4 – 5	526.03(5)	493.46(7)
1	1 – 2	531.19(6)	420.03(5)
6	3 – 4	535.64(7)	482.87(6)

Figure 4.8 indicates that most of the stability margins calculated by GCF are smaller than the accurate CPF margins. However, the performance of GCF is still efficient enough to rank the 5-bus system even though mis-ranking still occurs. The GCF method can detect the rank of the 4 most critical branch outage contingencies correctly.

4.4.2 GCF simulation for the 39-bus power system

The GCF method is applied to the 39-bus New England test system shown in Figure 4.9, which contains 35 transmission lines, 11 generators, and 13 transformers. Details of this power system are given in Appendix A.

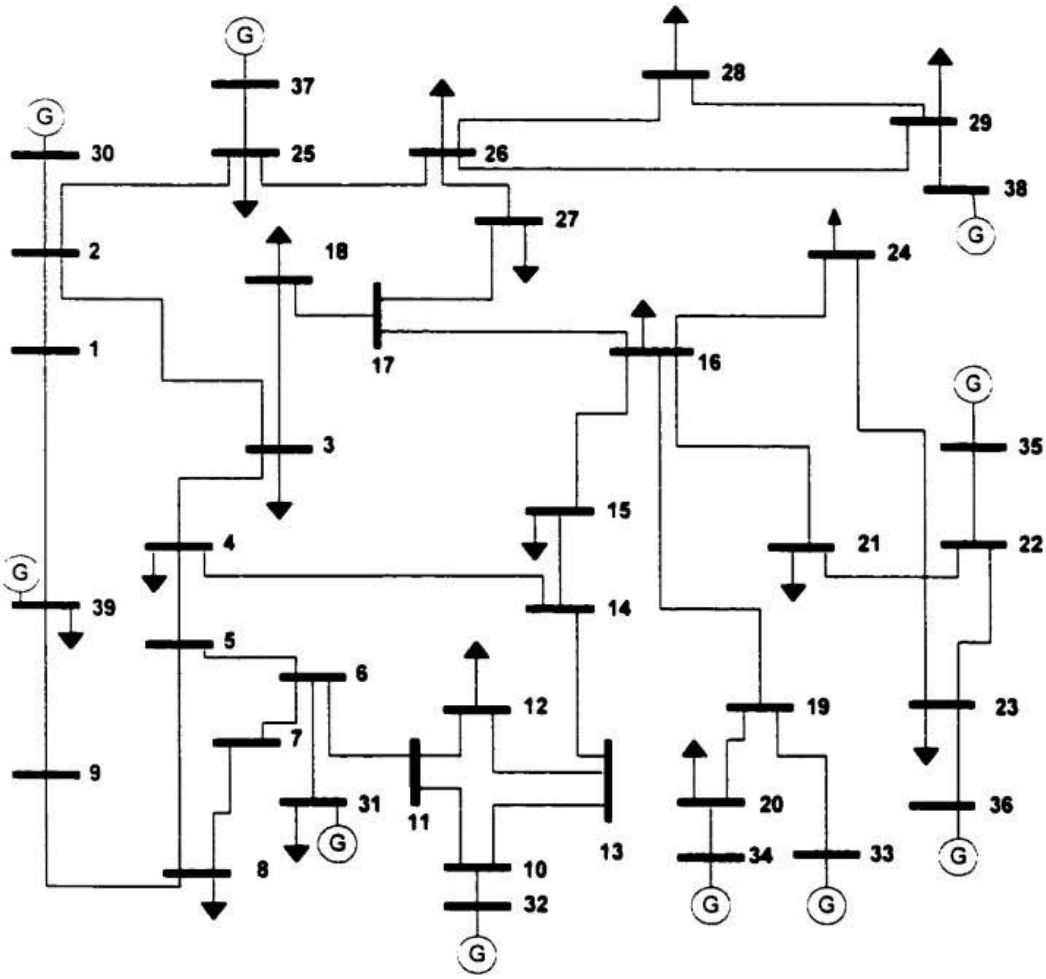

Figure 4.9. Single line diagram of the 39-bus power system

The normalized ranking results are shown in Figure 4.10. It shows that the stability margin given by the GCF method is much lower than that of CPF. However, GCF can still rank the 39-bus system, although mis-ranking exists. Table 4.11 shows the ten most critical branch outage contingency margins obtained by GCF and CPF methods. It can be seen that out of the 10 most critical branch contingencies, GCF mis-classifies only one.

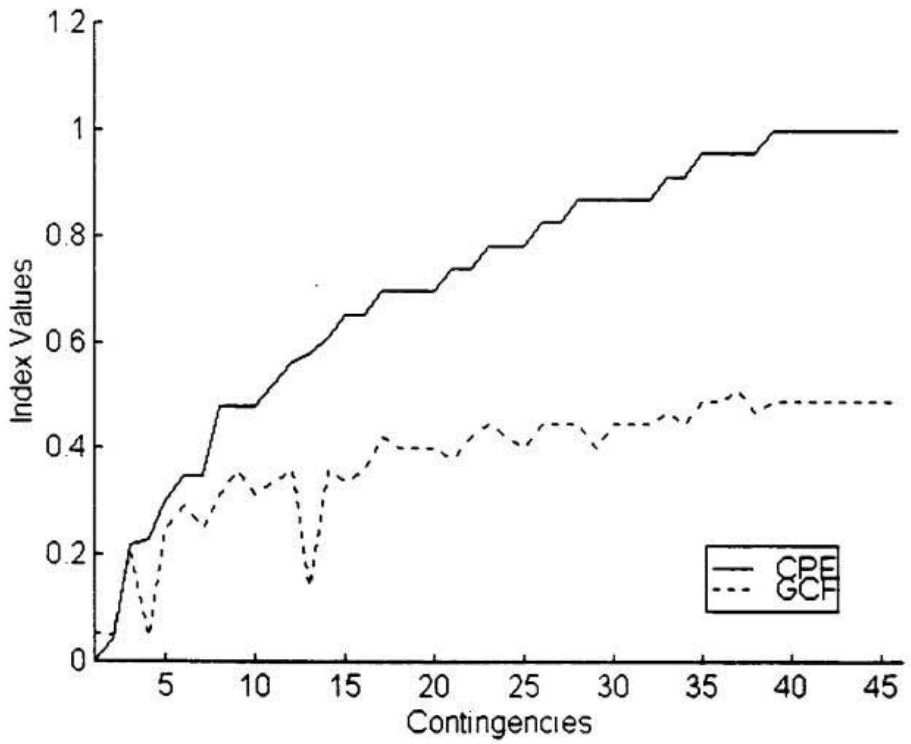

Figure 4.10 Normalized GCF index for the 39-bus system

CPF – Continuation power flow

GCF – Generalized curve fit

Table 4.11 The 10 critical branch outage contingency margins obtained by GCF and CPF for the 39-bus power system

Branch outage		Line/	CPF margin [Exact]		GCF margin [Estimate]	
From	To	Transformer	MW (rank)	VS%	MW (rank)	VS%
Pre-contingency			8200.5	133.3	5850	95.1
21	22	L	3600.5 (1)	58.54	3850 (3)	62.6
29	38	L	3800.5 (2)	61.79	3820 (2)	62.1
10	32	L	4600.5 (3)	74.80	4550 (5)	74.0
16	19	L	4657.1 (4)	75.72	3810 (1)	62.0
22	35	L	5000.5 (5)	81.30	4750 (6)	77.2
15	16	L	5200.5 (6)	84.56	4950 (8)	80.5
19	33	L	5200.5 (7)	84.56	4750 (7)	77.2
20	34	L	5800.5 (8)	94.31	5050 (9)	82.1
23	36	L	5800.5 (9)	94.31	5250 (13)	85.4
25	37	L	5800.5 (10)	94.31	5050 (10)	82.1

The parameter VS% shown in Table 4.11 is obtained by using equation (4.3),

$$VS\% = \frac{\text{margin}}{\text{Total basecase load in the study area}} \times 100\% \qquad (4.3)$$

At the pre-contingency case, for example, the stability margin is 8200.5MW, while the total base case load is 6150 MW. Thus, $VS\% = 8200.5/6150 \times 100\% = 133.3\%$. For the contingency case, line 21-22 out of service, the margin is 3600.5 MW, the total base case load remains the same. Hence, $VS\% = 3600.5/6150 \times 100\% = 58.54\%$.

4.4.3 GCF simulation for the 118-bus power system

The ranking results obtained by GCF for the IEEE 118-bus power system are not accurate. Figure 4.11 depicts the normalized margins of GCF and CPF for this test system. As seen from Figure 4.11, for most contingency cases, the estimated margins by GCF for the 118-bus system are smaller than those accurate ones by CPF.

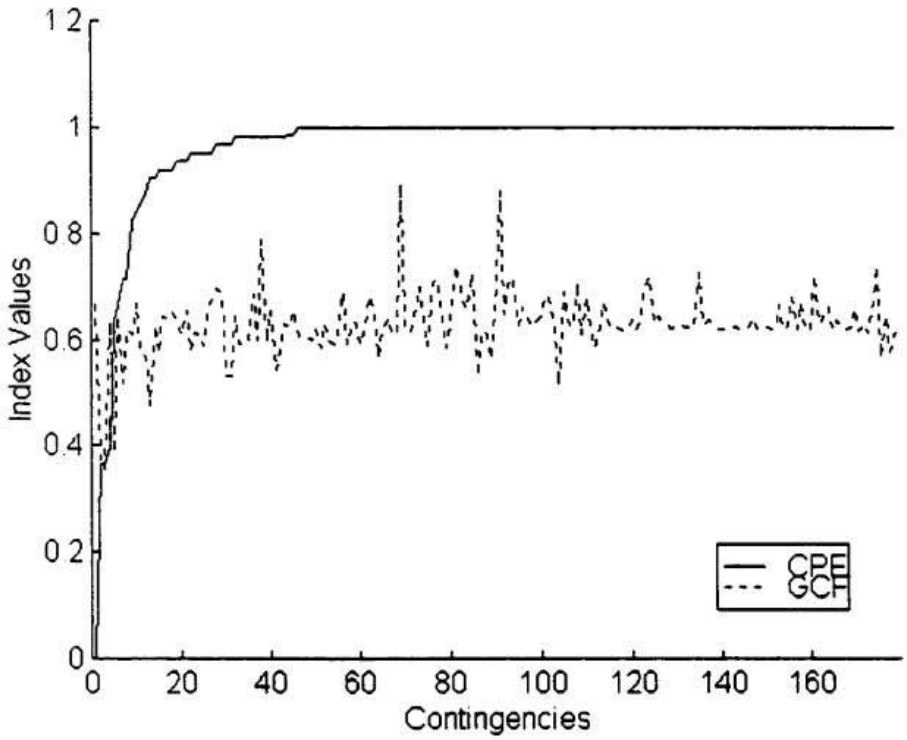

Figure 4.11 Normalized GCF index for the 118-bus system
CPF – Continuation power flow
GCF – Generalized curve fit

Table 4.12 shows the margins of the 10 most critical branch outage contingencies. Out of the 10 most critical contingencies, GCF mis-classifies 6 for the 118-bus system. Therefore, GCF results provide very poor information about the severity of the branch outage contingencies for the 118-bus systems.

Table 4.12 The 10 critical branch outage contingency margins obtained by GCF and CPF for the 118-bus power system

Branch outage From	To	Line/ Transformer	Rating	CPF margin [Exact]		GCF margin [Estimate]	
				MW (rank)	VS%	MW (rank)	VS%
Pre-contingency				4140	112.9	3282	80.5
8	5	T	-	980 (1)	25.9	3047 (145)	83.1
8	9	L	-	2100 (2)	57.25	2103.5 (2)	57.3
9	10	L	-	2120 (3)	57.25	2074.7 (1)	56.6
75	118	L	-	2200 (4)	59.97	2947 (113)	80.3
38	37	T	-	2980 (5)	80.42	2172 (3)	59.2
76	77	L	-	3060 (6)	83.15	2979 (125)	81.2
38	65	L	-	3220 (7)	87.24	2578 (6)	70.3
100	103	L	-	3220 (8)	87.24	2898.8 (55)	79.0
4	5	L	-	3580 (9)	96.78	2869.7 (40)	78.2
69	75	L	-	3600 (10)	98.14	3056 (146)	83.3

4.4.4 GCF simulation for the 300-bus system

The GCF method is applied to the IEEE 300-bus power system, which contains 304 transmission lines, 106 transformers, and 69 generators. Details of this power system are given in Appendix A. For the 150 most critical branch outage contingencies, the loading margins obtained by GCF and CPF for the 300-bus systems are illustrated in

Figure 4.12. It is seen that the margins obtained by GCF are inaccurate. Several estimated margins even become negative, which is abnormal.

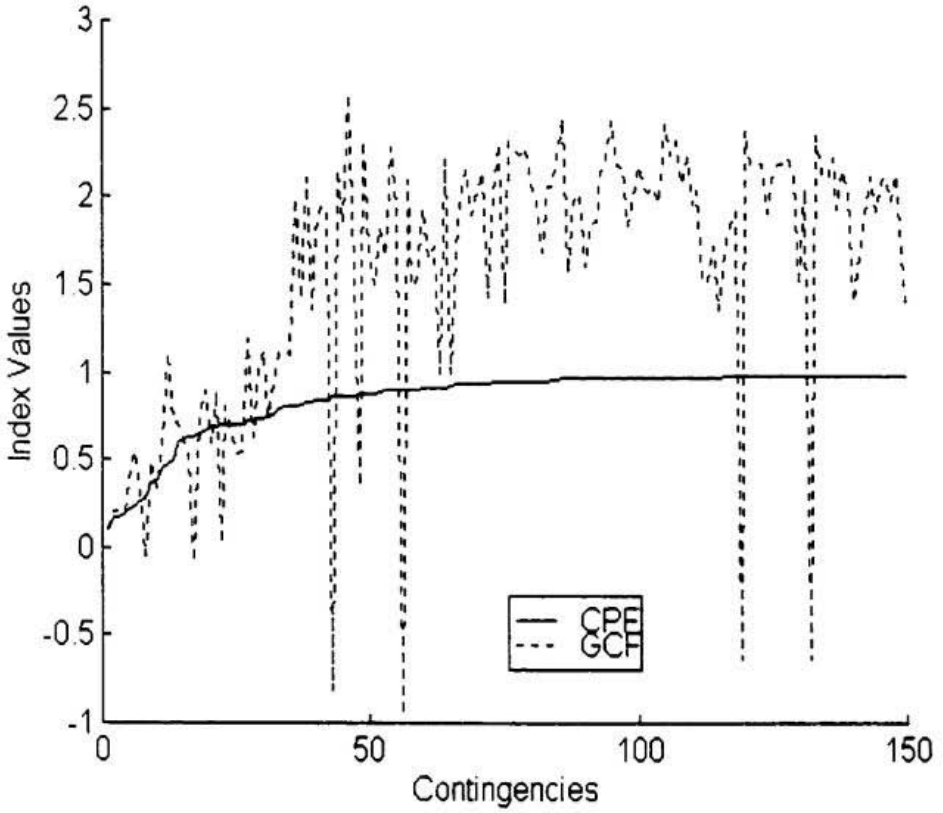

Figure 4.12 Normalized GCF index for the 300-bus system
CPF – Continuation power flow
GCF – Generalized curve fit

Table 4.13 shows that the GCF method misclassifies 6 out of the 10 most critical contingencies.

Table 4.13 The 10 critical branch outage contingency margins obtained by GCF and CPF for the 300-bus power system

Branch outage		Line/	Rating	CPF margin [Exact]		GCF margin [Estimate]	
From	To	Transformer	(kV)	MW (rank)	VS%	MW (rank)	VS%
Pre-contingency				1140	4.9	2400	10.3
57	63	L	115	119.9 (1)	0.516	114.4 (8)	0.49
46	81	L	345	200.0 (2)	0.86	234.3 (11)	1.01
16	42	L	345	200.0 (3)	0.86	232.5 (10)	1.00
7071	71	T	13.8/115	219.9 (4)	0.946	228.2 (9)	0.98
231	232	T	345/138	246.2 (5)	1.059	431.8 (15)	1.86
202	211	T	66/115	259.9 (6)	1.118	620.8 (19)	2.67
37	49	L	115	299.9 (7)	1.29	378.9 (12)	1.63
159	117	T	230/115	319.9 (8)	1.376	-54.55 (6)	-0.23
45	46	T	230/345	419.9 (9)	1.807	556.9 (16)	2.40
45	60	L	230	439.9 (10)	1.893	383.7 (13)	1.65

4.4.5 GCF simulation for the 600-bus power system

Similarly, the margins obtained by GCF for the 600-bus system are presented in Figure 4.13, in which the estimated margins oscillate around their exact ones. Several of them even become negative.

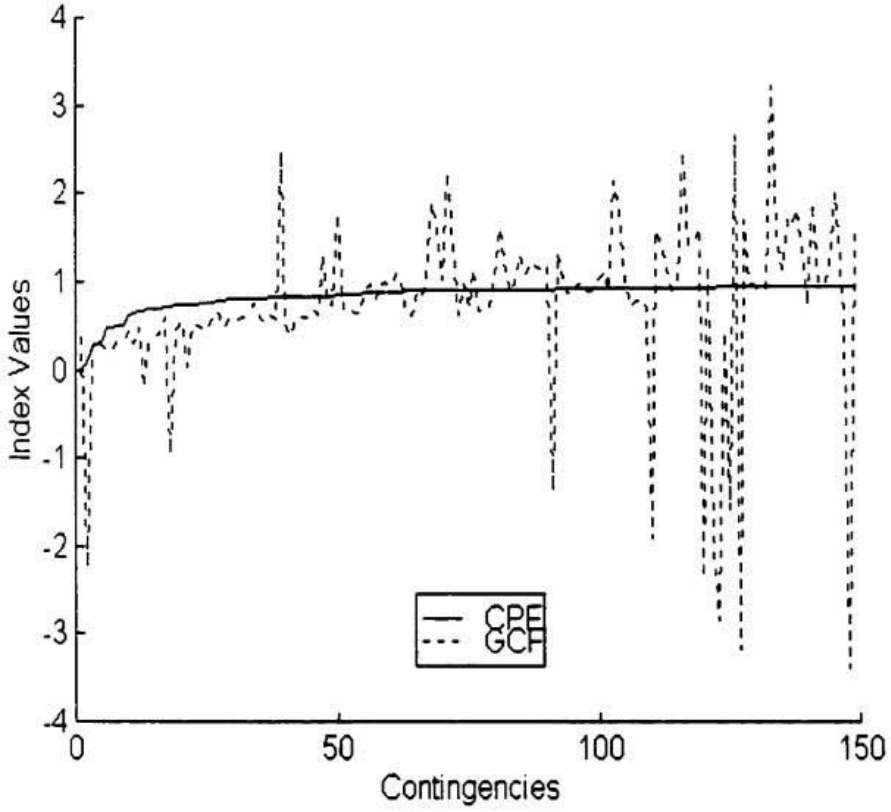

Figure 4.13 Normalized GCF index for the 600-bus system
CPF – Continuation power flow
GCF – Generalized curve fit

Table 4.14 shows that out of the 10 most critical branch outage contingencies, the GCF misclassifies 9. Hence, the GCF results cannot provide any useful ranking for the 600-bus power system.

Table 4.14 The 10 critical branch outage contingency margins obtained by GCF and CPF for the 600-bus power system

Branch outage		Line/	Rating	CPF margin [Exact]		GCF margin [Estimate]	
From	To	Transformer	(kV)	MW (rank)	VS%	MW (rank)	VS%
Pre-contingency				1140	4.6	768.2	3.1
226	227	L	118	20 (1)	0.081	405.2 (21)	1.65
8	299	T	230/220	80.01 (2)	0.325	-2508.9 (5)	-10.20
16	350	L	500	300.01 (3)	1.22	273.4 (15)	1.11
9	15	L	500	319.99 (4)	1.301	406.2 (22)	1.65
15	19	L	500	340.01 (5)	1.382	331.6 (17)	1.35
92	108	T	220/24	549.29 (6)	2.233	240.5 (13)	0.98
92	110	T	220/24	549.29 (7)	2.233	240.5 (14)	0.98
93	112	T	220/24	572.76 (8)	2.329	371.6 (19)	1.51
93	113	T	220/24	572.76 (9)	2.329	372.5 (20)	1.51
459	464	L	118.05	700 (10)	2.846	491.4 (27)	2.00

4.4.6 GCF simulation for B.C Hydro 197-bus power system

The GCF method is applied to the BC Hydro 197-bus power system, which contains 317 transmission lines and 21 generators. Detials of this power system are privided in Appendix B. The performance of the GCF method is quite good for this 197-bus power system. The simulation results are depicted in Figure 4.14, which shows that the estimated margins can roughly follow the exact pattern.

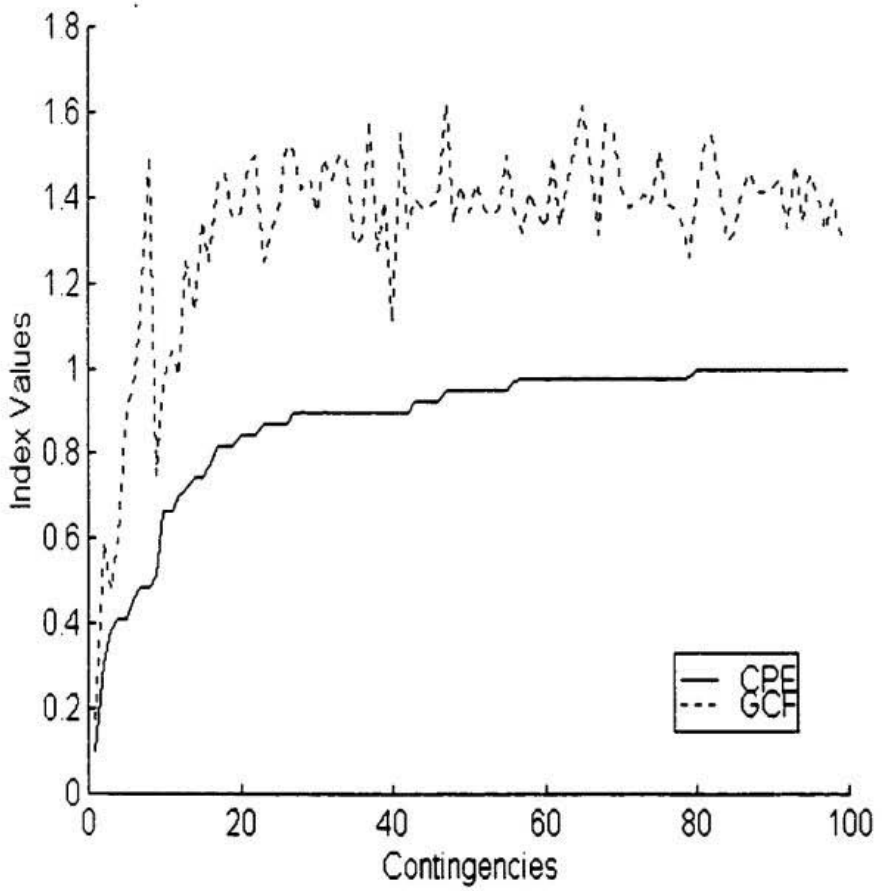

Figure 4.14 Normalized GCF index for the 197-bus power system
CPF – Continuation power flow
GCF – Generalized curve fit

Out of the 10 most critical branch outage contingencies, the GCF method misclassifies 2, which is shown in Table 4.15.

Table 4.15 The 10 critical branch outage contingency margins obtained by GCF and CPF for the 197-bus power system

Branch outage From	To	Line/ Transformer	Rating (kV)	CPF margin [Exact] MW (rank)	VS%	CGF margin [Estimat] MW (rank)	VS%
Pre-contingency				780	23.65	1031	31.3
4144	4145	T	132/230	80 (1)	2.426	135.5 (1)	4.1
4074	4080	L	287	240 (2)	7.278	460.2 (3)	14.0
4087	4099	L	500	300 (3)	9.098	374.8 (2)	11.4
4058	4099	L	500	320 (4)	9.704	468.4 (4)	14.2
4143	4142	T	132/13.8	320 (5)	9.704	706.8 (6)	21.4
4032	4137	L	500	360 (6)	10.918	746.5 (7)	22.6
4032	4136	L	500	380 (7)	11.524	872.9 (12)	26.5
4046	4043	T	500/13.8	380 (8)	11.524	1168 (87)	35.4
4028	4078	L	500	400 (9)	12.131	583.1 (5)	17.7
4015	4020	L	16.5	520 (10)	15.77	757.3 (8)	23.0

4.4.7 GCF simulation for Ontario Hydro 1254-bus power system

The GCF method is applied to the Ontario Hydro 1254-bus power system, which contains 1970 transmission lines and 268 generators. Detials of this power system are privided in Appendix C. The simulation results for the 1254-bus system by GCF, which are shown in Figure 4.15, contain much turbulance. Thus, it is very difficult to find the relationship between the margins obtained by GCF and CPF.

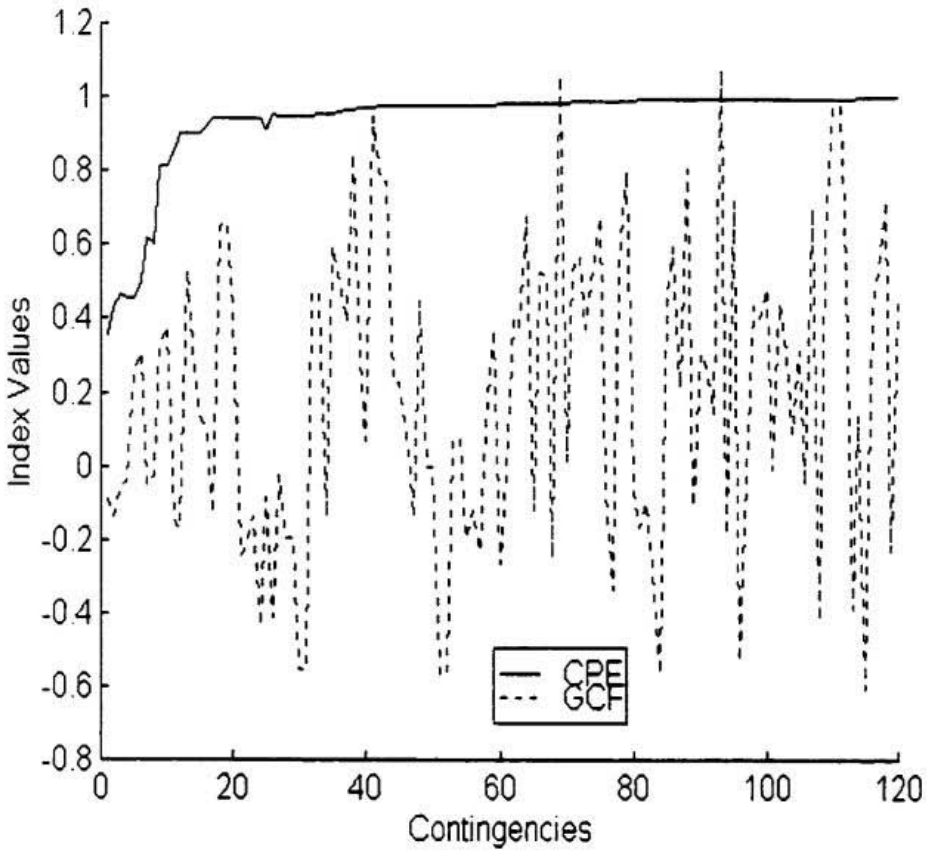

Figure 4.15 Normalized GCF index for the 1254-bus power system

CPF – Continuation power flow

GCF – Generalized curve fit

Table 4.16 shows that the GCF method cannot capture any of the 10 most critical branch outage contingencies for the Ontario Hydro 1254-bus power system.

Table 4.16 The 10 critical branch outage contingency margins obtained by GCF and CPF for the 1254-bus power system

Branch outage From To	Line/ Transformer	Rating (kV)	CPF margin [Exact]		GCF margin [Estimate]	
			MW (rank)	VS%	MW (rank)	VS%
Pre-contingency			900	4.20	600	2.79
11940 12174	L	220	320.04 (1)	1.49	-82.23 (36)	-0.38
12635 12638	L	220	390.03 (2)	1.82	-125.43 (27)	-0.58
12636 12637	L	220	419.99 (3)	1.96	-45.46 (41)	-0.21
12595 12600	L	220	410.02 (4)	1.91	-38.95 (43)	-0.18
12596 12600	L	220	410.02 (5)	1.91	227.94 (65)	1.06
10826 10856	L	118.05	452.16 (6)	2.11	275.15 (69)	1.28
12555 12615	L	220	560.03 (7)	2.61	-48.71 (40)	-0.23
12555 12616	L	220	540.02 (8)	2.52	-21.85 (46)	-0.10
12695 12600	L	345	729.16 (9)	3.40	299.03 (73)	1.39
12696 12600	L	345	731.3 (10)	3.41	343.34 (77)	1.60

4.5 Summary

In this chapter, three contingency screening and ranking (CS&R) methods, Continuation Power Flow (CPF), Reactive Support Index (RSI), and Generalized Curve Fit (GCF), are applied to different power systems, such as 5-bus, 39-bus, 118-bus, 300-bus, 600-bus, BC Hydro 197-bus, and Ontario Hydro 1254-bus power systems.

Simulation results show that RSI is a relatively stable method for contingency screening and ranking. It works well not only for small systems but also for larger power systems with some misclassifications. However, GCF is an unstable method. It can detect

most severe contingencies for small systems such as 5-bus and 39-bus power systems, but fails to give correct classification for larger systems, such as 118-bus, 300-bus, 600-bus, and Ontario Hydro 1254-bus power systems.

In view of the poor performance of the existing contingency ranking methods, this research focused on alternate approaches. The results of this investigation are presented in the next chapter.

Chapter 5

Proposed Methods for Contingency Screening and Ranking

5.1 Introduction

The GCF method has a good performance of contingency screening and ranking for 5-bus and 39-bus systems, while its performance degrades for the IEEE 118-bus, 300-bus, and a 600-bus, as well as the two utility systems (BC Hydro 197-bus and Ontario Hydro 1254-bus power systems). Compared with GCF, RSI is a relatively stable method. Simulation results show that the misclassification of RSI is still unacceptable for several large sample power systems. In this chapter, two improved methods for GCF, *reselecting curve fitting points* and *filtering out unreasonable nose points*, proposed by the author will be introduced. This chapter is divided into two parts. The first part introduces the proposed methods, while the second part deals with the simulation results by applying these two methods to a variety of power systems when branch outage contingencies occur. The effectiveness of these two methods is demonstrated by applying them to rank branch outage contingencies of the power systems listed above. Simulation results on

these power systems show that the performance of GCF is enhanced significantly by these two methods [28,29].

5.2 Reselecting Curve Fitting Points (R-GCF)

In previous GCF ranking results for large power systems, the estimated nose points of the PV curve at load buses are not accurate. The reason is that the three fitting points are far away from their nose point, especially the third one. In view of this, the last two fitting points are rearranged, while the first point is kept fixed. The third point is reselected to be closer to the nose point, i.e. in Figure 5.1, point P_3 is moved closer to λ^*.

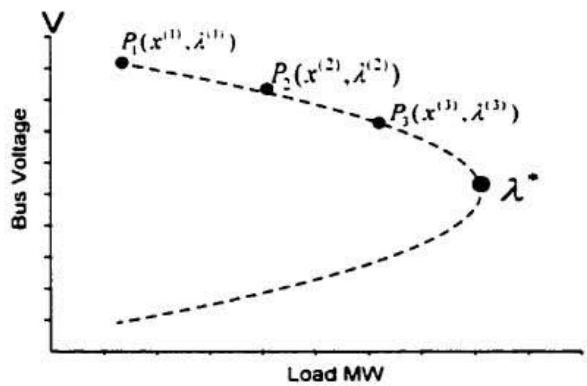

Figure 5.1 Illustration of the generalized curved fit method

The implementation of this method can be carried out by the following steps:

1. Choose a contingency from the list of pre-defined contingencies.

2. Determine operating point P_2 and a stressed operating point P_3. To determine the stressed operating point P_3, use CPF to find the nose point of the pre-contingency case. Then, decrease the load from the nose point and calculate this stressed case using any

power flow method for each contingency. For the solved cases (majority), use this operating point as a fitting point. For the unsolved contingency cases (minority), reduce the load and solve power flow equations again until they are solved or the load is less than the well defined operating point. Figure 5.2 presents the details of this computation. A similar approach was proposed in [5] and described in chapter 3.4.6.

3. Estimate the nose points for all the load buses in the study area based on the curve fitting method that uses the previously calculated three operating points.

4. Determine the mean value of these nose points. This is the estimate of the voltage stability margin for the chosen contingency.

5. Repeat the above steps for all the pre-defined contingencies.

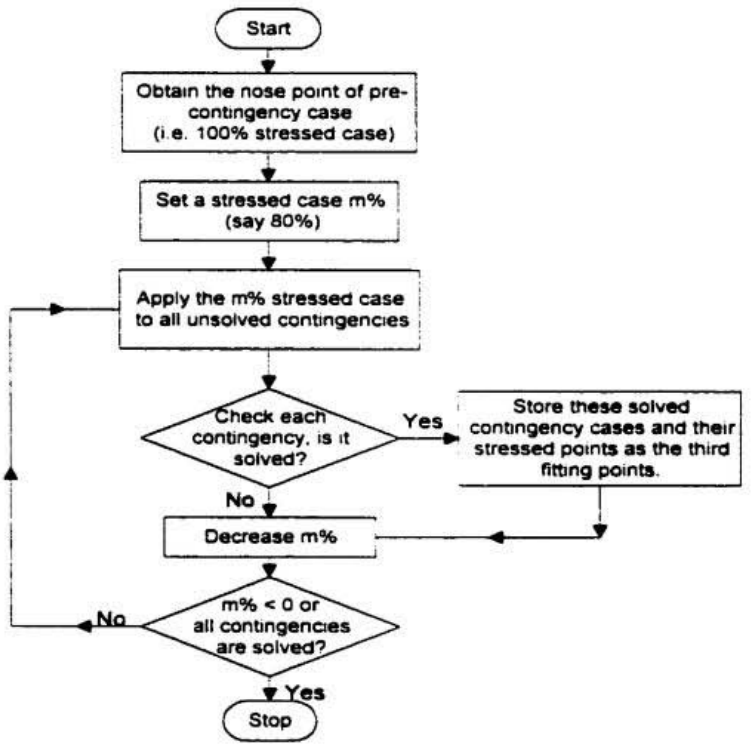

Figure 5.2 The flow chart to obtain the stressed case for each contingency

This method is referred to as R-GCF in the following sections.

5.3 Filtering out Unreasonable Nose Points (F-GCF)

The GCF method assumes that each PV curve of a load bus can be approximated as a quadratic equation, and its stability margin, obtained by GCF, is the average of the margins corresponding to the load buses in the study area. Reference [6] has proved that power flow equation can be expressed as a quadratic function only at the nose point of a power system. However, the GCF method has assumed that the complete PV curve can be defined by a quadratic equation, which is not always true. This will cause significant error if some of the calculated nose points are far away from the actual nose point. For certain contingencies it is observed that some nose points are extremely bigger than the actual nose point, as shown in Figure 5.3. In Figure 5.3 the solid line is the actual PV curve and the dotted line represents the estimated PV curve. In some cases the margin obtained by the curve fitting method can even be negative as illustrated in Figure 5.4.

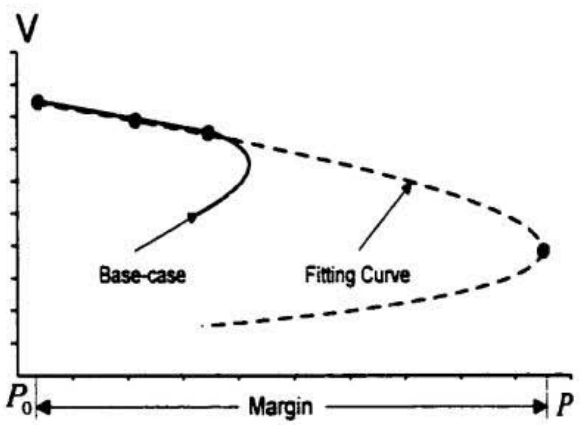

Figure 5.3 Abnormal nose point obtained by GCF (extremely big)

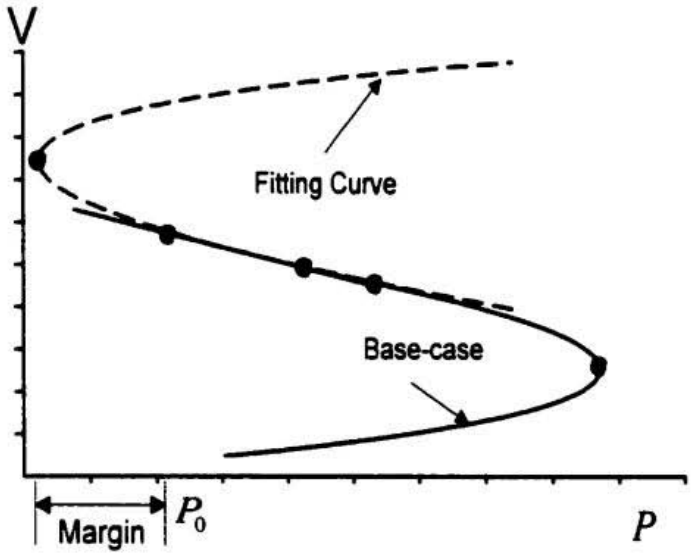

Figure 5.4 Abnormal nose point obtained by GCF (Negative margin)

To eliminate these unreasonable nose points, a 'band-pass filter', as shown in Figure 5.5, is used. If the nose points obtained by GCF are out of this band, these nose points will not be counted when estimating the approximate voltage collapse point. This 'band' is considered to be equal to twice the pre-contingency voltage stability margin. The application of this method follows the steps discussed in chapter 5.2, except that after step 3, the 'band-pass filter' is used to eliminate the unreasonable nose points.

This method is referred to as F-GCF in the following sections.

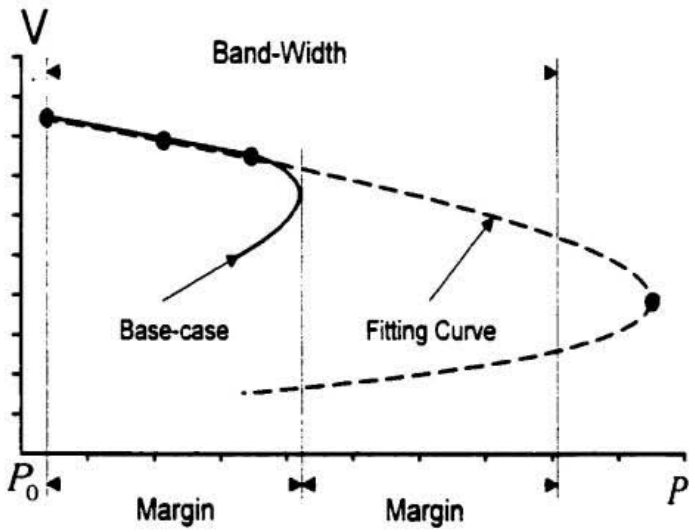

Figure 5.5 Illustration of a 'band-pass filter'

5.4 Simulation Results for Reselecting Curve Fitting Points (R-GCF)

Assuming that the load at each load bus is increased according to a given pattern, by following the implementation steps stated in chapter 5.2, three reselected curve fitting points at every load bus can be obtained for each branch outage contingency. Among these three points, the last point is closest to the voltage collapse point. The R-GCF method is applied to the 5-bus, 39-bus, 118-bus, 300-bus, 600-bus, BC Hydro 197-bus, and Ontario Hydro 1254-bus systems. With the exception of the last two systems, the load and generation in all systems are increased in a pattern such that the load of all PQ buses is increased in proportion to their MVA. For BC Hydro 197-bus and Ontario Hydro 1254-bus power systems, since the load centers are known, the load is increased only at the selected load centers; the generation is also picked up by all generators in proportion to their capabilities. The simulation results are discussed in the following sections.

5.4.1 Simulation of the 5-bus system using R-GCF

When the R-GCF method is applied to the 5-bus system, the margins obtained by R-GCF and CPF are recorded. The results of R-GCF and CPF are shown in Figure 5.6, where the outage of the seven lines is considered one at a time. This figure shows that normalized index values obtained by R-GCF can follow those of the CPF method very well (The normalized index value is described in chapter 4.3.1). Compared with Figure 4.8, Figure 5.6 indicates that the accuracy of the GCF method is improved by reselecting curve fitting points. Detailed results in Table 5.1 indicate that the R-GCF method can precisely rank the 4 most critical line outage contingencies for the 5-bus system. The margins obtained by R-GCF are also close to those of CPF.

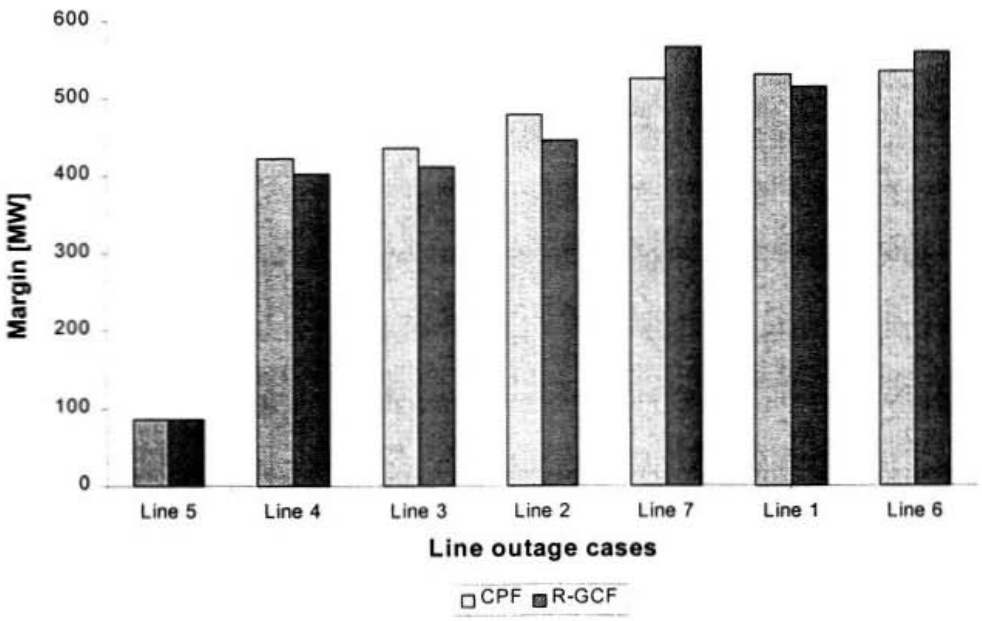

Figure 5.6 Normalized R-GCF index for the 5-bus system
CPF : Continuation power flow
R-GCF : GCF by reselecting curve fitting points

Table 5.1 Line outage contingency margins obtained by R-GCF and CPF for the 5-bus system

Branch outage		Line/	CPF margin [Exact]		R-GCF [Estimate]	
From	To	Transformer	MW (rank)	VS%	MW (rank)	VS%
Pre-contingency			643.34	443.68	605.20	417.40
2	5	L	85.64 (1)	59.06	86.56 (1)	59.69
2	4	L	422.8 (2)	291.58	402.98 (2)	277.91
2	3	L	435.89 (3)	300.61	412.03 (3)	284.16
1	3	L	479.36 (4)	330.59	446.09 (4)	307.64
4	5	L	526.03 (5)	362.78	567.42 (7)	391.32
1	2	L	531.19 (6)	366.34	514.66 (5)	354.93
3	4	L	535.64 (7)	369.41	559.61 (6)	385.94

5.4.2 Simulation of the New England 39-bus system using R-GCF

The R-GCF method is applied to the New England 39-bus power system, and the normalized index values obtained by R-GCF and CPF are presented in Figure 5.7. Compared with Figure 4.10, Figure 5.7 shows that the R-GCF method can follow the accurate results of CPF very well. Table 5.2 presents the margins and ranking results obtained by both methods. Among the 10 most critical branch outage contingencies, the R-GCF method has no misclassification.

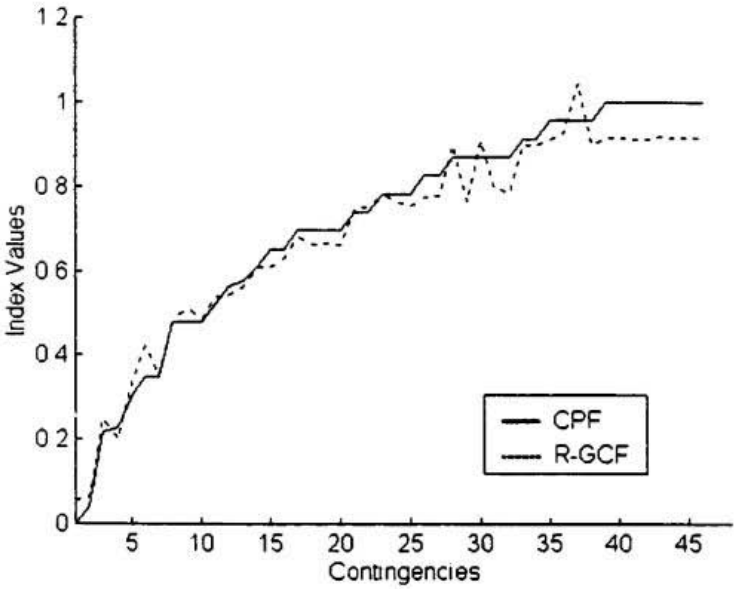

Figure 5.7 Normalized R-GCF index for the 39-bus power system

CPF : Continuation power flow

R-GCF : GCF by reselecting curve fitting points

Table 5.2 The 10 most critical branch outage contingency margins obtained by R-GCF and CPF for the 39-bus system

Branch outage From	To	Line/ Transformer	CPF margin [Exact]		R-GCF [Estimate]	
			MW (rank)	VS%	MW (rank)	VS%
Pre-contingency			8200.5	133.3	8105	131.1
21	22	L	3600.5 (1)	58.54	3854 (1)	62.67
29	38	L	3800.5 (2)	61.79	3885 (2)	63.17
10	32	L	4600.5 (3)	74.80	4755 (4)	77.32
16	19	L	4657.1 (4)	75.72	4525 (3)	73.58
22	35	L	5000.5 (5)	81.30	5137 (5)	83.53
15	16	L	5200.5 (6)	84.56	5542 (7)	90.11
19	33	L	5200.5 (7)	84.56	5216 (6)	84.81
20	34	L	5800.5 (8)	94.31	5822 (8)	94.67
23	36	L	5800.5 (9)	94.31	5963 (10)	96.96
25	37	L	5800.5 (10)	94.31	5822 (9)	94.67

5.4.3 Simulation of the IEEE 118-bus system using R-GCF

The margins obtained by applying R-GCF and CPF to the 118-bus system are illustrated in Figure 5.8. This figure shows that the margins obtained by R-GCF give optimistic estimations of the exact load margins. Table 5.3 reveals that the R-GCF method can still provide useful information for line contingency ranking, even though the differences of the margins between the two methods are not negligible. Out of the 10 most critical contingencies, the R-GCF method misclassifies 2 of them.

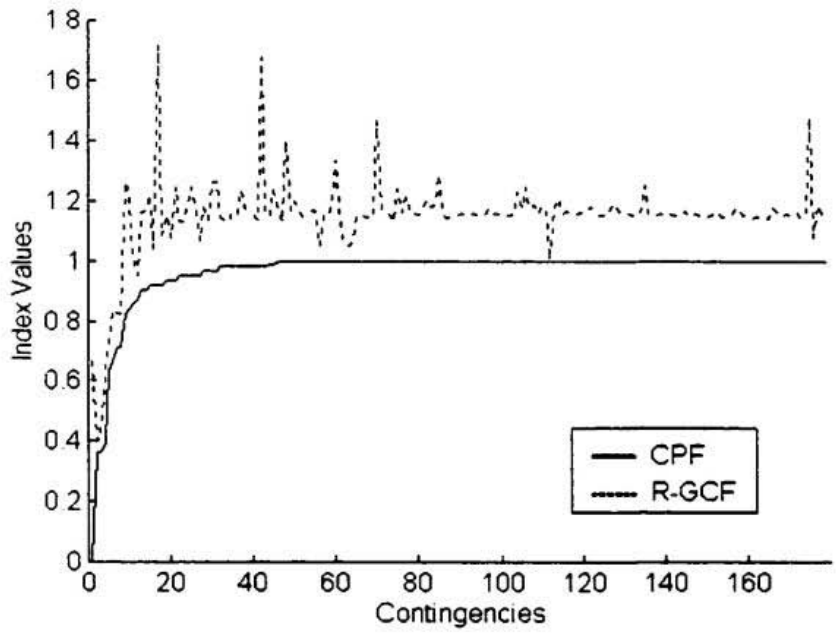

Figure 5.8 Normalized R-GCF index for the 118-bus power system
CPF : Continuation power flow
R-GCF : GCF by reselecting curve fitting points

Table 5.3 The 10 most critical branch outage contingency margins obtained by R-GCF and CPF for the 118-bus system

Branch outage		Line/	CPF margin [Exact]		R-GCF [Estimate]	
From	To	Transformer	MW (rank)	VS%	MW (rank)	VS%
Pre-contingency			4140	112.9	4598.7	125.37
8	5	T	980 (1)	25.9	3047.8 (4)	83.09
8	9	L	2100 (2)	57.252	2208.4 (1)	60.21
9	10	L	2120 (3)	57.252	2238.3 (2)	61.02
75	118	L	2200 (4)	59.978	2942.4 (3)	80.22
38	37	T	2980 (5)	80.425	3234.1 (5)	88.17
76	77	L	3060 (6)	83.152	3594.2 (8)	97.99
38	65	L	3220 (7)	87.241	3547.6 (6)	96.72
100	103	L	3220 (8)	87.241	3552.3 (7)	96.85
4	5	L	3580 (9)	96.783	4933 (172)	134.49
69	75	L	3600 (10)	98.146	4749 (158)	129.50

5.4.4 Simulation of the IEEE 300-bus system using R-GCF

When the R-GCF method is applied to the 150 most critical branch contingencies obtained by CPF, when VSTAB software is used, the normalized margins that result by R-GCF and CPF are presented in Figure 5.9. As seen in Figure 5.9, the margins obtained by R-GCF are much larger than those of CPF. However, the trend of the R-GCF can partially provide the severity of the branch contingencies. Compared with Figure 4.12, Figure 5.9 shows that the performance of GCF has been improved by reselecting the

curve fitting points. Table 5.4 shows that R-GCF has 2 misclassifications out of the 10 most critical branch outage contingencies.

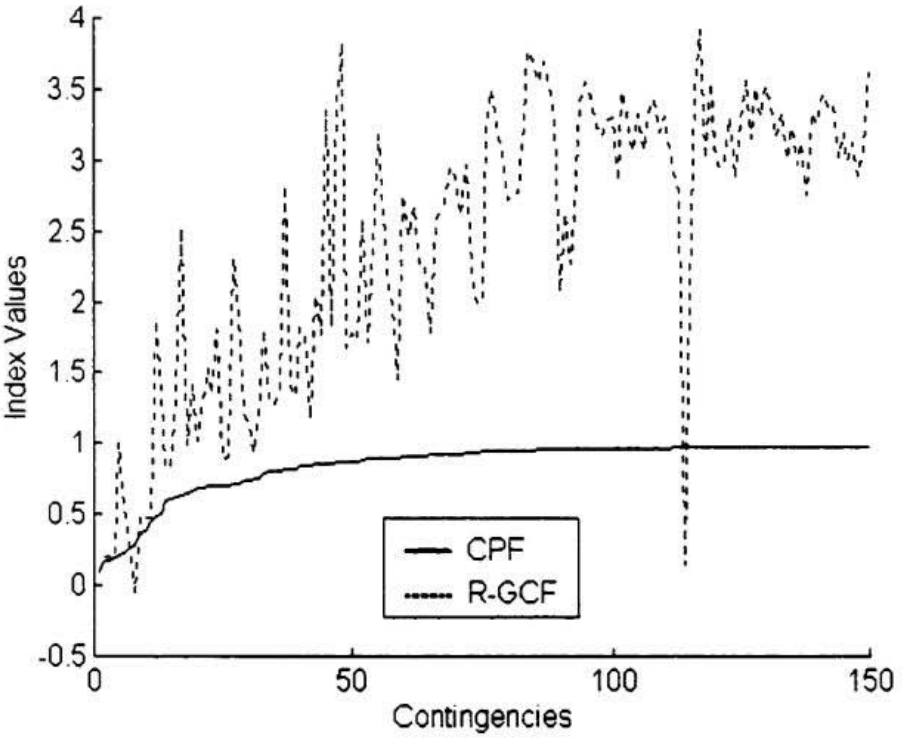

Figure 5.9 Normalized R-GCF index for the 300-bus power system

CPF : Continuation power flow

R-GCF : GCF by reselecting curve fitting points

Table 5.4 The 10 most critical branch outage contingency margins obtained by R-GCF and CPF for the 300-bus system

Branch outage		Line/	Rating	CPF margin [Exact]		R-GCF [Estimate]	
From	To	Transformer	(kV)	MW (rank)	VS%	MW (rank)	VS%
Pre-contingency				1140	4.9	3970	17.08
57	63	L	115	119.9 (1)	0.516	114.4 (2)	0.49
46	81	L	345	200.0 (2)	0.86	234.3 (6)	1.01
16	42	L	345	200.0 (3)	0.86	232.5 (5)	1.00
7071	71	T	13.8/115	219.9 (4)	0.946	228.2 (4)	0.98
231	232	T	345/138	246.2 (5)	1.059	1147.6 (18)	4.93
202	211	T	66/115	259.9 (6)	1.118	620.8 (11)	2.67
37	49	L	115	299.9 (7)	1.29	378.9 (7)	1.63
159	117	T	230/115	319.9 (8)	1.376	-54.55 (1)	-0.23
45	46	T	230/345	419.9 (9)	1.807	572.0 (10)	2.46
45	60	L	230	439.9 (10)	1.893	548.2 (9)	2.35

5.4.5 Simulation of the 600-bus system using R-GCF

Figure 5.10 shows the margins obtained by both the R-GCF and CPF methods for the 600-bus system. From Figure 5.10, it is seen that the R-GCF method can follow most of the CPF results with a few exceptions. From Table 5.5, it is evident that out of the 10 most critical branch outage contingencies, the R-GCF method misclassifies 2 of them. However, the R-GCF method gives the rank 149 when line 8-299 is broken, while its

actual rank of 2 is obtained by CPF. This wrong information is unacceptable for on-line power system security assessment. Therefore, the accuracy of R-GCF still needs to be improved.

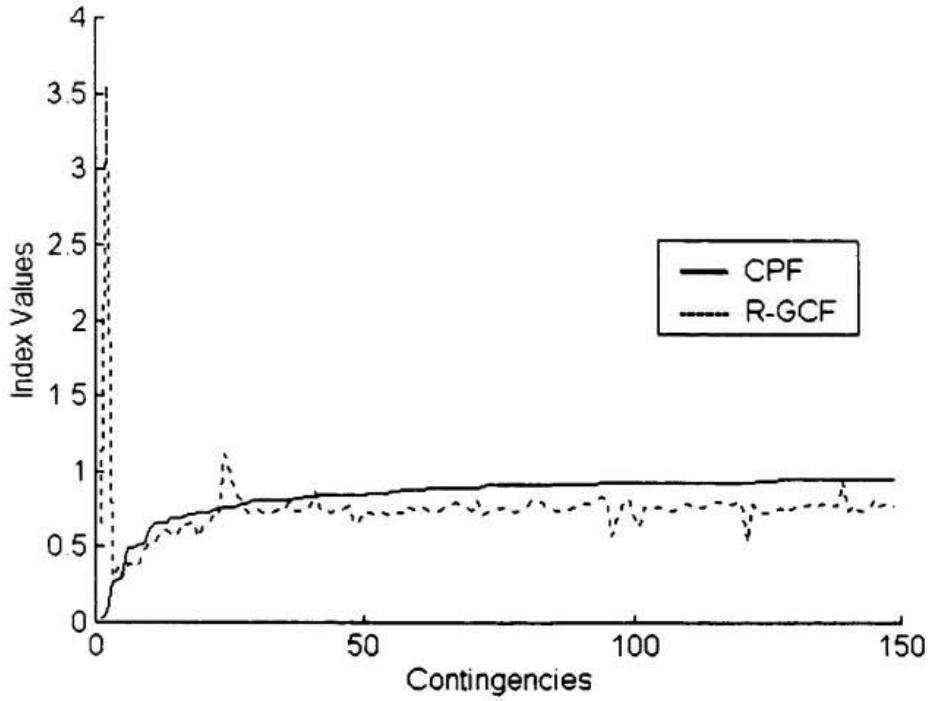

Figure 5.10 Normalized R-GCF index for the 600-bus power system
CPF : Continuation power flow
R-GCF : GCF by reselecting curve fitting points

Table 5.5 The 10 most critical branch outage contingency margins obtained by R-GCF and CPF for the 600-bus system

Branch outage From	To	Line/ Transformer	Rating (kV)	CPF margin [Exact] MW	VS%	R-GCF [Estimate] MW	VS%
Pre-contingency				1140	4.6	900	3.66
226	227	L	118	20.0 (1)	0.081	737.9 (23)	3.00
8	299	T	230/220	80.0 (2)	0.325	3977 (149)	16.17
16	350	L	500	300.0 (3)	1.22	273.5 (1)	1.11
9	15	L	500	319.9 (4)	1.301	406.2 (3)	1.65
15	19	L	500	340.0 (5)	1.382	331.6 (2)	1.35
92	108	T	220/24	549.3 (6)	2.233	440.0 (5)	1.79
92	110	T	220/24	549.2 (7)	2.233	440.0 (6)	1.79
93	112	T	220/24	572.7 (8)	2.329	417.2 (4)	1.70
93	113	T	220/24	572.8 (9)	2.329	540.1 (7)	2.20
459	464	L	118.05	700.0 (10)	2.846	591.8 (8)	2.41

5.4.6 Simulation of BC Hydro 197-bus system using R-GCF

The 197-bus power system is a simplified BC Hydro system. The load is increased only in main load centers located at the Lower Mainland and Vancouver Island, BC, Canada. The structure of single line power systems in these two areas is shown in Appendix B. The margins obtained by R-GCF in Figure 5.11 show that R-GCF can capture most of the severe contingencies, even though the margins are larger than actual

ones. Table 5.6 shows that out of the 10 most critical contingencies, this method misclassifies 2 of them.

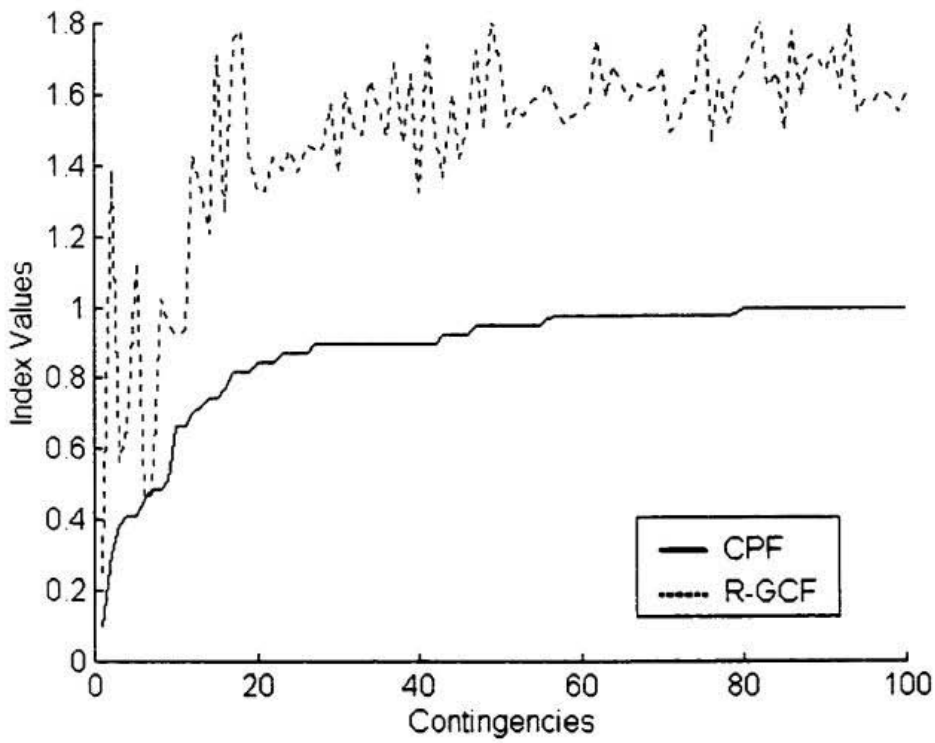

Figure 5.11 **Normalized R-GCF index for the 197-bus power system**
CPF : Continuation power flow
R-GCF : GCF by reselecting curve fitting points

Table 5.6 The 10 most critical branch outage contingency margins obtained by R-GCF and CPF for the 197-bus system

Branch outage From	To	Line/ Transformer	Rating (kV)	CPF margin [Exact] MW	VS%	R-GCF [Estimate] MW	VS%
Pre-contingency				780	23.65	1330	40.35
4144	4145	T	132/230	80 (1)	2.426	196.3 (1)	5.95
4074	4080	L	287	240 (2)	7.278	1084.1(21)	32.88
4087	4099	L	500	300 (3)	9.098	441.73 (4)	13.40
4058	4099	L	500	320 (4)	9.704	514.06 (5)	15.59
4143	4142	T	132/13.8	320 (5)	9.704	881.23 (10)	26.72
4032	4137	L	500	360 (6)	10.918	356.8 (2)	10.82
4032	4136	L	500	380 (7)	11.524	371.89 (3)	11.28
4046	4043	T	500/13.8	380 (8)	11.524	798.45 (9)	24.21
4028	4078	L	500	400 (9)	12.131	743.85 (8)	22.56
4015	4020	L	16.5	520 (10)	15.77	716.35 (6)	21.72

5.4.7 Simulation of Ontario Hydro 1254-bus system using R-GCF

The 1254-bus system is a simplified Ontario Hydro power system. Its main structure is presented in Appendix C. Once the R-GCF method is applied to this system, the margins acquired by R-GCF and CPF are shown in Figure 5.12. In this figure, the R-GCF results are oscillating around those of CPF. As seen in Table 5.7, the R-GCF method misclassifies 4 out of the 10 most critical branch outage contingencies.

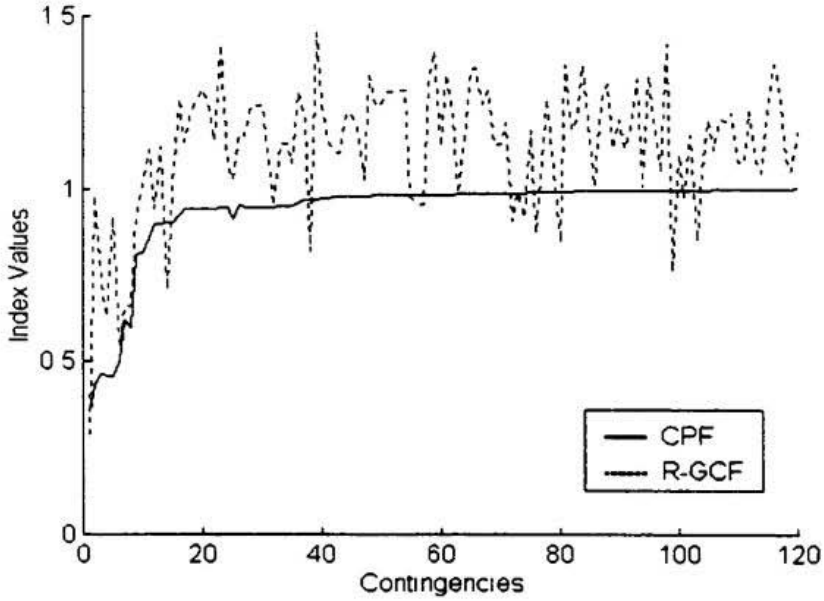

Figure 5.12 Normalized R-GCF index for the 1254-bus power system

CPF : Continuation power flow

R-GCF : GCF by reselecting curve fitting points

Table 5.7 The 10 most critical branch outage contingency margins obtained by R-GCF and CPF for the 1254-bus system

Branch outage From To	Line/ Transformer	Rating (kV)	CPF margin [Exact]		R-GCF [Estimate]	
			MW (rank)	VS%	MW (rank)	VS%
Pre-contingency			900	4.20	1052	4.9
11940 12174	L	220	320.04 (1)	1.49	259.78 (1)	1.21
12635 12638	L	220	390.03 (2)	1.82	881.97 (23)	4.11
12636 12637	L	220	419.99 (3)	1.96	653.71 (7)	3.05
12595 12600	L	220	410.02 (4)	1.91	567.86 (3)	2.65
12596 12600	L	220	410.02 (5)	1.91	828.2 (16)	3.86
10826 10856	L	118.05	452.16 (6)	2.11	491.94 (2)	2.29
12555 12615	L	220	560.03 (7)	2.61	593.65 (4)	2.77
12555 12616	L	220	540.02 (8)	2.52	593.92 (5)	2.77
12695 12600	L	345	729.16 (9)	3.40	827.3 (15)	3.86
12696 12600	L	345	731.35 (10)	3.41	910.5 (29)	4.25

From the above simulation results, it is seen that the R-GCF method can rank the contingencies of the 5-bus and 39-bus systems very well, and that the margins obtained by R-GCF are very close to those of CPF. However, for the 118-bus, 300-bus, 600-bus, BC Hydro 197-bus, and Ontario Hydro 1254-bus systems, the trend of the R-GCF margins can only partially detect the severety of branch outage contingencies with several misclasifications, and the differences between R-GCF and CPF are still not acceptable.

5.5 Simulation Results for Reselecting Curve Fitting Points and Filtering out Unreasonable Nose Points

For a certain contingency, if we check every nose point obtained by GCF at each load bus of the previously studied power systems, it is visible that some noses are incredibly big and some noses are even smaller than the current operating point (shown in Figure 5.3 and Figure 5.4). These abnormal phenomena are caused by the approximated quadratic equation.

To eliminate these unreasonable nose points, a 'band-pass filter', introduced in chapter 5.3, is employed. If the nose points obtained by GCF are out of the band interval, which is from the operating point to operating point + 2 × margin, those nose points will not be counted. By applying the two improved methods, *reselecting curve fitting points* (R-GCF) and *filtering out unreasonable nose points* (F-GCF), to the 118-bus, 300-bus, 600-bus, BC Hydro 197-bus, and Ontario Hydro 1254-bus power systems, estimates of the stability margins can be obtained. These results are presented in Figure 5.13 to Figure

5.17 for these power systems, respectively. Detailed results are also listed in Table 5.8 to Table 5.12.

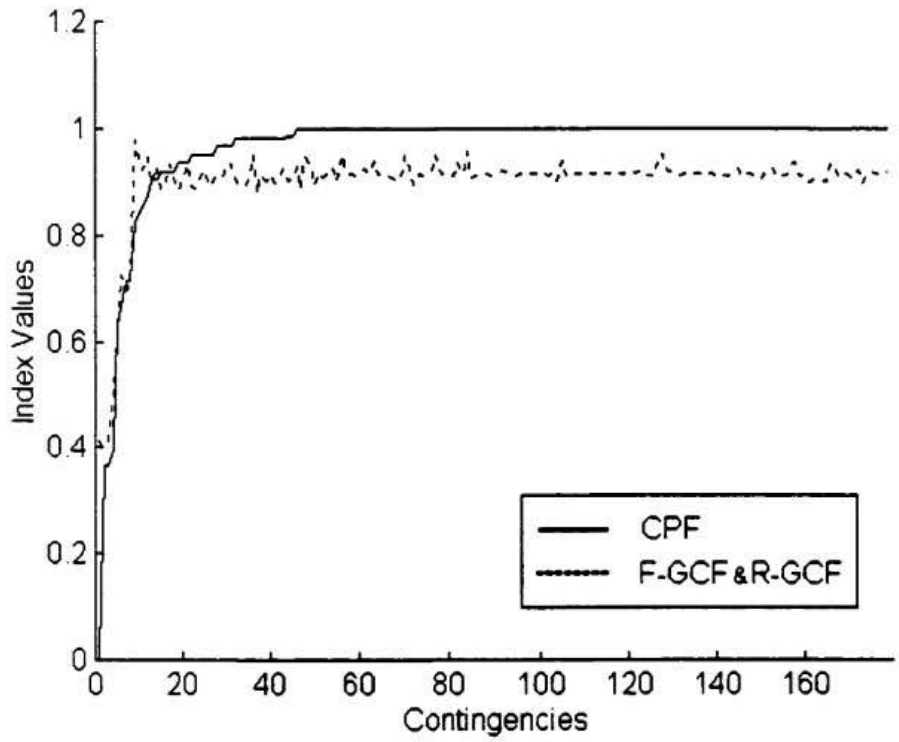

Figure 5.13 Normalized F-GCF & R-GCF index for the 118-bus power system

CPF : Continuation power flow

F-GCF & R-GCF : GCF by using both improved methods

Table 5.8 The 10 most critical branch outage contingency margins obtained by F-GCF & R-GCF, and CPF for the 118 bus-system

Branch outage		Line/	Rating	CPF margin [Exact]		F-GCF & R-GCF [Estimate]	
From	To	Transformer	(kV)	MW (rank)	VS%	MW (rank)	VS%
Pre-contingency				4140	112.9	3852	105
8	5	T	-	980 (1)	25.9	2245.9 (3)	61.23
8	9	L	-	2100 (2)	57.25	2208.4 (1)	60.21
9	10	L	-	2120 (3)	57.25	2238.3 (2)	61.02
75	118	L	-	2200 (4)	59.97	2548.4 (4)	69.47
38	37	T	-	2980 (5)	80.42	2879.4 (5)	78.50
76	77	L	-	3060 (6)	83.15	3232 (8)	88.11
38	65	L	-	3220 (7)	87.24	3148.1 (6)	85.82
100	103	L	-	3220 (8)	87.24	3188.4 (7)	86.92
4	5	L	-	3580 (9)	96.78	4029.6(179)	109.86
69	75	L	-	3600 (10)	98.14	3920.8(169)	106.89

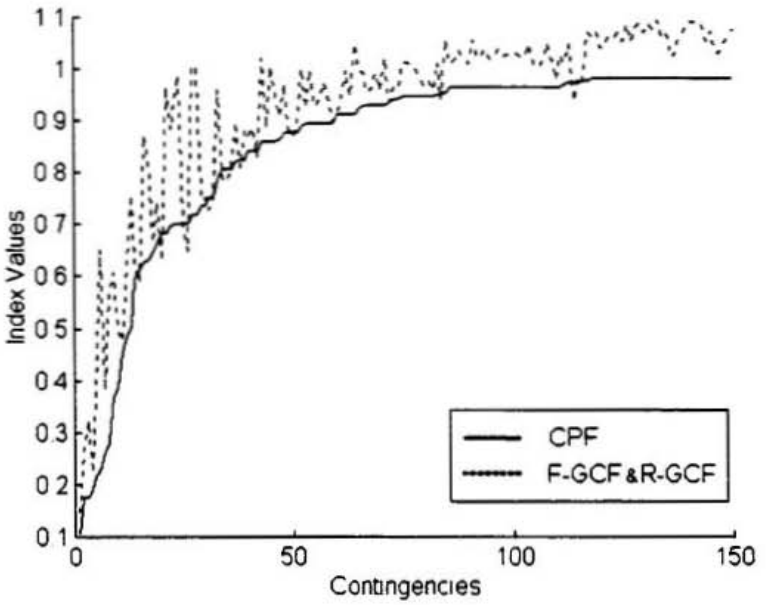

Figure 5.14 Normalized F-GCF & R-GCF index for the 300-bus power system

CPF : Continuation power flow

F-GCF & R-GCF : GCF by using both improved methods

Table 5.9 The 10 most critical branch outage contingency margins obtained by F-GCF & R-GCF, and CPF for the 300-bus system

Branch outage From	To	Line/ Transformer	Rating (kV)	CPF margin [Exact] MW (rank)	VS%	F-GCF & R-GCF [Estimate] MW (rank)	VS%
Pre-contingency				1140	4.9	1303	5.6
57	63	L	115	119.9 (1)	0.516	168.62 (1)	0.725
46	81	L	345	200.0 (2)	0.86	300.13 (3)	1.291
16	42	L	345	200.0 (3)	0.86	368.0 (4)	1.583
7071	71	T	13.8/115	219.9 (4)	0.946	253.28 (2)	1.09
231	232	T	345/138	246.2 (5)	1.059	576.21 (5)	2.479
202	211	T	66/115	259.9 (6)	1.118	785.5 (16)	3.379
37	49	L	115	299.9 (7)	1.29	434.1 (6)	1.867
159	117	T	230/115	319.9 (8)	1.376	665.83 (9)	2.864
45	46	T	230/345	419.9 (9)	1.807	718.6 (11)	3.091
45	60	L	230	439.9 (10)	1.893	592.4 (8)	2.548

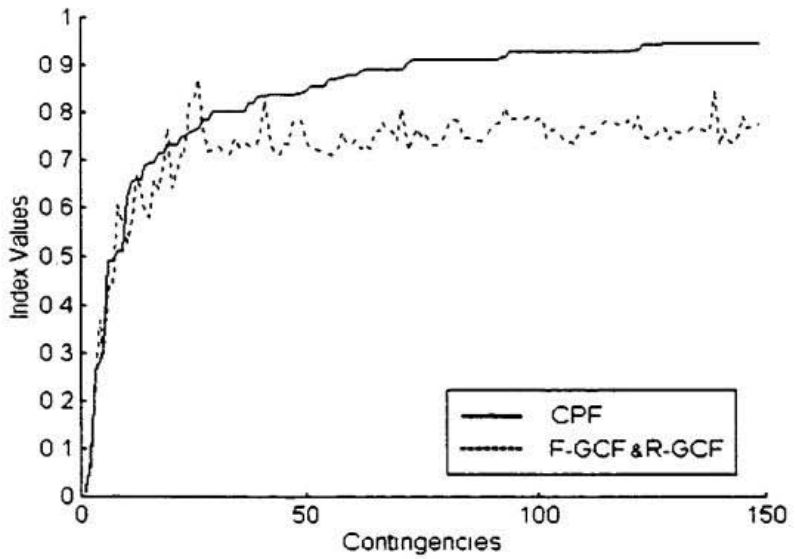

Figure 5.15 Normalized F-GCF and R-GCF index for the 600-bus power system

CPF : Continuation power flow

F-GCF & R-GCF : GCF by using both improved methods

Table 5.10 The 10 most critical branch outage contingency margins obtained by F-GCF & R-GCF, and CPF for the 600-bus system

Branch outage From	To	Line/ Transformer	Rating (kV)	CPF margin [Exact] MW (rank)	VS%	F-GCF & R-GCF [Estimate] MW (rank)	VS%
Pre-contingency				1140	4.6	910	3.7
226	227	L	118	20 (1)	0.081	8.67 (1)	0.035
8	299	T	230/220	80.01 (2)	0.325	90.97 (2)	0.37
16	350	L	500	300.01 (3)	1.22	275.99 (3)	1.122
9	15	L	500	319.99 (4)	1.301	412.43 (5)	1.677
15	19	L	500	340.01 (5)	1.382	333.95 (4)	1.358
92	108	T	220/24	549.29 (6)	2.233	488.02 (6)	1.984
92	110	T	220/24	549.29 (7)	2.233	488.02 (7)	1.984
93	112	T	220/24	572.76 (8)	2.329	678.52 (11)	2.759
93	113	T	220/24	572.76 (9)	2.329	637.83 (9)	2.593
459	464	L	118.05	700 (10)	2.846	591.76 (8)	2.406

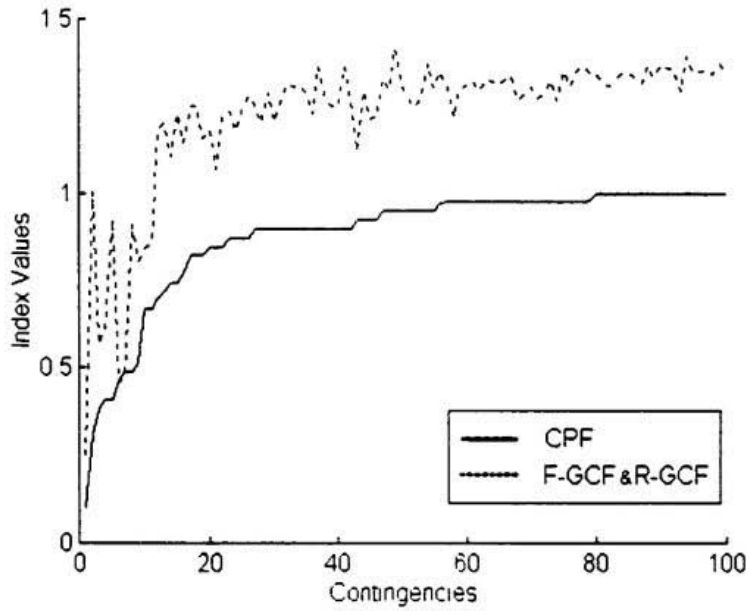

Figure 5.16 Normalized F-GCF &R-GCF index for the 197-bus power system

CPF : Continuation power flow

F-GCF & R-GCF : GCF by using both improved methods

Table 5.11 The 10 most critical branch outage contingency margins obtained by F-GCF & R-GCF, and CPF for the 197-bus system

Branch outage From	To	Line/ Transformer	Rating (kV)	CPF margin [Exact] MW (rank)	VS%	F-GCF & R-GCF [Estimate] MW (rank)	VS%
Pre-contingency				780	23.6	1083	32.8
4144	4145	T	132/230	80 (1)	2.4	196.3 (1)	5.95
4074	4080	L	287	240 (2)	7.3	781.2 (11)	23.7
4087	4099	L	500	300 (3)	9.1	441.7 (4)	13.4
4058	4099	L	500	320 (4)	9.7	481.7 (5)	14.6
4143	4142	T	132/13.8	320 (5)	9.7	719.1 (10)	21.8
4032	4137	L	500	360 (6)	10.9	356.8 (2)	10.8
4032	4136	L	500	380 (7)	11.5	371.8 (3)	11.3
4046	4043	T	500/13.8	380 (8)	11.5	710.9 (9)	21.5
4028	4078	L	500	400 (9)	12.1	629.1 (6)	19.1
4015	4020	L	16.5	520 (10)	15.7	654.2 (7)	19.8

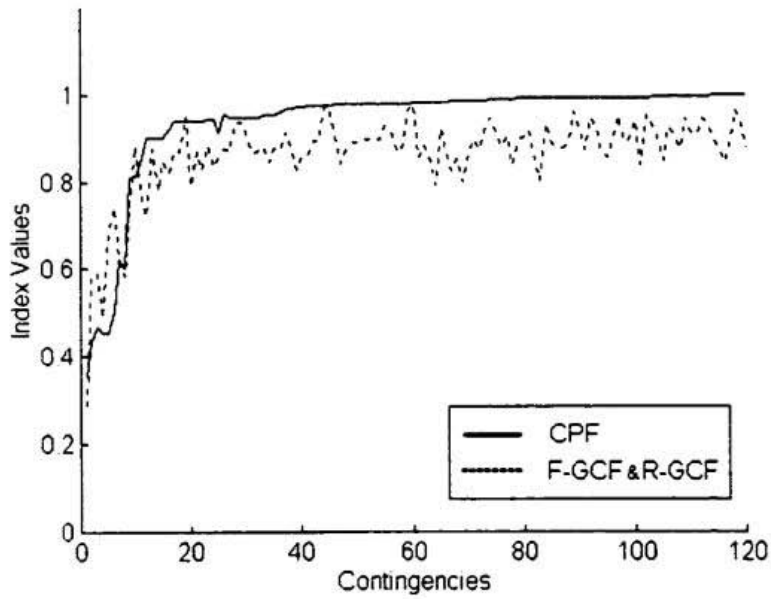

Figure 5.17 Normalized F-GCF & R-GCF index for the 1254-bus power system

CPF : Continuation power flow

F-GCF & R-GCF : GCF by using both improved methods

Table 5.12 The 10 most critical branch outage contingency margins obtained by F-GCF & R-GCF, and CPF for the 1254-bus system

Branch outage From To	Line/ Transformer	Rating (kV)	CPF margin [Exact]		F-GCF & R-GCF [Estimate]	
			MW (rank)	VS%	MW (rank)	VS%
Pre-contingency			900	4.20	1046	4.88
11940 12174	L	220	320.04 (1)	1.49	259.7 (1)	1.21
12635 12638	L	220	390.03 (2)	1.82	525.9 (5)	2.45
12636 12637	L	220	419.99 (3)	1.96	531.5 (7)	2.48
12595 12600	L	220	410.02 (4)	1.91	440.4 (3)	2.05
12596 12600	L	220	410.02 (5)	1.91	615.6 (6)	2.87
10826 10856	L	118.05	452.16 (6)	2.11	667.6 (10)	3.11
12555 12615	L	220	560.03 (7)	2.61	561.2 (9)	2.62
12555 12616	L	220	540.02 (8)	2.52	526.7 (2)	2.46
12695 12600	L	345	729.16 (9)	3.40	677.5 (65)	3.16
12696 12600	L	345	731.35 (10)	3.41	794.2 (97)	3.70

Compared to the figures presented in section 5.4, these figures obtained by filtering out unreasonable nose points (F-GCF), as well as reselecting curve fitting points (R-GCF), well approximate the CPF curves. Moreover, the nose points obtained by the improved GCF method are very close to the desired ones. From these tables, it is evident that out of the ten most critical branch outage contingencies, improved GCF method misclassifies two for the 118-bus system, two for the 300-bus system, one for the 600-bus system, one for the BC Hydro 197-bus system, and two for the Ontario Hydro 1254-bus system.

5.6 Summary

In this chapter, two improved methods, *reselecting curve fitting points* (R-GCF) and *filtering out unreasonable nose points* (F-GCF), for Generalized Curve Fitting (GCF) method were proposed. Contingency screening and ranking for voltage stability was carried out on a variety of power systems by using the first method alone and a combination of both methods. Their ranking results were also compared with the results obtained by the well-known Continuation Power Flow (CPF) method. Table 5.13 compares the results of GCF and its improved methods with the accurate contingency ranking results provided by VSTAB. This table shows that the proposed methods improve the accuracy of the GCF method dramatically. Table 5.14 provides the computation performance of the improved GCF (F-GCF & R-GCF) method, on a Dec-Alpha Workstation.

Table 5.13 The misclassification of the proposed methods

System	39-bus	118-bus	300-bus	600-bus	197-bus	1254-bus
GCF	1	6	6	9	2	10
R-GCF	0	2	2	2	1	4
F-GCF & R-GCF	N/A	2	2	1	1	1

Table 5.14 CPU time for the 10 most critical contingencies to different systems

System	118-bus	300-bus	600-bus	197-bus	1254 bus
CPU time in second*	5.02	18.15	34.37	3.09	20.2
Total load buses monitored by modified GCF in study area	65	231	445	40**	300**

* CPU time does not include the time to determine the three curve fitting points
** Load is increased only at these buses located at selected load centers

The simulation results show that the proposed methods, *reselecting curve fitting points* and *filtering out unreasonable nose points*, have the ability to provide a fast estimate of voltage stability margins, and thus select the most severe contingencies.

Chapter 6

Conclusions

6.1 Contributions of this research

Power system operators have a vital role to play in ensuring system security and efficient operation. The primary role of power system operators is to ensure that the system is operating in a healthy condition and take corrective action in the event of any contingency. In performing this task, the system operator has the help of powerful tools like the Energy Management System (EMS). One of the important functions of the EMS is voltage stability assessment, which includes Contingency Screening and Ranking (CS&R). It is expected that in the near future, EMS will be equipped with capabilities for on-line voltage stability assessment functions, so as to enable the system operator to implement preventive or corrective controls.

In order to quantify voltage instability and rank the most critical contingencies of a power system, researchers have recently developed a number of voltage stability indices and contingency screening and ranking indices. This thesis has studied two popular voltage stability methods and presented simulations on test power systems. The first is the well-known continuation power flow (CPF) method. It is found that the

voltage collapse point obtained by CPF is accurate, but the CPF method requires significant computation time [5]. The second method investigated for voltage stability index is the 'minimum singular value' method. When a power system is under stressed conditions, the minimum singular value of the Jacobian matrix of the power flow equations will also decrease. At the collapse point, its Jacobian matrix becomes singular. However, the behavior of the minimum singular value is non-linear, especially when the dimension of the Jacobian matrix is decreased due to some PV buses (voltage controlled buses) changing to PQ buses (load buses). These indices are all computation intensive and require repeated power flow solutions. For large power systems, this can be quite time-consuming, and heavy investments in terms of computer hardware are required if real-time response is desired. Therefore, it is impractical to use these indices for on-line contingency screening and ranking. This has been the motivation to find fast algorithms, which are inexpensive in terms of computation for CS&R.

In this thesis, several existing CS&R methods are reviewed. Then, two of them, Reactive Support Index (RSI) and Generalized Curve Fitting (GCF) methods, are investigated on various power systems. RSI method is a new, fast ranking algorithm proposed by BC Hydro for CS&R. It is defined as the extra amount of reactive generation from all the existing dynamic Var devices (generation, SVC, etc) for each contingency, when their reactive limits are ignored. GCF method is another rapid CS&R method, which assumes that each PV curve of a load bus can be approximated as a quadratic equation. The stability margin obtained by GCF is the average of the margins corresponding to the load buses in the study area. To assess the performance of these two methods for CS&R, simulations are carried out at a certain load increase pattern and

generator dispatch scheme on various power systems, such as 5-bus, 39-bus, 118-bus, 300-bus, 600-bus, BC Hydro 197-bus, and Ontario Hydro 1254-bus power systems. Their results are also compared with those of CPF method, which are considered accurate. CPF simulations show that only a limited number of contingencies have a significant impact on the load margins to these test systems, while most contingencies would not affect the security of power systems greatly. Therefore, it is very important to capture these few critical contingencies from a large number of well-defined contingency cases. RSI results show that this method can obtain several most of the critical contingencies of all the test systems, except some misclassifications. However, the performance of GCF method is quite unstable. For 5-bus, 38-bus, and BC Hydro 197-bus power systems, it can capture most of the critical contingencies with some exceptions; for the other test systems, GCF cannot provide any useful information about the severity of each contingency.

To enhance the performance of GCF, a novel method derived from GCF for CS&R is proposed by the author. Based on the assumption that each PV curve of a load bus can be approximated as a quadratic equation (which is not always true), this can cause significant errors. For a certain contingency, it is found that some estimated nose points are far away from the actual ones. In some cases, the margin obtained by GCF can even be negative which is abnormal. To reduce the abnormal phenomena, two improved methods, *reselecting curve fitting points* and *filtering out unreasonable nose points*, were employed. The first method reselects the three fitting points: the first point is kept fixed, while the other two are rearranged to be closer to the collapse point, especially the last one. The second method employed a 'band-pass filter'. If the nose points obtained by GCF exceed the operating point by twice the margin, these nose points will not be

counted. The simulations were also carried out on the test systems by using the two proposed methods.. The results showed that the proposed methods have the ability to provide a fast estimate of voltage stability margin and thus the most severe contingencies. Therefore, the proposed methods have the potential to be implemented in any on-line voltage stability assessment scheme.

6.1.1 Summary of the main contributions of this research

- Application of Continuation Power Flow (CPF) and Minimum Singular Value for voltage stability analysis.
- Analysis of six available methods for contingency screening and ranking.
- Application of Continuation Power Flow (CPF), Reactive Support Index (RSI), and Generalized Curve Fit (GCF) for contingency screening and ranking for sample power systems including BC Hydro and Ontario Hydro systems.
- Development of new methods for contingency screening and ranking. These methods incorporate the 'reselecting curve fitting points' and ' filtering out unreasonable nose points' techniques.
- Evaluation of the proposed methods for contingency screening and ranking of different power systems.
- The research presented in this thesis shows that the proposed methods can provide a fast estimate of voltage stability margins for branch outage contingencies. These estimates can then be used to rank potential contingencies. The computation time for this method is not very large. These methods have the potential to be implemented in any on-line voltage stability assessment scheme. Once the potential contingencies are

ranked, control actions can be implemented to enhance the security of the power system with respect to voltage instability.

6.2 Suggestions for future work

The work reported in this thesis can be extended in the following areas:

- The proposed methods still use all the PQ buses at all studied areas, which are the same as the GCF. To speed up the calculation, it is possible to choose a few 'typical' PQ buses for curve fitting instead of all PQ buses in load increase areas. The participation factor proposed in [30] might be one of the candidates to decide the 'typical' PQ buses.
- To improve the accuracy of the proposed methods, the combination of this method with the *Iterative filtering* method proposed in [5] is a potential approach.
- The objective of contingency ranking for on-line voltage stability assessment is to assist in the implementation of suitable preventive and corrective control actions to enhance the security of the power system. There is a significant potential for research in this direction.
- Recently there has been considerable interest in the use of FACTS (Flexible AC Transmission Systems) devices for power system control. The effectiveness of these devices for voltage stability enhancement should be investigated.

References

[1] P. Kundur, *Power System Stability and Control*, McGraw-Hill, Inc, New York, 1993.

[2] J. Grainger, W. Stevenson, *Power System Analysis*, McGraw-Hill, Inc, New York, 1994.

[3] C.W. Taylor, *Power System Voltage Stability*, McGraw-Hill, Inc., New York, 1994.

[4] G.C. Ejebe, G.D. Irisarri, etc., "Methods for Contingency Screening and Ranking for Voltage Stability Analysis of Power Systems", IEEE Trans. on Power Systems, Vol. 11, No. 1, February 1996, pp. 350-356.

[5] E. Vaahedi, C. Fuchs, W. Xu, Y. Mansour, H. Hamadanizadeh, and G. K. Morison, "Voltage Stability Contingency Screening and Ranking," IEEE Trans. on Power Systems, Vol. 14, No.1, February, 1999, pp. 256-265.

[6] H.D. Chiang, C.S. Wang and A.J. Flueck, "Look-ahead Voltage and Load Margin Contingency Selection Functions for Large Scale Power Systems," IEEE Trans. on Power Systems, Vol. 12, No. 1, February, 1997, pp. 173-180

[7] S.Greene, I. Dobson, F.L. Avlarado, "Contingency Ranking for Voltage Collapse via Sensitivities from a Single Nose Curve", IEEE Trans. on Power Systems, Vol. 14, No.1, February, 1999, pp. 232-240.

[8] S. C. Vallabhan, *Application of Artificial Neural Networks for Voltage Stability Evaluation of Power Systems*, M.Eng. thesis, Memorial University of Newfoundland, Canada, August 1995.

[9] G. D. Irisarri, X. Wang, J. Tong, S. Mokhari, "Maximum Loadability of Power Systems using Interior Point Non-Linear Optimization Method", IEEE Trans. on Power Systems, Vol., 12, No. 1, February 1997, pp. 162-174.

[10] B. Jeyasurya, "Artificial Neural Networks for Power System Steady-state Voltage Instability Evaluation", Electrical Power Research, Vol. 29, 1994, pp. 85-90.

[11] Y. Mansour, W. Xu, F. Alvarado, C. Rinzin, "SVC Placement Using Critical Modes of Voltage Instability", IEEE Trans. on Power Systems, Vol.. 9, No. 2, May 1994, pp. 757-763.

[12] R. P. Klump, T. J. Overbye, "Assessment of Transmission System Loadability", IEEE Trans. on Power Systems, Vol. 12, No. 1, February 1997, pp. 416-423.

[13] N. Yorino, S. Harada, H. Cheng, "A Method to Approximate a Closest Loadability Limit Using Multiple Load Flow Solutions", IEEE Trans. on Power Systems, Vol. 12, No. 1, Fabruary 1997, pp. 424-429.

[14] Z. Yang, P. Cao, M. L. Crow, "A New Voltage Stability Index Based on the Continuation Power Flow Method", Proc. of the 30th North American Power Symposium (NAPS98), Cleveland State University, Cleveland, Ohio, October,1998, pp. 42-47

[15] Einar Larsen, Nicholas Miller, Stig Nilsson, and Lindgren, "Benefits of GTO-Based Compensation Systems For Electric Utility Applications," IEEE Trans. on Power Delivery, vol. 7, No. 4, October 1992, pp. 2056-2062

[16] Laszlo Gyugyi, "Dynamic Compensation of AC Transmission Lines By Solid-state Synchronous Voltage Sources," IEEE Trans. on Power Delivery, Vol. 9. No. 2, April, 1994, pp. 904-911

[17] Voltage Stability Analysis Program – VSTAB Version 4.1, Power Tech Lab Inc., B.C, Canada, 1996.

[18] Stagg and El-Abiad, "Computer Methods in Power System Analysis", McGraw-Hill Book Company, 1968

[19] V. Ajjarapu and C. Christy, " The Continuation Power Flow: A Tool for Steady Voltage Stability Analysis," IEEE Trans. on Power Systems, Vol. 8, No. 1, Feb. 1992, pp. 416-423.

[20] C.A. Canizares and F.L. Alvarado, "Point of Collapse and Continuation Methods for Large AC/DC Systems," IEEE Trans. on Power Systems, Vol. 8, No. 1, Feb. 1993, pp 1-7.

[21] V. A. Venokov, V.I. Stroes, V. I. Indelchuk, and V. I. Tatasov, " Estimation of Electic Power System steady State Stability in Load Flow Calculations", IEEE Trans. on Power Systems, Vol., 94, No. 3, May 1975, pp. 1034-1038.

[22] MATLAB version 5.1, The MathWorks Inc., Natick, Massachusetts, 1997

[23] A. Berizzi, P. Finazzi, D. Dosi, and P. Marannino, " First and Second Order Methods for Voltage Collapse Assessment and Security Enhancement", IEEE Trans. On Power Systems, Vol., 13, No., 2, May, 1998, pp. 543-551

[24] Z. Feng, V. Ajjarapu, D.J. Maratukulam, "A Practical Minimum Load Shedding Strategy to Mitigate Voltage Collapse", IEEE Trans. on Power System, Vol. 13, No. 4, Nov. 1998, pp. 1285-1291

[25] X. Wang, G.C. Ejebe, J. Tong, J.G. Waight, "Preventive/Corrective Control for Voltage Stability Using Direct Interior Point Method", IEEE Trans. on Power Systems, Vol. 13, No. 3, Aug. 1998, pp. 878-883.

[26] H.D. Chiang and R. Jean-Jumeau, "Toward a Practical Performance Index for Predicting Voltage Collapse in Electric Power Systems," IEEE Trans. on Power Systems, Vol. 10, No. 1, March 1995, pp. 582-592.

[27] Y. Tamura, H Mori, and S. Iwamoto, "Relationship Between Voltage Instability and Multiple Load Flow Solutions in Electric Power Systems", IEEE Trans. on Power Apparatus and System, Vol. PAS-102, May 1983, pp. 1115-1123.

[28] Z. Jia, B. Jeyasurya, "Contingency Analysis for on-line voltage stability assessment", the Eighth Newfoundland Electrical and Computer Engineering Conference (NECEC'98), November, 1998, Memorial University, St. John's, Newfoundland.

[29] Z. Jia, B. Jeyasurya, "Contingency Ranking for On-line Voltage Stability Assessment" , accepted for publication in IEEE Transactions on Power Systems, letter from IEEE Power Engineering Society, June 7, 1999.

[30] B. Gao, G. K. Morison, and P.Kundur, " Voltage Stability Evaluation Using Model Analysis", IEEE Trans. on Power Systems, Vol7, No.4, November 1992, pp. 1529-1536.

[31] Yokout Mansour, "Suggested Techniques for Voltage Stability Analysis", Report No. 93TH0620-5PWR, IEEE Power Engineering Society,1993

Appendix A

Summary of Different Power System Models

A.1 5-bus Power System

Table A.1 5-bus power system component data

Buses	5
Generators	2
Lines	7

Table A.2 5-bus power system base-case load flow summary

	Real Power (MW)	Reactive Power (Mvar)
From generation	149.62	13.85
To load	145.00	30.00
From line charging	0.00	29.99
To losses	4.62	13.87

System diagram is shown in Figure 4.1.

A.2 New England 39-bus Power System

Table A.3 New England 39-bus power system component data

Buses	39
Generators	11
Bus shunts	2
Lines	35
Transformers	13

Table A.4 New England 39-bus system base case load flow summary

	Real Power (MW)	Reactive Power (Mvar)
From generation	6192.55	1108.29
To load	6150.50	1508.90
To bus shunts	0.00	-213.39
From line charging	0.00	1120.62
To losses	42.04	933.21

System diagram is shown in Figure 4.9.

A.3 IEEE 118-bus Power System

Table A.5 IEEE 118-bus power system component data

Buses	118
Generators	54
Bus shunts	14
Lines	177
Transformers	9

Table A.6 IEEE 118-bus power system base case load flow summary

	Real Power (MW)	Reactive Power (Mvar)
From generation	3803.40	0.00
To load	3668.00	1438.00
To bus shunts	0.00	-84.41
From line charging	0.00	1338.86
To losses	133.03	784.62

A.4 IEEE 300-bus Power System

Table A.7 IEEE 300-bus power system component data

Buses	300
Generators	69
Bus shunts	29
Lines	304
Transformers	106

Table A.8 IEEE 300-bus power system base case load flow summary

	Real Power (MW)	Reactive Power (Mvar)
From generation	23200.44	8014.65
To load	23246.87	7787.97
To bus shunts	1.19	599.63
From line charging	0.00	5901.35
To losses	410.88	5528.35

A.5 600-bus Power System

Table A.9 600-bus power system component data

Buses	600
Generators	123
Bus shunts	368
Lines	1019
Transformers	372

Table A.10 600-bus power system base case load flow summary

	Real Power (MW)	Reactive Power (Mvar)
From generation	25148.90	6838.50
To load	24594.60	14112.10
To bus shunts	0.00	-10048
From line charging	0.00	6564.2
To losses	555.30	9339.70

Appendix B

197-bus BC Hydro Power System Summary

One of the power system models used in the research is BC Hydro 197-bus power system. In this power system, most of the available sources of hydroelectric power are distant from the southwest part of the province, where most of the demand is located. Figure B.1 shows the entire 500kV network and the subtransmisison network of the major load centers of Lower Mainland (around the city of Vancouver) and the south part of Vancouver Island (around the city of Victoria). The transmission network is interconnected with the TransAlta Utilities system in the Province of Alberta, the West Kootenay power and Light System in the southeast part of British Columbia, and the interconnected Western System of the U. S. A in the south. Figure B.2 shows the geographic location of BC Hydro transmission network.

The major generation system of BC Hydro consists of those on the Peace and Columbia Rivers. (Table B.1 shows the information of the main power plants of BC Hydro power system) [31]. The Peace River system (G. M. Shrum and Peace Canyon generating stations), located at the northern part of the Province, has a generating capacity of 3400 MW. The majority of this capacity is transmitted about 1000 km through 500 kV transmission to the load centers. The Columbia River system (Mica, Revelstoke, Seven Miles, and Kootenay Canal generating stations), located in the south interior region of the province, has a generating capacity of 4730 MW at distances

ranging from 200 to 500 km from the load centers. The transfer over the part of the 500 kV network feeding the Lower Mainland and Vancouver Island is limited by voltage stability [31].

The BC Hydro power system data file used in the research is generated using the power system model for the WSCC (Western Systems Coordination Council) 8313-bus power system PTI file. Table B.2 shows the WSCC 8313-bus power system component data, and Table B.3 shows the WSCC 8313-bus power system base case load flow summary. The data are obtained from the web site: http://www.ferc.fed.us/electric/f715/f715data.htm. These data are for the 1998 summer loading condition.

The general procedure for the derivation of the 197-bus BC Hydro power system data file is shown below:

(1) Obtain the basic power system parameters (bus data and transmission line data) from WSCC.RAW file on the above website and change it to CDF (IEEE Common Data Format) file.

(2) Find the 11 tie transmission lines connecting BC Hydro power system to the other subsystems and all the power transferred through the tie lines using Powerworld Viewer software (test edition), which is available on web site: http://www.powerworld.com.

(3) Cut off all the tie transmission lines between BC Hydro and all the other subsystems, and install the equivalent real power and reactive power exchange through the tie lines on the buses in BC Hydro accordingly.

(4) Change initial values for iteration in the new BC Hydro power system data file so that the initial values are close to the converged value for power flow. Thus, the final equivalent BC Hydro 197-bus power system CDF data file is obtained. Table B.4 shows the BC Hydro 197-bus power system component data; table B.5 shows the BC Hydro 197-bus power system base case load flow.

This BC Hydro 197-bus power system load flow data is used for contingency screening and ranking.

Table B.1 BC Hydro main power plant summary

Power Station Name	Type (Hydro or Thermal)	Capacity (MW)	Bus Number	Power Generation (MW)	Power Generation (Mvar)	Terminal Voltage (P.U / kV)	Voltage Angle (Degree)
Burrard	Thermal	912	4015	0	-138.32	0.965 / 15.9	-36.40
Cheakmus	NA*	NA	4026	144.00	18.74	1.02 / 14.1	-24.25
Gorden M. Shrum (G. M. S)	Hydro	2730	4042	1122.00	-205.35	0.978 / 13.5	-1.23
			4043	663.39	261.67	1.049 / 14.5	-2.24
			4047	400.00	-96.9	0.979 / 13.5	-2.65
Kootenay Canal	Hydro	549	4064	529.00	-46.76	0.969 / 13.4	4.52
Kelly L. k	NA	NA	4069	0	21.55	1.014 / 12.7	-25.64
L. M. EQIV	NA	NA	4081	209.00	8.53	1.00 / 13.8	-32.99
Mica	Hydro	1736	4088	1700.00	38.58	0.961 / 15.4	6.50
Peace Canyon	Hydro	700	4111	530.00	23.15	0.985 / 13.6	-3.47
Revel Stoke	Hydro	1843	4117	1818.75	105.00	1.009 / 16.1	0
Seven Mile	Hydro	594	4130	590.00	-19.86	0.985 / 13.6	-1.02
V. I. T	NA	NA	4140	0	-36.09	1.006 / 12.7	-45.84
			4141	0	-36.09	1.023 / 13.0	-45.87
VA. IS. EQ	NA	NA	4142	279.00	-28.06	1.00 / 13.8	-40.17
Whatshan	NA	NA	4153	55.00	9.93	1.05 / 14.5	-9.84
Willston	NA	NA	4154	0	-67.5	0.928 / 11.6	-19.32
DMRSVC	NA	NA	4182	0	150.5	1.119 / 21	-42.22
Kemano	NA	NA	4186	810	294.69	1.078 / 14.9	-4.93
Bridge River	Hydro	480	4210	175.00	2.30	1.02 / 14.1	-15.76
			4211	200.00	2.30	1.023/ 14.1	-18.45
Data from Powerworld Viewer				Data from 197-bus load flow (IPFLOW)			

*NA : Not Available

Table B.2 WSCC 8313- bus power system component data

Buses	8313
Generators	1320
Bus shunts	1059
Lines	7767
Transformers	2951
Phase Shifters	16
DC Converters	6

Table B.3 WSCC 8313-bus power system base case load flow summary

	Real Power (MW)	Reactive Power (Mvar)
From generation	132686.78	25619.00
To load	127642.73	31644.42
From line charging	0.00	50329.89
To losses	4557.74	59391.75

Table B.4 BC Hydro 197- bus power system component data

Buses	197
Generators	21
Bus shunts	120
Lines	317

Table B.5 BC Hydro 197-bus power system base case load flow summary

	Real Power (MW)	Reactive Power (Mvar)
From generation	9223.8	242.65
To load	8803.8	2521.03
From line charging	0.00	7044.73
To losses	420.01	4762.40

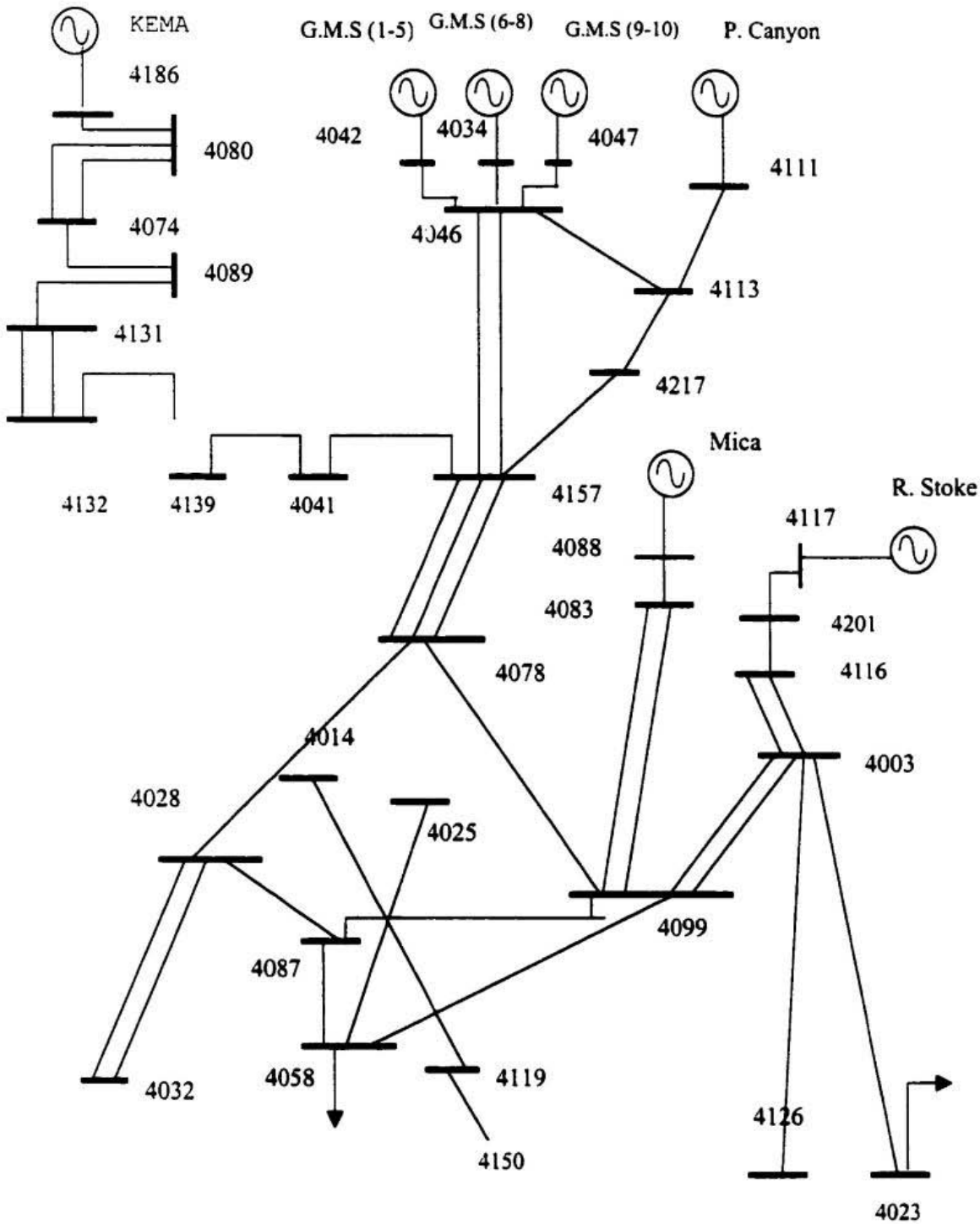

Figure B.1 Main structure of BC Hydro power system

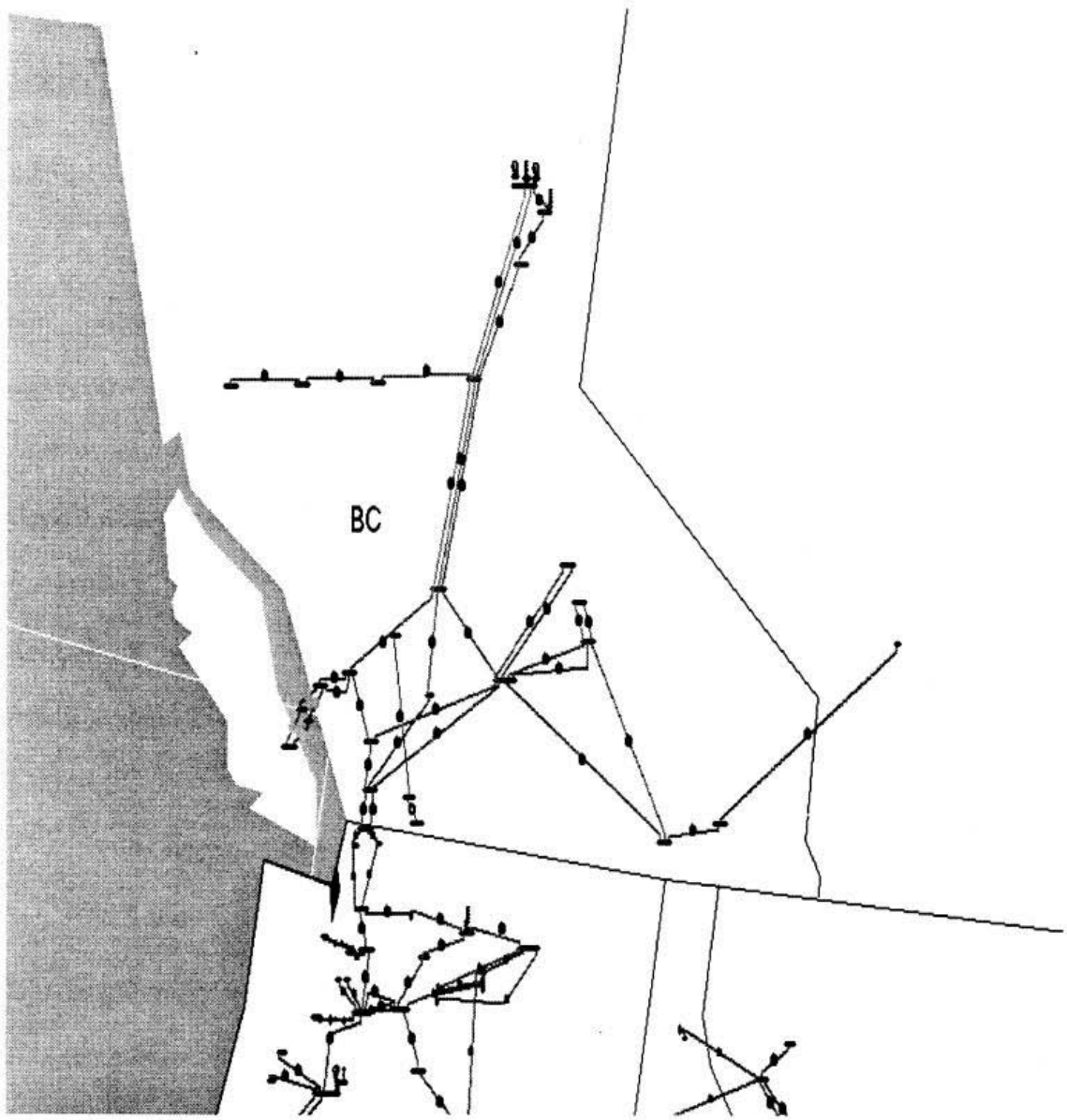

Figure B.2 Geographic location of BC Hydro transmission network

Appendix C

1254-bus Ontario Hydro Power System Summary

Another power system model used in the research is Ontario Hydro 1254-bus power system. In this power system, most of the electricity is provided by Hydro and nuclear power plants, which are located at northern part of the province and around the Great Lakes respectively, while most of the load is located around the Great Lakes. The transmission network of Ontario Hydro is interconnected with other power systems through 13 transmission lines. Figure C.1 shows the main structure of Ontario Hydro power system; Figure C.2 gives the geographic location of Ontario Hydro transmission network.

The Ontario Hydro power system data file used in the research is generated from a 13715-bus power system, which is obtained from web site: http://www.powerworld.com/fercNEPP.html. These data are for 1998 summer load of New England Power Pool. Table C.1 shows the information of the main generators of Ontario Hydro power system. Table C.2 presents the 13715-bus power system component data. The base case load flow summary is given in Table C.3.

The general procedure for derivation of the Ontario Hydro 1254-bus power system data file is shown below:

(1) Obtain the basic power system parameters from the above web site and change it to RAW data file.

(2) Find the 13 tie transmission lines connecting Ontario Hydro to other sub-systems and all the power transferred through the tie lines using powerworld viewer software, which can be download from web site: http://www.powerworld.com.

(3) Cut off all the tie transmission lines between Ontario Hydro and all the other sub-systems, and install the equivalent real and reactive power exchange through the tie lines on the buses in Ontario Hydro accordingly. Thus, the equivalent Ontario Hydro 1254-bus RAW data file is obtained.

Table C.4 shows the Ontario Hydro 1254-bus power system component data; Table C.5 shows the base case load flow for this power system. The equivalent Ontario Hydro 1254-bus power system RAW data file is used as a sample system for contingency screening and ranking.

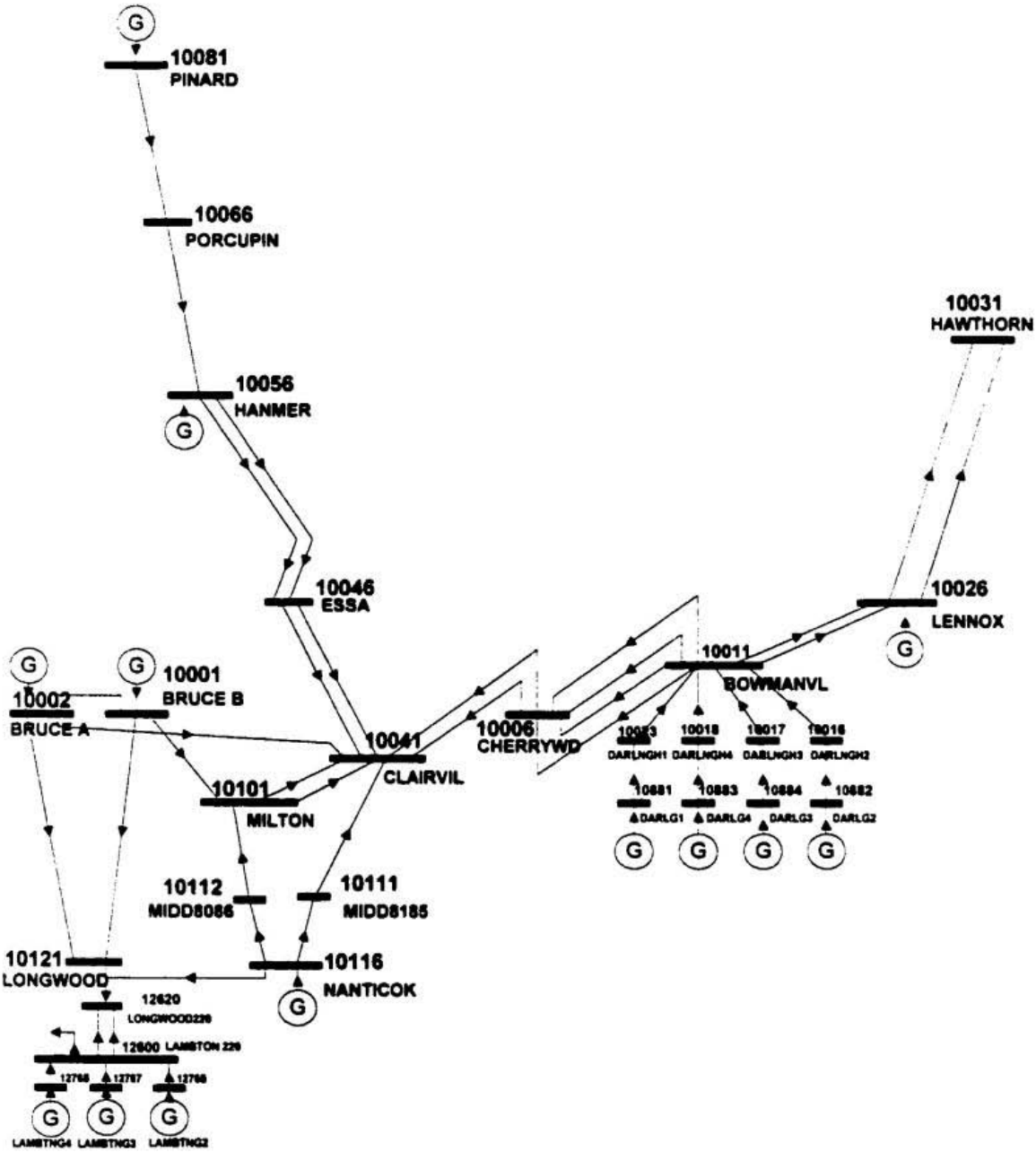

Figure C.1 Main structure of Ontario Hydro power system

Table C.1 Ontario Hydro main generator summary

Generator Name	Capacity (MW)	Bus Number	Power Generation (MW)	Power Generation (Mvar)	Terminal Voltage (p.u / kV)	Voltage Angle (Degree)
BRUCEBG8	1025.0	10326	750.00	209.22	0.9990/24.0	-4.70
BRUCEBG6	1025.0	10327	750.00	209.22	0.9984/24.0	-4.77
BRUCEBG5	1025.0	10328	750.00	209.22	0.9987/24.0	-4.67
BRUCEBG7	1025.0	10329	750.00	209.22	0.9988/24.0	-4.72
DARL G1	1101.0	10881	1192.89	578.00	1.0548/23.2	-4.43
DARL G2	1101.0	10882	930.00	52.76	0.9900/21.8	-5.94
DARL G4	1101.0	10883	930.00	52.58	0.9902/21.8	-5.93
DARL G3	1101.0	10884	930.00	52.58	0.9902/21.8	-5.93
PIC B G7	635.30	10911	540.00	101.67	0.9988/24.0	-12.27
PIC B G8	635.30	10912	540.00	101.67	0.9987/24.0	-12.27
PIC B G5	635.30	10913	540.00	75.48	0.9913/23.8	-12.14
PIC B G6	635.30	10914	540.00	75.48	0.9913/23.8	-12.09
LENNOXG2	675.00	11422	570.00	73.69	0.9507/19.0	-1.59
LENNOXG1	675.00	11423	570.00	73.69	0.9507/19.0	-1.32
NANTICG7	675.00	11764	500.00	93.10	0.9753/21.5	-6.04
NANTICG6	675.00	12765	500.00	93.10	0.9764/23.3	-11.88
Data from Powerworld Viewer			Data from 1254-bus load flow (IPFLOW)			

Table C.2 NEPP 13,715- bus power system component data

Buses	13,715
Generators	3,533
Bus shunts	495
Lines	25,125

Table C.3· NEPP 13,715-bus power system base case load flow summary

	Real Power (MW)	Reactive Power (Mvar)
From generation	460557.6	83536.3
To load	451355.6	165226.7
From line charging	670.8	-104092.6
To losses	8603.64	22615.79

Table C.4 Ontario Hydro 1254- bus power system component data

Buses	1254
Generators	268
Bus shunts	173
Lines	1970

Table C.5 Ontario Hydro 1254-bus power system base case load flow summary

	Real Power (MW)	Reactive Power (Mvar)
From generation	23989.07	3490.74
To load	23439.60	12465.27
From line charging	0.00	7003.85
To losses	438.80	8261.11

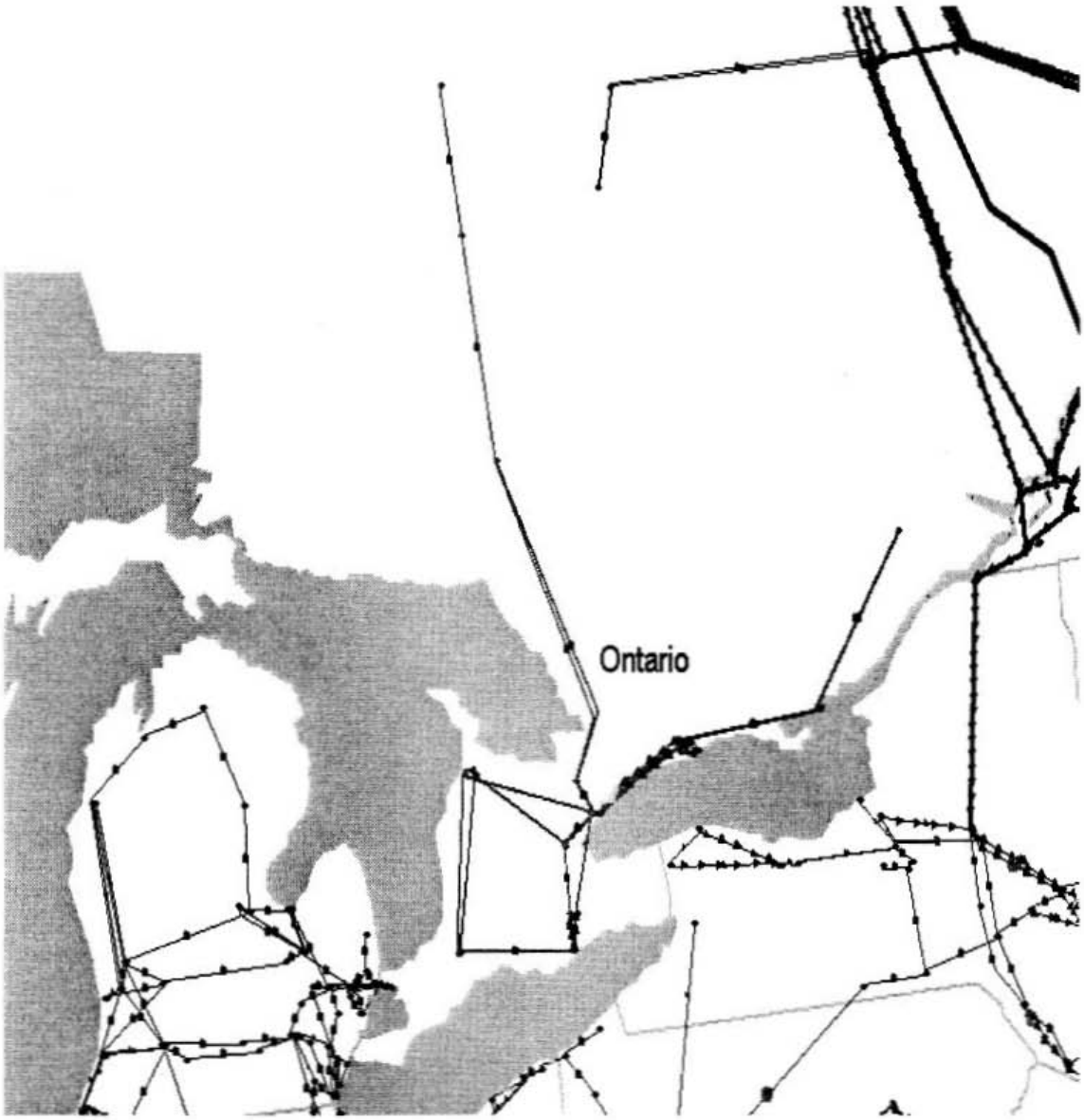

Figure C.2 Geographic location of Ontario Hydro transmission network